

CONSTRAINING THE ORIGIN OF MULTIPLE
STELLAR POPULATIONS IN STELLAR
CLUSTERS

Ivan Cabrera Ziri Castro

A thesis submitted in partial fulfilment of the requirements of
Liverpool John Moores University
for the degree of
Doctor of Philosophy.
May 5, 2017

“¿Por dónde le entra el agua al coco?”

-I. Cabrera-Ziri, 2015

Abstract

Globular clusters were among the first luminous objects to form in the Universe. They are dense collections of hundreds of thousands of stars. Globular cluster formation is a major unsolved problem in astrophysics. A new constraint on the problem came from the discovery of unexpected star-to-star variations in the abundances of some light elements. These abundance variations (or multiple stellar populations) are ubiquitous to all globular clusters studied to date. The pursuit to explain this longstanding problem using these new constraints (i.e. the abundance variations), has reinvigorated the study of globular clusters, and at the same time has challenged our understanding of nucleosynthesis and stellar evolution.

Several scenarios have been put forward to explain the presence of multiple stellar populations in globular clusters, nearly all requiring multiple generations of stars. The basic hypothesis in these models is that a second generation of stars is born during the early life of the globular cluster from the chemically-processed ejecta of some first generation stars in order to account for the signature multiple stellar populations observed in old globular clusters today. Many of these scenarios are mutually exclusive. Therefore, to determine which of them fits the current evidence the best became the priority of globular cluster studies.

Modern observational facilities cannot resolve the globular cluster formation process in the early Universe. However, none of the scenarios for the origin of globular cluster and their multiple stellar populations make any distinctions between star/cluster formation at the present day and earlier epochs of the universe. Accordingly, the processes invoked in these scenarios can, in principle, be constrained by studies of the forma-

tion of young massive star clusters in the local Universe, which have similar sizes and masses as present-day globular clusters, but are significantly younger.

In this work, I present some of the strongest constraints from such studies coming from the gas content of young massive clusters and their star formation histories. These studies showed that: 1) young massive clusters are consistent with a single star formation burst, and 2) there is no significant cool gas reservoirs left within young massive clusters that can fuel future star-formation events.

These results are in stark contrast with the predictions of nearly all the scenarios that have been proposed to explain the origin of abundance variations in globular cluster stars, which require that young massive clusters should host multiple star formation events.

Publications

- Bastian, N.; Cabrera-Ziri, I.; Niederhofer, F.; de Mink, S.; Georgy, C.; Baade, D.; Correnti, M.; Usher, C.; Romaniello, M. “*A high fraction of Be stars in young massive clusters: evidence for a large population of near-critically rotating stars*”, 2017, MNRAS, 465, 4795 – Contribution: Providing comments on science.
- Niederhofer, F.; Bastian, N.; Kozhurina-Platais, V.; Larsen, S.; Hollyhead, K.; Lardo, C.; Cabrera-Ziri, I.; Kacharov, N.; Platais, I.; Salaris, M.; Cordero, M.; Dalessandro, E.; Geisler, D.; Hilker, M.; Li C.; Mackey, D.; Mucciarelli, A. “*The Search for Multiple Populations in Magellanic Cloud Clusters II: The Detection of Multiple Populations in Three Intermediate-Age SMC Clusters*”, 2017, MNRAS, 465, 4159 – Contribution: Providing comments on science.
- Niederhofer, F.; Bastian, N.; Kozhurina-Platais, V.; Larsen, S.; Salaris, M.; Dalessandro, E.; Mucciarelli, A.; Cabrera-Ziri, I.; Cordero, M.; Geisler, D.; Hilker, M.; Hollyhead, K.; Kacharov, N.; Lardo, C.; Li, C.; Mackey, D.; Platais, I. “*The Search for Multiple Populations in Magellanic Cloud Clusters I: Two Stellar Populations in the Small Magellanic Cloud Globular Cluster NGC 121*”, 2017, MNRAS, 464, 94 – Contribution: Providing comments on science.
- Cabrera-Ziri, I.; Lardo, C.; Davies, B.; Bastian, N.; Beccari, G.; Larsen, S. S.; Hernandez, S. “*Searching for GC-like abundance patterns in young massive clusters*”, 2016, MNRAS, 460, 1869
- Bastian, N.; Niederhofer, F.; Kozhurina-Platais, V.; Salaris M.; Larsen S.;

- Cabrera-Ziri, I.; Cordero, M.; Ekstrm, S.; Geisler, D.; Georgy, C.; Hilker, M.; Kacharov, N.; Li, C.; Mackey, D.; Mucciarelli, A.; Platais, I. “*A Young Cluster With an Extended Main Sequence Turnoff: Confirmation of a Prediction of the Stellar Rotation Scenario*”, 2016, MNRAS, 460, L20 – Contribution: Providing comments on science.
- Cabrera-Ziri, I.; Niederhofer, F.; Bastian, N.; Rejkuba, M.; Balbinot, E.; Kerzendorf, W. E.; Larsen, S. S.; Mackey, A. D.; Dalessandro, E.; Mucciarelli, A.; Charbonnel, C.; Hilker, M.; Gieles, M.; Hénault-Brunet, V. “*No evidence for young stellar generations within intermediate age massive clusters NGC 1783, NGC 1806 and NGC 411*”, 2016, MNRAS, 459, 4218
 - Cabrera-Ziri, I.; Bastian, N.; Hilker, M.; Davies, B.; Schweizer, F.; Kruijssen, J. M. D.; Mejía-Narváez, A.; Niederhofer, F.; Brandt, T. D.; Rejkuba, M.; Bruzual, G.; Magris, G. “*Is the escape velocity in star clusters linked to extended star formation histories? Using NGC 7252: W3 as a test case*”, 2016, MNRAS, 457, 809
 - Niederhofer, F.; Bastian, N.; Kozhurina-Platais, V.; Hilker, M.; de Mink, S. E.; Cabrera-Ziri, I.; Li, C.; Ercolano, B. “*Controversial Age Spreads from the Main Sequence Turn-Off and Red Clump in Intermediate-Age Clusters in the LMC*”, 2015, A&A, 586, A148 – Contribution: Providing comments on science.
 - Bastian, N.; Cabrera-Ziri, I.; Salaris, M. “*A general abundance problem for all self-enrichment scenarios for the origin of multiple populations in globular clusters*”, 2015, MNRAS, 449, 3333 – Contribution: Providing comments on science.
 - Cabrera-Ziri, I.; Bastian, N.; Longmore, S. N.; Brogan, C.; Hollyhead, K.; Larsen, S. S.; Whitmore, B.; Johnson, K.; Chandar, R.; Henshaw, J. D.; Davies, B.; Hibbard, J. E. “*Constraining globular cluster formation through studies of young massive clusters - V. ALMA observations of clusters in the Antennae*”, 2015, MNRAS, 448, 2224

- Magris, G.; Mateu, J.; Mateu, C.; Bruzual, G.; Cabrera-Ziri, I.; Mejía-Narváez, A. “*On the Recovery of Galaxy Properties from SED Fitting Solutions*”, 2015, PASP, 127, 16 – Contribution: Providing comments on science.
- Bastian, N.; Hollyhead, K.; Cabrera-Ziri, I. “*Constraining globular cluster formation through studies of young massive clusters - IV. Testing the fast rotating massive star scenario*”, 2014, MNRAS, 445, 378 – Contribution: Providing comments on science.
- Cabrera-Ziri, I.; Bastian, N.; Davies, B.; Magris, G.; Bruzual, G.; Schweizer, F. “*Constraining globular cluster formation through studies of young massive clusters - II. A Single Stellar Population Young Massive Cluster in NGC 34*”, 2014, MNRAS, 441, 2754
- Bastian, N., Cabrera-Ziri, I.; Davies, B. “*Constraining globular cluster formation through studies of young massive clusters - I. A lack of ongoing star formation within young clusters*”, 2013, MNRAS, 436, 2852 – Contribution: Providing comments on science.

Contents

Contents	viii
List of Tables	xii
List of Figures	xiii
1 Introduction	1
1.1 Globular clusters' background	1
1.1.1 Star-to-star abundance variations	3
1.1.2 The basic ideas behind the GC formation scenarios	5
1.1.3 Complex CMDs in intermediate-age clusters and GC formation link	6
1.2 Young massive clusters as test beds for GC formation	7
1.2.1 Evidence from YMCs in the Milky Way, LMC and SMC	8
1.3 Testing GC formation scenarios	10
2 Star formation history of young massive clusters	12
2.1 A Single Stellar Population Young Massive Cluster in NGC 34	12
2.1.1 Data	15
2.1.2 DynBaS fitting	16

2.1.3	Degeneracies and Uncertainties	19
2.1.4	Discussion	23
2.1.5	Conclusions from Cabrera-Ziri et al. (2014)	23
2.2	Is the Escape Velocity in Star Clusters Linked to Extended Star Formation Histories?	24
2.2.1	Data	27
2.2.2	Age and mass of NGC 7252: W3	28
2.2.3	Synthetic SED experiments	34
2.2.4	Discussion	38
2.2.5	Summary and Conclusions from Cabrera-Ziri et al. (2016a)	46
2.3	Constraints from resolved LMC/SMC clusters	48
2.3.1	HST photometry	49
2.3.2	Densities and luminosity functions of the young stars	50
2.3.3	Reducing background contamination in L16	51
2.3.4	Performance of L16 background decontamination	52
2.3.5	Significance of the L16 detections	56
2.3.6	Spatial distribution of the populations	58
2.3.7	Summary and conclusions from Cabrera-Ziri et al. (2016b)	60
3	Gas content of young massive clusters	62
3.1	Background	62
3.2	ALMA data	65
3.3	Molecular gas and stellar mass estimates	66

3.4	Discussion	68
3.4.1	AGB scenario: The essentials	69
3.4.2	Toy model	73
3.4.3	Accretion of pristine gas	76
3.4.4	D’Ercole et al. (2008) prediction of the gas reservoir mass	77
3.4.5	Why are YMCs gas free?	78
3.5	Conclusions from Cabrera-Ziri et al. (2015)	80
4	Abundance variations in young massive clusters	83
4.1	RSG stars and YMCs	85
4.2	XSHOOTER data	86
4.3	Analysis	86
4.3.1	Expectations from different GCs	88
4.3.2	[Al/Fe] spreads: results from YMCs in the context of GCs	91
4.4	Discussions and conclusions from Cabrera-Ziri et al. (2016c)	93
5	Present day properties of GCs and expectations from formation scenarios	97
5.1	Predicted properties	97
5.2	Unexpected correlations	98
5.2.1	Mass budget	99
5.2.2	Comments on Schiavon et al. (2013) results	100
6	Conclusions	101
6.1	Future work	103

A	Degeneracies of the continuum normalized fit of NGC 7252: W3	108
B	Cluster disruption in the SMC/LMC	111
	Bibliography	114

List of Tables

2.1	WFPC2 photometry of NGC 7252: W3 from Cabrera-Ziri et al. (2016a)	28
2.2	Results of DynBaS fitting NGC 7252: W3	29
2.3	Number and surface density of young stars in the Li et al. (2016) clusters and field	49
3.1	Properties of Cabrera-Ziri et al. (2015) clusters	68
4.1	Metallicities and aluminium abundance spread of Galactic GCs.	90

List of Figures

1.1	Ultraviolet CMDs of two GCs with very different MPs signatures . . .	5
1.2	CMD of NGC 1846, an intermediate-age cluster displaying an extended main-sequence turn-off	7
1.3	Correlation between inferred age spread and cluster age	9
1.4	Similarities between a YMC and a GC	10
2.1	DynBaS fits to YMC NGC 34: S1 from Cabrera-Ziri et al. (2014) . . .	18
2.2	Representation of the degeneracies of the DynBaS fit to NGC 34: S1 .	21
2.3	Uncertainties of the DynBaS fit of NGC 34: S1	22
2.4	DynBaS fits to the MagE spectrum of NGC 7252: W3 from Cabrera-Ziri et al. (2016a)	30
2.5	DynBaS fits to the continuum-normalised spectrum of NGC 7252: W3 from Cabrera-Ziri et al. (2016a)	31
2.6	Comparison of NGC 7252: W3 HST photometry with SSPs of different ages	32
2.7	Star formation histories of three synthetic YMCs following Goudfrooij et al. (2014) SFH predictions	37
2.8	Comparison of W3 MagE spectrum with predicted SEDs from Goudfrooij et al. (2014)	37

2.9	Similar to Fig. 2.8 but shown as a close-up around the age-sensitive Ca II K line	38
2.10	Pseudo-age distributions from G14 for three synthetic clusters	39
2.11	Comparison of W3 MagE spectrum with SEDs built according to SFH from Fig. 2.10	39
2.12	Similar to Fig. 2.8 but shown as a close-up around the Ca II K line	40
2.13	Young and old populations in Li et al. (2016) clusters	50
2.14	Cumulative LFs of the young populations in the clusters and field regions from Li et al. (2016)	51
2.15	Spatial distribution of the cluster and field stars used in Cabrera-Ziri et al. (2016b) experiments	53
2.16	Field subtraction experiments from Cabrera-Ziri et al. (2016b)	54
2.17	CMD of NGC 1783 produced by Li et al.'s decontamination technique	56
2.18	Probability of the stars in the CMD of NGC 1783 to belong to the LMC field	57
2.19	Significance of Li et al. (2016) detections	58
2.20	Radial profiles of the populations within the Cabrera-Ziri et al. (2016b) clusters	59
3.1	YMCs from Cabrera-Ziri et al. (2015)	65
3.2	ALMA spectra of Cabrera-Ziri et al. (2015) clusters	66
4.1	Comparison of <i>J</i> -band median spectrum of Davies et al. (2015) stars with the integrated spectrum pf NGC 1705: 1	87
4.2	Similar to Fig. 4.1 but centred around two Al lines	89

4.3	RSG models from Cabrera-Ziri et al. (2016c)	91
4.4	Aluminium abundance spread as a function of GC metallicity	92
6.1	Parameter space occupied by multiple stellar populations in GCs	104
6.2	Distribution of stars from Schiavon et al. (2017a)	106

Chapter 1

Introduction

It is likely that some stars are born essentially in isolation (de Wit et al., 2005; Bressert et al., 2010), however most stars seem to be born in stellar clusters and associations (Lada & Lada, 2003). Stellar clusters are physically associated groups of stars, bound permanently or temporarily by gravity, while moving together through space. Historically stellar clusters have been classified in two main categories: open and globulars. Open clusters are collections of dozens to thousands of stars, usually in an irregular shape and loosely bound (cf. Moraux, 2016, for a recent review of open clusters and associations). On the other opposite end of the stellar cluster mass distribution we have globular clusters (GCs), which are much denser collections of approximately hundreds of thousands of stars forming a roughly spherical shape, hence the term “globular”.

In this chapter I will present the basic ideas and concepts involved in the tests of the formation scenarios of GCs.

1.1 Globular clusters’ background

GCs span a wide range of properties. However, in order to give a general idea of their attributes I will describe the characteristics of the largest fraction of the GCs in our Galaxy. They usually have masses between $\sim 10^4 - 10^6 M_{\odot}$, half-light radii

between $\sim 2 - 20$ pc (Krause et al., 2016) and are found in the halo. The distribution is spherically symmetric around the centre of the Galaxy, and concentrated (in terms of their numbers per unit volume) mostly around the Sagittarius–Scorpius–Ophiuchus region. The majority of them have low metallicities, typically between $-2.5 < [\text{Fe}/\text{H}] < -0.5$ ¹ (Gratton et al., 2012). Having said that, there is a subset that can reach very high metallicities (close to solar) and are located in the Galactic bulge (e.g., Schiavon et al., 2017b). Most GC also tend to be very old $\sim 10 - 13$ Gyr (VandenBerg et al., 2013).

The fact that GCs are rather old became clear already in the 1950s, when the main-sequence turn-off luminosities of GC stars were found to be close to solar (cf. Sandage 1986 and references therein). But later refinements in nuclear physics and stellar structure calculations, as well as improvements in distance moduli and abundance measurements in fact soon demonstrated that they were older than the Sun and indeed contained some of the oldest stars in the Galaxy (Kraft, 1994). Due to this, detailed studies of the chemical composition of their stars were expected to provide important clues and constraints upon the formation and early chemical evolution of the Galaxy (e.g. Wheeler et al. 1989).

However, as the evidence of GC star-to-star abundance variation of e.g. C, N, Al, Na and O started to pile up (cf. Kraft 1979 and references therein), it became difficult to conclude at the time if the measured abundances were primordial (i.e. initial chemical composition) or were due to changes in the chemical composition of the stars product of stellar evolution in the giant stars that were the subject of these studies (i.e. the only stars bright enough to be accessible with the instrumentation of the time). Since then, a lot of attention was devoted to a new set of problems related to the evolution of low-mass stars and stellar nucleosynthesis.

It was not until 1980 when a major breakthrough was made. Hesser & Bell (1980) analysed the low-resolution spectra of seven unevolved (i.e. main-sequence) stars of

¹The abundance of a given element, el , is reported as $[el/H] = \log(el/H)_* - \log(el/H)_\odot$. In this field $[\text{Fe}/\text{H}]$ is routinely used as a “surrogate” of metallicity, i.e. the fraction of elements heavier than He. This amounts to at most $Z \sim 0.05$, is $Z_\odot \sim 0.02$ for the Sun, and can be as little as $Z \sim 0.0001$ in the most metal-poor Galactic GCs (Van Loon, 2010)

47 Tucanae (NGC 104), and found differences in the CN band strength that were due to variations in the N abundance, and were similar to the ones reported previously in the evolved stars of the same cluster. This was clear evidence that these abundance variations were primordial and could not be accounted entirely by the stellar evolution.

Understanding the origin of these star-to-star abundance variations has been a challenge ever since. In the rest of this section I will tally the main present-day properties of these abundance variations²; summarise the latest scenarios that have been put forward to explain the origin of GCs and these variations; and introduce how massive clusters forming today can help us shed some light on the origin of GCs and their star-to-star abundance variations.

1.1.1 Star-to-star abundance variations

The field has come a long way since since the early studies mentioned above, and new techniques and technology have helped increase the inventory of the present-day properties of the star-to-star abundance variations observed in GCs. For example, *all* GCs that have been studied with a large enough sample of stars show spectroscopic and/or photometric evidence of such abundance variations (more on this, and some possible exceptions in Cordero et al., 2017). Evidence suggesting the presence of star-to-star abundance variations has even been reported in GCs in other local group galaxies like: Andromeda (M31), Large Magellanic Cloud (LMC), Small Magellanic Cloud (SMC), Sagittarius dwarf-Spheroidal (dSph), Fornax dSph and Wolf-Lundmark-Melotte (WLM) alike (e.g. Schiavon et al., 2013; Mucciarelli et al., 2009; Dalessandro et al., 2016; Carretta et al., 2014a; Larsen et al., 2014b,a).

These light-element abundance variations are not random. On the contrary, they follow very specific trends and patterns between different elements. For example, the abundance of N anti-correlates with that of C and O, while the sum of C+N+O remains constant within a factor of ~ 2 , resembling the products of H-burning through the CNO

²A complete summary of all the reported chemical variations in GCs is beyond the scope of this work. The reader interested in a comprehensive review on this subject is referred to Gratton et al. (2012).

cycle (e.g. Carretta et al., 2005). The Na abundance is also observed to anti-correlate with the O abundance, and similar anti-correlations can be found sometimes between the Al and Mg abundances of GC stars (e.g. Carretta et al., 2009b; Roediger et al., 2014). The trends between these elements are consistent as well with the ashes of very high temperature H-burning through the NeNa- and MgAl-chains (e.g. Gratton et al., 2012; Charbonnel, 2016, and references therein).

There is also some evidence of He-enrichment in some GC stars. Most of this evidence is inferred from the presence of multiple main-sequences (MS) and the morphology of the horizontal branch in the colour-magnitude diagram (CMD) of some GCs (e.g. Milone et al., 2015; Salaris et al., 2016). Such He abundance variations have also been confirmed spectroscopically in studies of the chromospheres of red-giant branch stars (RGB – e.g. Pasquini et al., 2011), however due to the intrinsic challenges of these measurements³, direct spectroscopic measurements of He-abundances remain very scarce at the present⁴.

Although it seems like the abundances of different species always correlate the same way, the complexity of the sub-populations within a GC can change significantly from cluster to cluster⁵. Perhaps the best exemplification of this fact comes from the ultraviolet CMDs of GCs⁶. For example, while some GCs like NGC 6171 show very discrete features in the CMD, in some others the distinction between sub-populations is not that clear, and can even resemble a continuous distribution like in NGC 6205, cf. Figure 1.1⁷.

All this complexity differs from the early idea of GCs being simple (or single) stellar

³He is hardly observable in cool stars, because no photospheric He lines are present in their atmospheres –see Pasquini et al. (2011) for details

⁴Other spectroscopic reports of He variations in GC stars include Dupree et al. (2011); Marino et al. (2014)

⁵Moreover, some global properties of the GCs like the mass for example, seem to be associated with how severe the changes in abundances of some elements are, and even the ratio between sub-populations within a GCs, see §5.

⁶Different levels of N-enhancement/C- and O-depletion can be distinguished by the use of precise photometry in regions with prominent molecular bands, like the OH-, NH-, CN- and CH-bands in the ultraviolet and blue spectrum ($\sim 2500 - 4500 \text{ \AA}$ e.g. Piotto et al., 2015; Niederhofer et al., 2017a)

⁷Here the differences between sub-populations are maximised in the bottom row, with the use of the pseudo-colour $C_{F275W,F336W,F438W} = (m_{F275W} - m_{F336W}) - (m_{F336W} - m_{F438W})$

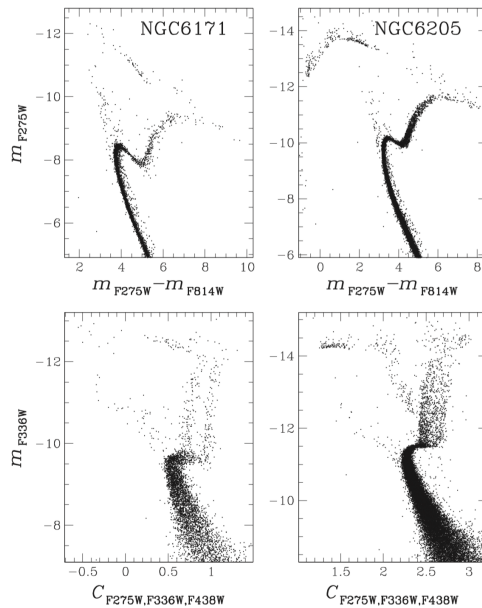


Figure 1.1: Ultraviolet CMDs of NGC 6171 (left) and NGC 6205 (right) from Piotto et al. (2015). In the bottom row is shown how the use of the pseudo-colour can maximise the differences between sub-populations in the CMD. NGC 6171 shows two very distinct sub-populations however, in NGC 6205 the distinction between sub-populations is not so clear.

populations (SSP), i.e. a group of stars born at the same time, in the same volume of space, and from a gas cloud of homogeneous chemical composition (Bruzual, 2010). Consequently, the community frequently refers to the star-to-star abundance variations observed in GCs, as being due to the presence of multiple populations (MPs).

1.1.2 The basic ideas behind the GC formation scenarios

There have been several scenarios proposed to explain the formation of GCs and how they ended up hosting MPs. In this section I will outline the most popular scenarios proposed in recent years.

All these scenarios were conceived around the following premisses – all supported by the evidence of the time although some may not necessarily in force today–, namely:

- MPs are found in any stage of the stellar evolution present in GCs, including the MS.
- The abundance patterns of MPs resemble the products of high temperature H-burning (see references in §1.1.1).
- Lack of variations in Fe-peak elements among GC stars – with the exception of

the most massive GCs like ω Centauri that shows clear photometric and spectroscopic evidence of large metallicity spreads.

- No evidence for MPs in the Galactic halo field stars, nor in open clusters.
- Most stars in GCs show chemical anomalies while a minority follow the same abundance patterns of field stars of similar metallicity.

The basic notion behind the scenarios is the following:

A first-generation is born as an SSP, i.e. all these stars have the same age, and homogeneous chemical composition. This will account for the fraction of GC stars that share abundances with field stars of similar metallicity. From now on, we will refer to this chemical composition as *pristine* composition.

Some of these stars born with pristine composition will return chemically processed material by high temperature H-burning back to the intra-cluster medium. These stars will be referred to as *polluters* henceforth. The cluster holds this polluted material within its gravitational potential well which allows a second generation of stars to form with a chemical signature which is distinct from the pristine, first stellar generation⁸.

The rationale behind the premises upon which these scenarios were built, as well as some relevant details about the mechanisms involved will be treated in due course.

1.1.3 Complex CMDs in intermediate-age clusters and GC formation link

Also relevant to the phenomenon of MPs in GCs and possibly their origin, is that observations of intermediate-age clusters ($\sim 1 - 2$ Gyr) in the LMC and SMC have shown the presence of extended main-sequence turn-offs (eMSTOs) that are not consistent

⁸It is worthy of note, that the term “multiple stellar populations” referring to the star-to-star abundance variations is often used as a synonym of “multiple stellar generations”, e.g. Gratton et al. (2012). This has led to unnecessary confusion in the literature, as the star-to-star abundance variations of He, C, N, Na, O, Al, etc. found in GCs hardly constitute any form of evidence for multiple star-formation events *per se*.

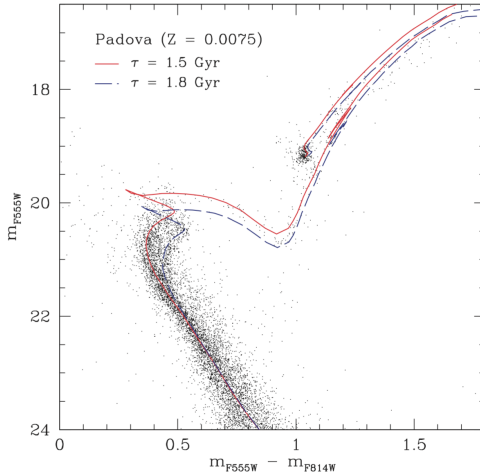


Figure 1.2: CMD of NGC 1846 from Mackey & Broby Nielsen (2007). Both red and blue isochrones have the same metal abundance $Z = 0.0075$, but different ages, 1.5 Gyr and 1.8 Gyr respectively. It is clear that the turn-off of this cluster cannot be reproduced by a single isochrone. This has been interpreted as evidence of extended star formation histories by some authors, see text.

with a single theoretical isochrone⁹ (e.g. Mackey & Broby Nielsen, 2007, see Figure 1.2). This was originally interpreted as evidence for a significant age spread present within the clusters, with a duration of $\sim 200 - 500$ Myr (e.g. Goudfrooij et al., 2009, 2011a,b; Milone et al., 2009; Rubele et al., 2013). Additionally, some clusters have “dual” red clumps (RC) in their CMDs which have also been interpreted as due to age spreads (e.g. Girardi et al., 2009).

A number of works have attempted to link these implied age-spreads with the anomalies in the ancient GCs (e.g. Conroy & Spergel, 2011; Keller et al., 2011, a more comprehensive review on this subject is presented in §2.2). Suggesting a common evolution for massive clusters (present-day masses $\gtrsim 10^5 M_{\odot}$), i.e. all massive clusters have undergone extended star-formation (SF) bursts, and second generation stars will form from *polluted* material that was retained in the cluster.

1.2 Young massive clusters as test beds for GC formation

Modern observational facilities cannot resolve the GC formation process in the early Universe. However, *none of the scenarios for the origin of GC and their MPs make any distinctions between star/cluster formation at the present day and earlier epochs of the*

⁹At any given time, the stars composing an SSP describe an isochrone in the theoretical Hertzsprung–Russell (HR) diagram, which can easily be transformed to an observational CMD (cf. Bruzual, 2010).

*universe*¹⁰. Accordingly, the processes invoked in these scenarios can, in principle, be constrained by studies of the formation of young massive star clusters (YMCs) today – as long as their masses are high enough to match those of young GCs.

Models that interpret the MPs in GCs and/or the complex CMDs of intermediate-age clusters as multiple star formation episodes, all make a common prediction, that YMCs with ages < 500 Myr should show ongoing star formation as well as gas/dust build-up within them that will eventually be used in the formation of a second generation. The duration of the age spread (or time between successive discrete star-forming episodes) depends on the model. If the second generation of GCs forms from the enriched material ejected from rapidly rotating massive ($\sim 20 - 120 M_{\odot}$) stars (FRMS – e.g. Prantzos & Charbonnel, 2006; Decressin et al., 2007a,b; Krause et al., 2012, 2013) or interacting binaries (e.g. de Mink et al. 2009), then the expected time between the first and second generation is expected to be short ($\sim 5 - 20$ Myr). On the other hand, if asymptotic giant branch (AGB) stars are the source of the second generation, then the time difference is expected to be $30 - 200$ Myr (e.g. D’Ercole et al., 2008; Conroy & Spergel, 2011). If the eMSTOs are due to extended star-formation histories (SFH), then young clusters should be seen forming stars continuously for $200 - 500$ Myr (see references in §1.1.3).

1.2.1 Evidence from YMCs in the Milky Way, LMC and SMC

Observations of young (< 10 Myr) massive (few $10^4 M_{\odot}$) clusters in the Galaxy, such as Westerlund 1, Westerlund 2 and NGC 3603, suggest an upper limit to age spreads of < 2 Myr (e.g. Kudryavtseva et al., 2012; Zeidler et al., 2015). Additionally, such massive clusters appear to be devoid of dense gas and its associated dust at an early age (e.g. Stolte et al., 2002). These time-scales are too short for any of the mechanisms proposed for the multiple populations of GCs to operate (see above). However, these clusters may be of too low mass for the mechanisms to work.

¹⁰D’Ercole et al. (2016) suggested only the characteristics found in disc galaxies at high redshift ($z \gtrsim 2$) were able to produce the necessary conditions to produce the MP phenomenon. However, evidence of GCs hosting MPs which formed at $z \sim 0.65$ – likely in a very different environment – argues otherwise (cf. Niederhofer et al., 2017b).

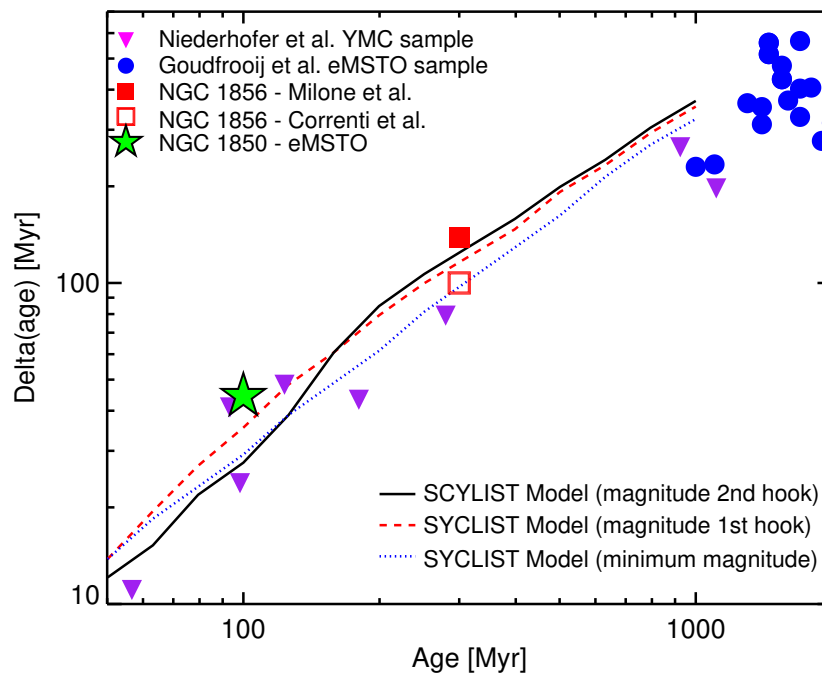


Figure 1.3: Image from Bastian et al. (2016) showing the correlation between cluster age and inferred age spread. The symbols represent the reported values from a number of observational studies. The lines represent predictions from the Geneva rotating stellar models (Georgy et al., 2013) of the inferred age spread expected if a spread in the turn-off due to rotation is misinterpreted as an age spread. Note the strong correlation between the age of the cluster and the inferred age spread, in good agreement with these model predictions.

For example, the scenario proposed by Conroy & Spergel (2011) predicts that clusters, at least in the LMC, with masses in excess of $10^4 M_{\odot}$ should be able to retain *polluted* material –and also accrete *pristine* material from the surroundings, more on this later, see §3 – in order to form a second generation of stars.

Massive (10^4 to $\sim 5 \times 10^5 M_{\odot}$) clusters in LMC and SMC, share the same mass range of present-day GCs. Some of these are the young- and intermediate-age clusters displaying eMSTO and “dual” RC in their CMDs. However, the eMSTO and “dual” RC do not seem to be in accord with extended star formation events (e.g. Bastian & Niederhofer, 2015; Niederhofer et al., 2016, and references therein).

Another model for the origin of eMSTOs, which appears to fit the data better, is that there exists a range of stellar rotation rates within the clusters (cf. Bastian & de Mink, 2009; Bastian et al., 2016, 2017; Brandt & Huang, 2015a,b; Niederhofer et al., 2015,

2016; Milone et al., 2016, and references therein). A key prediction of the stellar rotation scenario that has been observationally tested, is that the prominence of the eMSTO (i.e. how severe the eMSTO is) correlates strongly with the age of the cluster, in the sense that the width of the eMSTO –and as a consequence, the inferred age spread– is smaller/narrower the younger the cluster is, see Figure 1.3. This is not expected if age spreads are responsible of the eMSTO. By the time of writing this work, a direct measurement of the rotation rates of the stars is still missing, yet such measurements are expected to arrive soon.

With this in mind, the evidence indicates that no age spreads are present in these LMC and SMC clusters. This suggests that if clusters are able to retain the material to form multiple generations, it must be above a mass of $\sim 5 \times 10^5 M_{\odot}$.

1.3 Testing GC formation scenarios

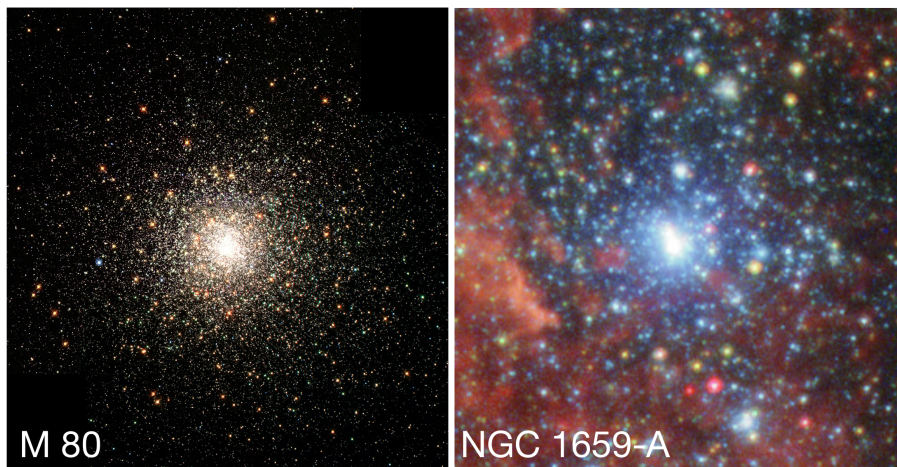


Figure 1.4: Image from Kruijssen (2014) comparing two massive stellar clusters. Left: the Galactic GC M 80 ($10^{5.6} M_{\odot}$; 1.8 pc – Harris, 1996). Right: NGC 1659-A the most massive YMC in a nearby dwarf starburst galaxy ($10^6 M_{\odot}$; 1.6 pc – Anders et al., 2004). The masses of M 80 and NGC 1659-A and half-light radii are very similar, but the ages differ strongly (10^{10} and 10^7 yr, respectively), showing that GC-like YMCs are still forming at the present day. Hence, YMCs like NGC 1659-A provide an unprecedented view in the formation and early evolution of GCs.

There are clusters in the local Universe that have masses similar to, and even significantly above GCs, that can be used to directly test the scenarios described above, see

Figure 1.4. These YMCs (see e.g. Portegies Zwart et al., 2010, for a recent review) have ages between a few Myr and a few hundred Myr, and masses between 10^4 and $10^8 M_{\odot}$, although note that the lower limit is a relatively arbitrary cut as the mass function of clusters extends smoothly below this limit.

In the following, I will present a summary of the main results that constrain the scenarios of GC formation and the origin of MPs using young ($< \text{few Gyr}$) massive ($> 10^5 M_{\odot}$) clusters, focusing namely in the following predictions from the scenarios for such clusters:

- There should be large reservoirs of gas/dust within these YMCs in order to fuel multiple SF events.
- Their SFHs should not be consistent with an SSP, but rather should show evidence of multiple discrete bursts.
- There should be signatures of abundance variations in YMCs similar to the ones in GCs.

Chapter 2

Star formation history of young massive clusters

In this chapter I summarise the relevant evidence I have gathered regarding the expected properties of YMCs according to some GC formation scenarios. Specifically that YMCs, given their current masses and densities should be able to retain and accrete gas which will eventually spawn secondary SF events – in these scenarios also responsible for the MPs. Here I review the constraints on the origin of MPs placed by the SFH of YMCs.

2.1 A Single Stellar Population Young Massive Cluster in NGC 34

As mentioned before, most models that attempt to explain the chemical anomalies and CMD morphology observed in GCs assume that these features are the product of multiple generations of stars. The basic idea is that a second generation of stars is created from the chemically processed ejecta of some very precise kinds of stars from the first generation (*polluter* stars). Stars that have been suggested to be *polluters* include: Asymptotic Giant Branch (AGB) stars (e.g. D’Ercole et al. 2008), fast rotating

massive stars (also known as FRMS e.g. Decressin et al. 2009), and massive stars in interacting binary systems (de Mink et al., 2009).

All these multiple-population scenarios do well reproducing some of the observed anomalies mentioned before, and they predict that star clusters forming today should undergo a second generation of star formation. If spin-stars or massive interacting binaries are the source of the enriched material, then the second generation is expected to form within ~ 10 Myr of the first generation. Alternatively, if AGB stars are the source, a difference of 30–200 Myr between the 1st and 2nd generation is expected (e.g. Conroy & Spergel 2011). However, these models require that a large fraction (90–95%) of the first generation of stars needs to be lost from the cluster in order to explain the fraction of first and second generation stars, which appears to be at odds with observations of the Fornax, WLM and IKN dwarf galaxies (Larsen et al., 2012, 2014a). Recently, an alternative scenario has been proposed that does not invoke multiple star formation events within massive clusters. In this scenario, Bastian et al. (2013b) suggest that the chemically enriched material is ejected by spin stars or high mass interacting binaries, and is accreted onto circumstellar disks of pre-main-sequence low mass stars of the same generation and eventually onto the host stars themselves.

Additionally it has been suggested that the observed extended main sequence turn-offs (eMSTO) and “dual red clumps” observed in intermediate age (1–2 Gyr) SMC and LMC clusters may be the product of extended (200–500 Myr) star formation events (e.g. Mackey & Broby Nielsen 2007; Goudfrooij et al. 2009, 2011a,b; Milone et al. 2009; Rubele et al. 2013). Some studies propose a common evolution of these intermediate age clusters with GCs (e.g. Conroy & Spergel 2011). On the other hand, there are some claims for the opposite, for example Mucciarelli et al. (2008) indicated that the eMSTO of intermediate-age clusters were not related to the multiple stellar populations seen in globular clusters, due to the lack of abundance spreads between the stars of the younger clusters. Alternatively, different mechanisms have been put forward to explain such anomalies in intermediate age clusters e.g. stellar rotation (e.g. Bastian & de Mink 2009; Yang et al. 2013) or interacting binaries (e.g. Yang et al. 2011).

In a pioneering work, Peacock et al. (2013) showed that there are detectable obser-

vational signatures of multiple formation events in the unresolved spectra of massive, young extragalactic star clusters. They pointed out what perhaps is one of the cleanest signatures of multiple SF events: the combined presence of emission lines from a very recently formed population of massive stars and absorption lines from a somewhat older population. Following on the work of Peacock et al. (2013), Bastian et al. (2013c) presented a catalog containing more than 100 young (10–1000 Myr) massive (10^4 – $10^8 M_{\odot}$) clusters where they do not find evidence of any ongoing star formation within the clusters, and concluded that any extended star formation within clusters lasting for hundreds of Myr are ruled out at high significance (unless strong stellar initial mass function -IMF- variations are invoked). Their study was sensitive to $\sim 2\%$ of the current cluster mass being formed today, in other words, if these clusters were forming more than $\sim 2\%$ of their current stellar mass this would have been detected. If such extended (200 – 500 Myr) star formation events were common, the authors estimate that roughly 50% of their sample should have shown evidence for ongoing star-formation.

In Cabrera-Ziri et al. (2014), we approached the problems of the origin of multiple populations in GCs and eMSTO detected in intermediate age clusters by analysing the integrated spectrum of a young massive star cluster, looking for evidence for multiple events of star formation within this cluster. The cluster we chose for this initial study is young (~ 150 Myr), is found in the wet-merger galaxy NGC 34 and does not show any evidence for ongoing star-formation, based on the lack of optical emission lines in its spectrum (e.g. Schweizer & Seitzer, 2007; Bastian et al., 2013c). This young globular cluster commonly known as “Cluster 1” (NGC 34: S1, hereafter) has an estimated mass of about 15 – $20 \times 10^6 M_{\odot}$ (Schweizer & Seitzer, 2007), which is 3–4 times more massive than that of ω Centauri, the most massive GC in the Galaxy. The fact that NGC 34: S1 is so massive and young makes it rather suitable to probe GC formation scenarios, given that it should be able to – according to MPs formation scenarios– easily retain the ejecta of the polluter stars of the first generation, and we should be able to find evidence of a second generation of stars if a secondary burst has already taken place in the cluster.

In the rest of this section I go through the analysis and results of this work in the

following way: In §2.1.1 we present the optical spectrum of NGC 34: S1 and in §2.1.2 we introduce the fitting method and models used in the SFH analysis. The degeneracies and uncertainties in the fits are discussed in §2.1.3, and finally the discussion of these results and conclusions are presented in §2.1.4 and §2.1.5, respectively.

2.1.1 Data

In Cabrera-Ziri et al. (2014) we analysed the integrated spectrum of one of the most massive clusters in NGC 34 (Mrk 938), NGC 34: S1. The spectrum was obtained by Schweizer & Seitzer (2007) (hereafter, SS07) with the Low Dispersion Survey Spectrograph (LDSS-2) of the Baade 6.5 m telescope at Las Campanas. This spectrum has a spectral resolution of $\sim 5.3 \text{ \AA}$ at 5000 \AA , and a wavelength coverage of about $3700\text{--}6850 \text{ \AA}$ (see SS07 for more details regarding instrument settings and reduction).

We note that the spectrograph used (LDSS-2) does not have an Atmospheric Dispersion Corrector and the targets were observed with a *non-parallactic slit* at airmasses of ca 1.1–1.2 (in order to include 2 clusters at a time for each slit placing). Therefore, differential refraction might have led to wavelength-dependent light losses and the wrong continuum shape.

Since the continuum of the spectrum may not be representative of the actual flux levels, the only SFH diagnostics of the spectrum that we can use are the line-to-continuum ratios of absorption features. Therefore we normalised the continuum for our SED fitting. To obtain the continuum we ran a median filter of 100 \AA width over the cluster spectrum, masking $2,000 \text{ km/s}$ around the core of each Balmer line. For the blue end of the spectrum (wavelengths on the blue side of $H\epsilon$) the pseudo-continuum was not properly reproduced with the median filter, and a handcrafted continuum was used over this wavelength range in order to improve the continuum fit.

We tested that our results are not affected by the exact choice of the continuum normalisation method (see also §2.1.3).

Once the (pseudo)continuum was found for the cluster SED, we divided the observed

spectrum by the continuum to produce the normalised spectrum employed in our analysis and shown in Fig. 2.1.

2.1.2 DynBaS fitting

We made use of a Dynamical Basis Selection spectral fitting algorithm (DynBaS) originally developed to recover the SFH of galaxies (Magris et al., 2015). Most SED fitting algorithms, e.g. MOPED, VESPA, STECMAP, STARLIGHT, ULySS (Heavens et al., 2000; Tojeiro et al., 2007; Ocvirk et al., 2006; Cid Fernandes et al., 2005; Koleva et al., 2009), use a fixed spectral basis to fit all target spectra. Instead, in DynBaSND¹ for each target spectrum a different and dynamically selected basis of N model spectra is used to obtain an optimal fit to the target spectrum. In practice, we fit the target spectrum using all possible combinations of N model spectra and store the resulting χ^2_ν for each solution. The DynBaSND solution is then the one with the minimum χ^2_ν , subject to the condition that the weight a_i assigned to the i th spectrum in the basis obeys $a_i \geq 0$ for $i = 1, \dots, N$. As argued by Magris et al. (2015), DynBaSND for $N = 2$ and 3 provide excellent fits to the target spectra, and the residuals of the recovered physical parameters for the target galaxies are less biased than for fixed-age, rigid basis methods.

These features make DynBaS a suitable tool to analyse the integrated spectra of young clusters since their SFHs are expected to comprise just a few star formation bursts of short length (e.g. Gratton et al., 2012). This gains an edge for the study of these clusters over conventional fixed basis SED fitting codes, since the latter may introduce a great number of artificial components (i.e. ages) to the fit while exploring the vast parameter space that is the set of ages of current stellar population synthesis models. For example Cid Fernandes & González-Delgado (2010) and Dias et al. (2010) found unphysical solutions for the multiple-populations fits to young and old stellar clusters, e.g. age differences of the order of 10 Gyr within clusters. On the other hand, DynBaS will adapt to each target spectrum's peculiarities, fitting it with the best linear combination

¹DynBaSND denotes that a basis of N spectra is used in the fits.

of N components from the whole set of ages available in the models, reducing the number of artificial components and simplifying the analysis.

2.1.2.1 Star Formation History

We used Bruzual & Charlot 2003 (hereafter BC03) stellar population synthesis models for the SED fitting, assuming a Chabrier (2003) IMF, computed using “Padova 1994” evolutionary tracks (Alongi et al., 1993; Bressan et al., 1993; Fagotto et al., 1994a,b; Girardi et al., 1996) and the stellar library STELIB (Le Borgne et al., 2003). We normalised the continuum for each SSP comprised in the models, using again a median filter with the same width and mask that we used for the observed spectrum, but on the blue end we fit a cubic spline between the pseudo-continuum between the Balmer lines. Finally, we divided each SED by its respective continuum.

For the fits we used the entire range of ages contained in the models, ranging from 10^5 to 2×10^{10} yr. The fits were performed between 3815–5500 Å, comprising the region most sensitive to age in the optical spectra (Schweizer & Seitzer, 1998), including most Balmer lines and some important metal indices (e.g. Fe5015, Fe5270, Fe5335 and Mgb) for metallicity estimation. For the fits we masked the CaII K line, since it might be contaminated by interstellar absorption within NGC 34 (SS07).

The cluster velocity dispersion was treated as a free parameter during the fits, as a means to emulate the true dispersion and as a correction factor to downgrade the resolution of the models to match the resolution of the data.

We estimated the S/N of the NGC 34: S1 spectrum to be 48 between 5000-5800 Å and we assumed it to be constant over the entire spectrum. Since we did not have a proper error spectrum for the fits, we used the observed flux divided by the S/N of our data as the error spectrum. Because the error spectrum is not real, the χ_ν^2 are not genuine either but they are comparable between different solutions that used the same error spectrum.

The χ_ν^2 obtained in our DynBaS1D fit was 1.27. For comparison reasons, we lowered the S/N estimated before dividing it by the value of our χ_ν ($\sqrt{1.27}$), then we calcu-

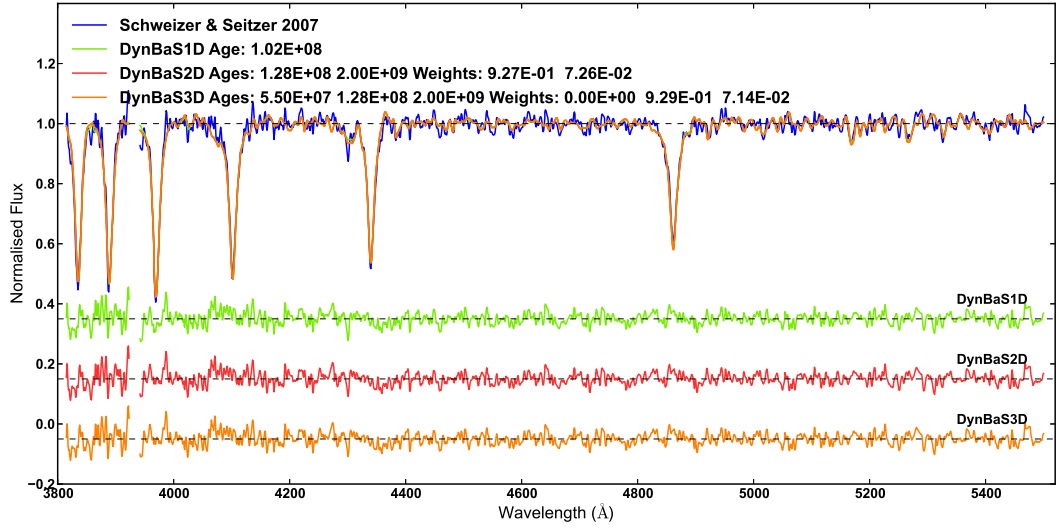


Figure 2.1: DynBaS1D, DynBaS2D and DynBaS3D fits to the continuum-normalised spectrum of NGC 34: S1. The DynBaS fits presented here were obtained using BC03 models of solar metallicity. On the bottom we plot the residuals (data - DynBaS fits) in the same vertical scale with 3 different offsets for clarity. The three solutions provide virtually the same SED. Note that the CaII K (3933 Å) line has been masked for the fit.

lated a new error spectrum for this value. This resulted in a value of $\chi^2_\nu = 1$ for our DynBaS1D solution using the new error spectrum, and made χ^2_ν values from the grids in §2.1.3 easier to compare with DynBaS results.

Figure 2.1 shows the DynBaS1D, DynBaS2D, and DynBaS3D fits to our NGC 34: S1 SED. DynBaS1D yields an age of 100 Myr. For DynBaS2D we find ages of 130 Myr (quite similar to DynBaS1D solution) and 2 Gyr, corresponding to 93% and 7% of the total mass of the cluster, respectively. Finally, the 3-component fit DynBaS3D yields ages of 55 Myr, 130 Myr and 2 Gyr for stellar populations containing <0.01%, 93% and 7% of the cluster mass, respectively.

As can be seen in the residuals plotted at the bottom of Fig. 2.1, the differences between the three fits are very small, and in principle each is as valid as the others. However, we can rule out the multiple population solutions (DynBaS2D and DynBaS3D) given the lack of physical meaning of the results. For example, we note that “very old” (>1 Gyr) populations in these clusters are not expected to exist, and it would imply that a low-mass cluster existed for more than a Gyr before a second generation formed within the cluster, with ~ 13 times the mass of the initial population.

In §2.1.3 we place more constraints on the multiple population solutions and estimate the uncertainties in our age determination.

2.1.2.2 Metallicity and Mass

In a previous work, SS07 estimated that NGC 34: S1 has an age of 150 ± 20 Myr and solar metallicity through the analysis of Lick line indices. Here we made various fits assuming metallicities of $Z = 0.4, 1$ and $2.5Z_{\odot}$ ($[Z] = -0.4, 0$ and 0.4) for the models, and we found that the best fits to spectra (specifically, the 5100–5400 Å region which hosts a number of important metallicity indicators, including Mgb, Fe5270, Fe5335 – González, 1993) were with the Z_{\odot} templates (values reported in §2.1.2.1). Given this result, we restrict ourselves to the Z_{\odot} models for the rest of the analysis.

The mass was estimated in the standard way, through a comparison between the observed cluster luminosity (corrected for distance and extinction) and predictions of SSP models for the corresponding age (which assume a metallicity and stellar initial mass function). We adopt the photometry of SS07 ($V=19.38$), an extinction of $A_V = 0.1$, and a distance of 85.2 Mpc, to derive an absolute V-band magnitude of $M_V = -15.36$ for this cluster. Comparing this to predictions from the BC03 models for solar metallicity, and an age of 100 Myr (adopting a Chabrier 2003 IMF) we estimate the mass of NGC 34: S1 to be $1.9 \times 10^7 M_{\odot}$. An uncertainty of 10% on the distance leads to an uncertainty of 20% on the estimated mass. Uncertainties related to adopting specific SSP models are also at the 20 – 30% level.

2.1.3 Degeneracies and Uncertainties

To assess possible degeneracies in our results (i.e. if other combinations of multiple populations reproduce the NGC 34: S1 SED equally well as our best solution) we performed theoretical experiments over grids of synthetic multiple-population clusters.

The grids were made up of synthetic cluster spectra for two events of star formation. These spectra were built using the same BC03 models we used for our DynBaS fits.

Each grid consisted of synthetic clusters with the same older population (Pop. 1 from here on) and different younger populations (Pop. 2). The masses of Pop. 2 could take values ranging from 10% to 90% of the mass of Pop. 1, and for the second population we allowed ages between 1 and 100 Myr distributed almost uniformly in log space. For Pop. 1 we used a wide extent of ages with very high resolution in age, creating a finely sampled parameter space (namely 140, 200, 290, 400, 510, 570, 720, 810 and 900 Myr).

We then applied to each synthetic cluster SED a Gaussian filter with the same velocity dispersion that DynBaS had recovered in the Z_{\odot} fit. Then for each element (synthetic 2-population cluster) of every grid we compared it with the spectrum of NGC 34: S1 obtaining a χ_{ν}^2 for each. The values of χ_{ν}^2 were computed using the same error spectrum we used to normalise the χ_{ν}^2 in the previous section.

Figure 2.2 presents the results of fitting NGC 34: S1 to three representative grids. In the figure we colour coded the solutions as a function of their χ_{ν}^2 . We found that for fits with $\chi_{\nu}^2 > 1.1$ it is possible to distinguish by eye that the spectral fits are poor (i.e. fail to reproduce the depths/profiles of the Balmer lines). The contours denote constant values of χ_{ν}^2 . Note how the areas with small values of χ_{ν}^2 rapidly shrink when we increase the age of Pop. 1 (areas enclosed by dark blue contours get smaller with older massive population). For grids with Pop. 1 values older than 200 Myr we can easily rule out the solutions at high significance.

We know that solutions with Pop. 2 ages younger than 10 Myr are not possible on account of the lack of emission lines produced by ionised gas. Such line emission can be detected down to limits of $\sim 2\%$ of the Pop. 1 mass (Bastian et al., 2013c). Hence, we can reject all solutions with these ages. As Fig. 2.2 shows, the “good fits” are only for massive and older Pop. 2 ages (Pop. 2 \simeq Pop 1.) or very young Pop. 2 and with small mass ratios ($M_2 \ll M_1$) when we increase the age of the main population Pop. 1.

We also carried out an additional experiment with a grid containing a Pop. 1 of 100 Myr (massive), but for this grid we allowed the Pop. 2 (less massive) ages to reach

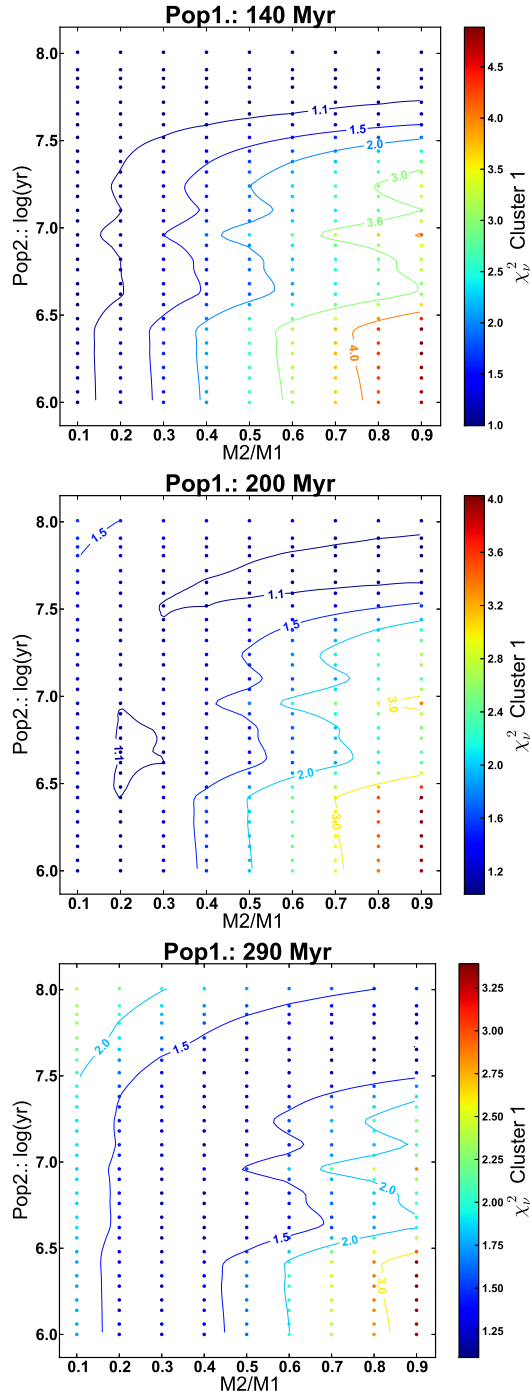


Figure 2.2: Results of fitting the normalised spectrum of NGC 34: S1 with each element of three representative grids of synthetic cluster spectra. The Pop. 1 ages are (from top to bottom) 140, 200, and 290 Myr. The vertical axis represents the age of the secondary (less massive) population, while the horizontal axis denotes the mass ratio between the first (older and more massive) and second population. Note that the χ^2_{ν} range changes for every panel, hence the colour coding does not represent the same values in different panels. For $\chi^2_{\nu} > 1.1$ we can spot the differences by eye between the synthetic clusters and the data, so those solutions are immediately excluded.

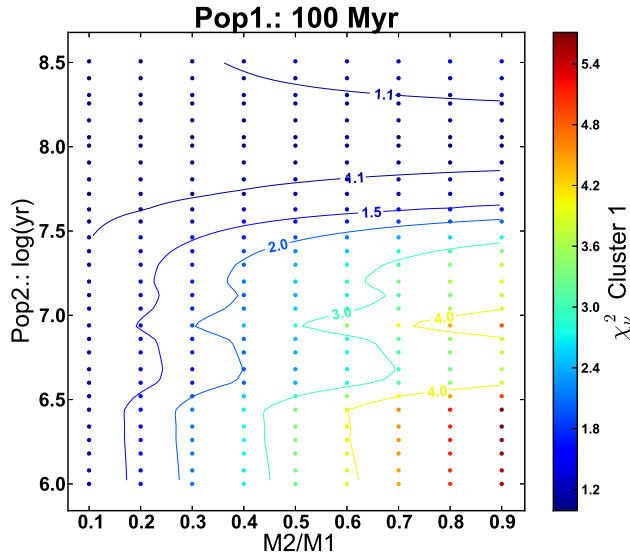


Figure 2.3: Results of fitting the normalised spectrum of NGC 34: S1 with each element of the 100 Myr extended grid. This grid shows that the solutions are consistent with the DynBaSID results (i.e. an SSP of ~ 100 Myr).

~ 300 Myr (i.e. to exceed the age of Pop. 1), with the results shown in Fig. 2.3. In this figure we can see a tendency where the best solution (fits) is the 100 Myr SSP (row with Pop. 2 $\log(\text{yr}) = 8.0$) with the quality of the fits (hence the likelihood of the solutions) gradually degrading in the direction of old massive Pop. 2, or young and less massive ones. With a main population of 100 Myr, the spectrum does not change significantly when adding a small amount of mass in a secondary population with older/younger ages, or a large amount of mass with an age close to 100 Myr. From Figs. 2.2 & 2.3 we can see that there are regions of parameter space where a second generation could be hidden (i.e. regions with $\chi^2_{\nu} < 1.1$). By looking at other young massive clusters with ages between 12 and 500 Myr, we should be able to sample all of these regions, and reduce degeneracies (e.g. Cabrera-Ziri et al., 2016a).

We emphasize that while experimenting with different ways to define the continuum in our data and models, defining different wavelength ranges for the fits, and assuming different S/N for the data *we always found that one-population solutions performed better than multiple-population solutions*. Almost all of these solutions lay within 10% of the reported age (100 Myr). We found the same behaviour (SSP solutions) when we performed the same trials with different metallicities.

2.1.4 Discussion

The tests performed (shown in Figs. 2.2 & 2.3) show that it is possible to construct a spectrum similar to that of NGC 34: S1 by combining SSP models of specific ages and mass fractions. However, we note that the DynBaS1D solution (i.e. single age model) to the observed spectra is preferred to the multiple generation model spectra. We use Fig. 2.3 to estimate an error for DynBaS1D solution of 30 Myr i.e. an age for NGC 34: S1 of 100 ± 30 Myr and a mass of $1.9 \pm 0.4 \times 10^7 M_{\odot}$. As an exploratory theoretical experiment, we also performed DynBaS fitting to artificial clusters with multiple star formation events. In these experiments, we were able to retrieve the extended star formation histories with DynBaS2D and DynBaS3D while the DynBaS1D solutions did not produce satisfactory fits. From this we conclude that if multiple populations like the ones of our grids were actually present in this cluster, we would have been able to recover them with DynBaS.

2.1.5 Conclusions from Cabrera-Ziri et al. (2014)

By fitting the normalised spectrum of NGC 34: S1 in NGC 34 with model SSP spectra, we have determined an age of 100 ± 30 Myr for the cluster and estimated a mass of $1.9 \pm 0.4 \times 10^7 M_{\odot}$, based on published photometry and SSP models for this age. We do not find evidence for multiple star formation episodes, and we can confidently rule out the presence of a 2nd generation of stars for ages outside the range from 70 to 130 Myr with mass ratios between the second and first generation greater than 0.1. These results are consistent with GC formation scenarios where multiple generations of stars are separated by < 30 Myr in age (e.g. Decressin et al., 2009; de Mink et al., 2009) or scenarios that do not invoke multiple star forming events (Bastian et al., 2013b).

Our results do not support any GC formation scenarios that involve multiple generations of stars separated by > 30 Myr in age. However, it is still possible that a secondary burst might happen in the future (i.e. with an age difference between the first and second generation of stars that is greater than 100 Myr). To improve our un-

derstanding of how GCs form, further spectroscopic studies of young massive clusters covering a wide range of ages are needed.

These results are consistent with the findings of Bastian et al. (2013c), who do not find any large age spreads in young massive LMC clusters, and they also disagree with GC formation scenarios that predict extended SFHs (e.g. Conroy & Spergel, 2011; Goudfrooij et al., 2014).

Finally, we conclude that DynBaS capabilities (i.e. SED fitting of just a few ages) are ideal for the study of the integrated spectra of young clusters, given that they reduce significantly the amounts of non-genuine components (i.e. ages) compared to traditional SED fitting algorithms, consequently simplifying the analysis of the results.

2.2 Is the Escape Velocity in Star Clusters Linked to Extended Star Formation Histories?

As mentioned before, some authors have associated the inferred age spreads derived from the eMSTO of young and intermediate-age clusters with the formation of a second generation of stars in GCs. A critical premise of this scenario is that in order to sustain extended or multiple episodes of star formation a cluster needs to be able to retain stellar ejecta and/or acquire new gas, which poses limits on the escape velocities of clusters hosting eMSTO. The current escape velocities of the clusters hosting eMSTOs are modest ($3\text{--}20\text{ km s}^{-1}$, see Goudfrooij et al., 2011a), and in many cases are below those estimated for young massive clusters that do not show evidence for extended star-formation episodes lasting $> 30\text{ Myr}$ (Bastian & Silva-Villa, 2013; Longmore et al., 2014; Kruijssen, 2014).

However, Goudfrooij et al. (2011b) have suggested that the intermediate-age clusters may have lost a significant fraction of their stars since their birth, in which case their initial escape velocities would have been much higher, potentially $> 15\text{ km/s}$, which the authors claim is a limit above which clusters can retain their stellar ejecta. In this

scenario, a first generation of stars forms in a near instantaneous burst, which is then followed by a lull that lasts between a few Myr and a few hundred Myr, and then by a further Gaussian-shaped extended star formation episode that lasts a few hundred Myr. In order to have enough matter available to form the second generation of stars a large amount of material needs to be accreted from the clusters' surroundings, because the material shed by the first generation is not sufficient to form the observed numbers of second generation stars. However, we note that a plausible mechanism for this accretion has not yet been identified.

A link between the eMSTO phenomenon in intermediate-age clusters and the MPs found in GCs has been proposed, suggesting a common evolution of massive clusters independent of the environment and time of formation (e.g. Keller et al. 2011; Conroy & Spergel 2011; Goudfrooij et al. 2011a,b, 2014, hereafter G11a,b and G14). The above scenario and its link with multiple populations in GCs have been tested by searching for abundance spreads within the eMSTO clusters, which are expected to be observed if these clusters are self-enriched. However, no evidence for abundance spreads has been found in the clusters with eMSTOs (Mucciarelli et al. 2008, 2014, Mackey et al. in prep.). Hence, self-enrichment is unlikely to have happened in the eMSTO clusters, and the eMSTO phenomenon does not appear to be linked to multiple populations in GCs.

The lack of ongoing star formation within young (< 1 Gyr) massive ($> 10^4 M_{\odot}$) clusters (YMCs) and the lack of extended star formation histories (SFHs) in resolved YMCs in the LMC are seemingly at variance with the age spreads inferred from the eMSTOs (Bastian & Silva-Villa, 2013; Niederhofer et al., 2015). In addition, some post-main-sequence evolutionary phases (e.g. the subgiant branch and red clump) of eMSTO clusters appear to be incompatible with the extended SFHs inferred from the analysis of their turnoffs (Bastian & Niederhofer 2015; Li et al. 2014; Niederhofer et al. 2016, although see Goudfrooij et al. 2015). This may indicate that alternative explanations are needed for these phenomena such as stellar evolutionary effects, e.g. stellar rotation, as has been suggested and explored by Bastian & de Mink (2009), Li et al. (2014) and Brandt & Huang (2015b).

In two recent studies of the resolved stellar populations in the young (~ 300 Myr) massive ($\sim 10^5 M_{\odot}$) LMC cluster NGC 1856 (Milone et al., 2015; Correnti et al., 2015), the authors found evidence for an eMSTO at young ages for the first time. Although these authors suggest a prolonged star-formation episode as the origin of the eMSTO, further analyses of post-main-sequence stars are necessary to see whether they are in agreement with this interpretation. However, note that the proposed duration of the secondary star-formation episode is significantly shorter than that inferred for the 1–2 Gyr old clusters (i.e. ~ 100 Myr vs. ~ 400 Myr). Niederhofer et al. (2016) have shown that there is a strong relation between the age of the cluster and the inferred age spread, suggesting that stellar evolutionary effects are the cause of the eMSTO phenomenon.

It has been suggested that the intermediate-age (1–2 Gyr) cluster population found in the LMC/SMC arose after these galaxies underwent a strong starburst during this epoch due to a three-body interaction with the Milky Way (G14). However, estimates of the SFH for both galaxies do not show clear evidence for such a burst, as the star-formation rate seems to be constant during this period within a factor of ~ 2 , cf. Harris & Zaritsky (2009); Weisz et al. (2013). The scenarios that propose extended star formation episodes as the origin of the eMSTO, also suggest that massive intermediate-age clusters, due to their large initial gravitational potential wells, were capable of retaining (and accreting) gas from which a second stellar generation was formed. Accordingly, one should see—in young massive clusters with escape velocities in excess of ~ 15 km s $^{-1}$ —clear signatures of younger generations of stars that formed after the initial, main burst in their integrated colours and SEDs. In Cabrera-Ziri et al. (2016a), we addressed the issue of the origin of the eMSTO of intermediate-age clusters by analysing the SED of W3, a YMC in the merger remnant NGC 7252 that has an escape velocity in excess of 193 km s $^{-1}$.

The cluster NGC 7252: W3 is an excellent candidate to test these scenarios given that with a mass of $\sim 10^8 M_{\odot}$ (Schweizer & Seitzer, 1998; Maraston et al., 2004) it is the most massive young cluster known to date. The age of W3 is constrained by optical photometry and spectroscopy (e.g. Schweizer & Seitzer, 1998; Maraston et al., 2001,

2004), as well as numerical simulations of NGC 7252, which suggest that its last major merger event took place about 600 Myr ago (Hibbard & Mihos, 1995; Chien & Barnes, 2010). This event has been proposed to trigger the star formation episode that gave birth to the YMC population observed in NGC 7252 (Whitmore et al., 1993; Miller et al., 1997; Schweizer & Seitzer, 1998). The age of ~ 600 Myr for W3, places it right in the range when the extended star-formation episode should be going on (or just have ceased), according to the SFHs inferred for eMSTO clusters by G14. All this makes this cluster ideal to test whether the eMSTO of intermediate-age clusters has its origin in extended periods of star formation.

In this section I will explain the analysis undertaken in Cabrera-Ziri et al. (2016a) and the relevant conclusions. In §2.2.1 we present the *HST* photometry and the MagE spectrum of W3. In §2.2.2 we show the procedure used to estimate the age, mass and escape velocity of W3. The experiments with synthetic SEDs are described in §2.2.3. Finally, we discuss our results and present our conclusions in §2.2.4 and §2.2.5, respectively.

2.2.1 Data

We took the WFC3 photometry of W3 from Bastian et al. (2013a) (bands $F336W$, $F475W$ and $F775W$).² Additionally, we performed aperture photometry on WFPC2 images taken with the filters $F336W$, $F439W$, $F555W$ and $F814W$.³ The *HST* pipeline processed images were first cleaned of cosmic rays by using the LACOS IRAF⁴ routine (van Dokkum, 2001), and then we performed aperture photometry with the task PHOT from DAOPHOT under IRAF adopting the same aperture sizes as Bastian et al. (2013a), i.e. a circular aperture with 0.4 arcsec radius centred on W3 and a sky annulus of inner radius 1.325 arcsec with a width of 0.25 arcsec. The results of our photometry on the WFPC2 images can be found in Table 2.1.

²*HST* programme GO-11554 (PI: Bastian; see Bastian et al. 2013a)

³*HST* programme GO-5416 (PI: Whitmore; see Miller et al. 1997).

⁴ IRAF is distributed by the National Optical Astronomy Observatories, which is operated by the Association of Universities for Research in Astronomy, Inc., under cooperative agreement with the National Science Foundation.

Table 2.1: WFPC2 photometry of NGC 7252: W3.

$F336W$ (mag)	$F439W$ (mag)	$F555W$ (mag)	$F814W$ (mag)
18.64 ± 0.06	18.41 ± 0.02	18.19 ± 0.13	17.36 ± 0.06

A spectrum of this cluster was obtained on Aug 23rd of 2009 with the MagE echellette spectrograph (Marshall et al., 2008) on the Clay 6.5-m telescope at Las Campanas. The $10 \text{ arcsec} \times 0.7 \text{ arcsec}$ slit was placed across the cluster at parallactic angle. The 2.3 hr total exposure was broken into seven 20 minute subexposures, during which the airmass decreased from 1.49 to 1.04 and the seeing was $\sim 0.7 \text{ arcsec}$. To permit flux calibration, six standard stars were also observed at parallactic angle throughout the night.

The reduction of the MagE spectrum included pipeline processing to flat-field and coadd frames, rectify spectral orders, calibrate wavelengths, and subtract the galaxy-plus-sky background spectrum. The final extracted spectrum of W3 covers the wavelength range $3300\text{--}8250 \text{ \AA}$, extracted from orders $18\text{--}8$, at a spectral resolution of $R \approx 5500$. Due to small wiggles in the spectral continuum introduced by the digital splicing together of the various overlapping orders, we here restrict our use of the spectrum to its highest-quality range of $3300\text{--}5500 \text{ \AA}$. However, the overall SED of W3 is a good representation of the actual flux levels of this cluster, as we will show via the good agreement with *HST* photometry in §2.2.3 (see below).

2.2.2 Age and mass of NGC 7252: W3

We used DynBaS, a Dynamical Basis Selection spectral fitting algorithm (Cabrera-Ziri et al., 2014; Magris et al., 2015) to recover the SFH of W3. Basically, the DynBaS algorithm finds the best simple stellar population (SSP) template or the best linear combination of two or three SSPs templates to fit the target spectrum (with their relative weights/masses, as discussed in the previous section). Here, we outline briefly the basics of our spectral fitting of W3 and refer the reader interested in a more detailed

Table 2.2: Results of DynBaS fitting: Ages and masses of each of the fit components, mass weighted ages, and total masses.

Fit	Solution	t_1/M_1 (Myr / %)	t_2/M_2 (Myr / %)	t_3/M_3 (Myr / %)	$\langle t \rangle_M^{(a)}$ (Myr)	M_{tot} (M_\odot)
<i>HST</i> photometry	DynBaS1D	509 / 100			509	1.00×10^8
	DynBaS2D	453 / 4.3	509 / 95.7		506	9.9×10^7
	DynBaS3D	453 / 65.3	719 / 14.4	5,750 / 20.3	815	1.19×10^8
MagE spectrum	DynBaS1D	571 / 100			571	9.9×10^7
	DynBaS2D	404 / 9.4	13,750 / 90.6		9,883	6.10×10^8
	DynBaS3D	360 / 2.6	404 / 6.2	13,750 / 91.2	10,057	6.24×10^8
MagE normalized spectrum ^(b)	DynBaS1D	571 / 100			571	-
	DynBaS2D	508 / 94.2	8,500 / 5.8		619	-
	DynBaS3D	508 / 93	1,700 / 2.6	8,500 / 4.4	589	-

^(a) $\langle t \rangle_M = 10 \sum_i \mu_i \log t_i$, with $\mu_i = M_i / \sum_i M_i$

^(b) Since there was no continuum in this spectrum we are not able to retrieve masses.

discussion of the limitations and uncertainties of our technique to the publications cited above.

We performed three different fits to W3 data:

1. ***HST* broad band photometry:** This was a full SED fit using the *HST*'s WFPC2 and WPC3 photometry described in §2.2.1 and assuming an $A_V = 0.083$ mag,⁵ and a distance to NGC 7252 of 64 Mpc (Bastian et al., 2013a). The results of all fits are presented in Table 2.2.⁶
2. **MagE spectrum:** This was also a full SED fit, using this time the flux-calibrated MagE spectrum instead of the *HST* photometry, and assuming the same A_V and distance as above. The results of these fits are shown in Fig. 2.4. From this figure, we can see that there is a slight offset between the SED and the synthetic stellar populations fitted by DynBaS. In order to determine whether these observed differences are due to the issues on the continuum calibration mentioned in §2.2.1, we decided to carry out an additional fit after normalizing the continuum, in order to assess the robustness of our age determination.

⁵this value was derived from the $A_{F475W} = 0.098$ reported in Bastian et al. (2013a) and assuming $A_g = 3.64 E_{(B-V)}$ from Jordán et al. (2004).

⁶We also carried out the fit including the K_s photometry from Maraston et al. (2001) and find that the results are unaffected.

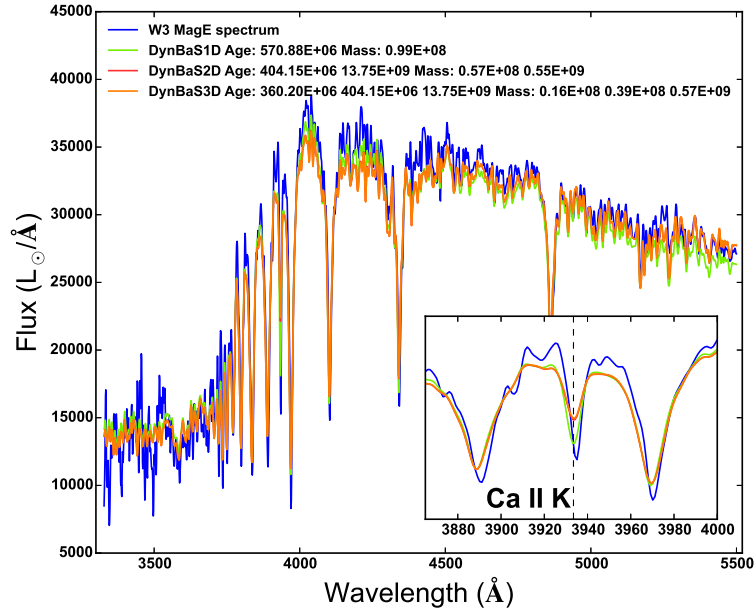


Figure 2.4: DynBaS1D, DynBaS2D and DynBaS3D fits (see the text) to the MagE spectrum of Cluster W3. The DynBaS fits presented here were obtained using stellar population models of solar metallicity. See text for a discussion of these results.

3. **MagE continuum-normalized spectrum:** We normalized the continuum of W3’s SED for our fitting. To obtain the continuum we ran a median filter of 100 \AA width over the cluster spectrum, masking 2000 km s^{-1} around the core of each Balmer line. Then we normalized the continuum for each SSP spectrum comprised in the Bruzual & Charlot (2003) models, using again a median filter with the same width and mask as we used for the observed spectrum. Next, we divided each model SED by its respective continuum. The spectral fit was then carried out on the normalized spectrum of W3 with the normalized SSP model spectra. The results of these fits are shown in Fig. 2.5.

Table 2.2 shows that all DynBaS1D solutions (i.e. best-fitting SSPs) are rather precise, i.e. in agreement within $\sim 60 \text{ Myr}$ of each other. Both fits of the MagE spectrum (unnormalized and normalized) yield a cluster age of 571 Myr , while the fit to the *HST* broad-band photometry yields a somewhat younger age of 509 Myr .

For both the photometry and the MagE spectrum fits, we see that the *multiple-population* solutions (i.e. DynBaS2D and DynBaS3D) consist of a young population relatively

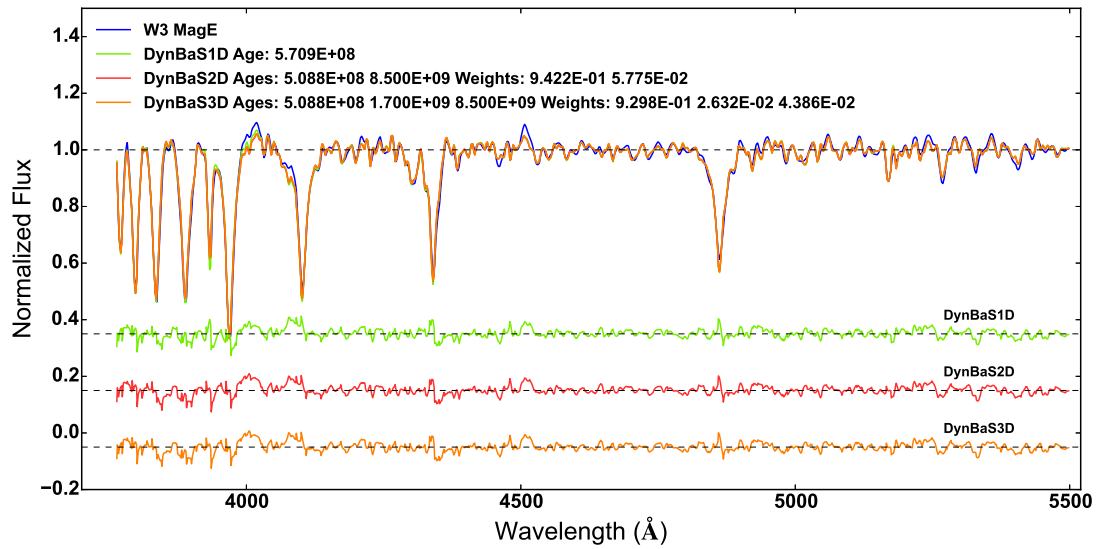


Figure 2.5: DynBaS1D, DynBaS2D and DynBaS3D fits to the continuum-normalised spectrum of W3. The DynBaS fits presented here were obtained using BC03 models of solar metallicity. On the bottom we plot the residuals (data - DynBaS fits) in the same vertical scale with 3 different offsets for clarity. The three solutions provide virtually the same spectrum. We can rule out the DynBaS2D and DynBaS3D solutions using the same arguments that were used for NGG 34: S1, see text for details.

close in age to the SSP solution, i.e. about 500 Myr, and an old (> 5 Gyr) population with a significant fraction of the total mass. The origin of these old components in the DynBaS fits is simple. Basically, they come from the fact that the mass-luminosity ratio increases with time for an SSP evolving passively, i.e. without any subsequent star formation events. This is shown in Fig. 2.6, where we plot the evolution of an SSP for a fixed mass. As the figure shows, the old (> 5 Gyr) populations are at least an order of magnitude fainter than a population of the same mass but younger age (i.e. few hundred Myr). Due to this, it is possible to allocate considerable important fractions of the mass into these old components during the fits, without affecting the overall SED of the younger populations in a significant way. In other words, if any component of the fit is attributed to an old population, due to the high mass to light ratio, it will necessarily be given a high mass.

However, although the overall multiple-population SED might appear to be in good agreement with the SED of the W3 and/or the SSP solution, we emphasize that the solutions with significant fractions of older components do not accurately reproduce

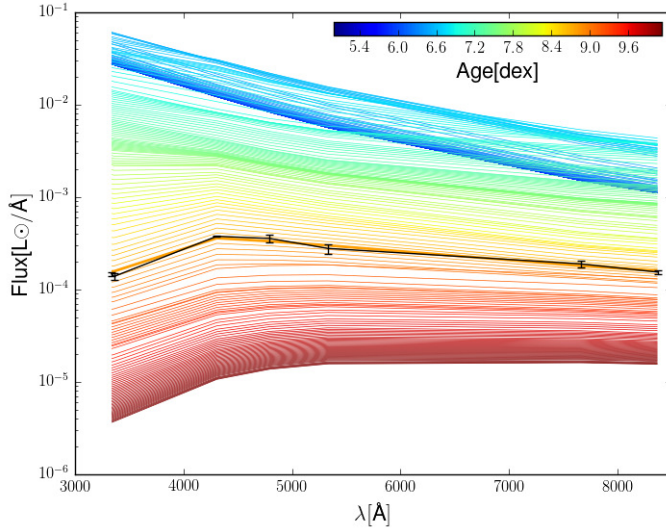


Figure 2.6: SED evolution of an SSP of Z_{\odot} over the *HST* filters mentioned in §2.2.1. The thick orange line represents the SSP age determined by the DynBaS continuum normalized fit (570 Myr). The black line represents the *HST* photometry of W3. We have scaled the stellar population templates to match the SED of W3 at 570 Myr. From this we infer a mass of $1.13 \times 10^8 M_{\odot}$ for W3. All SSP templates have been attenuated to the same extinction as reported for W3.

the Ca II K line, a spectral feature that is highly age sensitive (cf. Fig. 2.4, more on this in §2.2.4).

As was also found for the YMC NGC 34: S1 in Cabrera-Ziri et al. (2014), the multiple stellar-population solutions from the continuum-normalized spectral fit require a very old and low-mass burst to have happened ~ 8.5 Gyr ago, after which the cluster suffered a huge burst of 13–15 times the mass of the old population at a young (~ 500 Myr) age. These kinds of solutions would appear to be rather exotic, as discussed in Cabrera-Ziri et al. (2014). Very old populations arise when the code is forced to retrieve a multiple stellar-population solution, as they artificially improve the residuals between the observed spectrum and the stellar population templates on a very small level (i.e. less than tenths of reduced χ^2).

We carried out fits to the continuum-normalized spectrum of W3 using Bruzual & Charlot (2003) models with metallicities of $Z = 0.4, 1$ and $2.5 Z_{\odot}$ ($[Z] = -0.4, 0$ and 0.4), and we found that the best fits to the spectrum (specifically, the 5100–5400 Å region which hosts a number of important metallicity indicators, including Mgb, Fe5270, Fe5335; González 1993) were with the Z_{\odot} templates, as also found by Schweizer & Seitzer (1998).

Given that the DynBaS SSP solution for the continuum-normalized spectrum yields the most accurate fit of all our experiments, we adopt this solution, 570 Myr, as the age

of W3. Having derived the age, we are able to infer the cluster mass, scaling the SSP of 570 Myr to the *HST* photometry (corrected for extinction and distance). The match between W3 photometry and the SSP template of 570 Myr is also shown in Fig. 2.6. Additionally, we use this figure to make a conservative estimate of the uncertainties in age/mass. We adopt as uncertainties the values of the youngest/oldest SSP ages that lie within the photometric error bars. This yields an age for W3 of 570_{-62}^{+70} Myr and a mass of $1.13_{-0.13}^{+0.14} \times 10^8 M_{\odot}$ (we discuss the possible degeneracies of our age determination, in Appendix A).

These results are consistent with those from previous studies of this cluster. For example, Schweizer & Seitzer (1998) found an age of ~ 540 Myr and a mass of $1.8 \times 10^8 M_{\odot}$, a similar analysis by Maraston et al. (2001) found an age of 510 ± 10 Myr while Maraston et al. (2004) estimated the dynamical mass of W3 to be $8 \pm 2 \times 10^7 M_{\odot}$.

2.2.2.1 Escape velocity of NGC 7252: W3

We use equation (1) from Georgiev et al. (2009):

$$v_{esc} = f_c \sqrt{\frac{M_{cl}}{r_{eff}}} \text{ (km s}^{-1}\text{)},$$

to estimate the current escape velocity of W3. Here, f_c is a coefficient which takes into account the dependence of the escape velocity on the density profile of the cluster, i.e. its concentration $c = \log(r_t/r_c)$ where r_t and r_c are the tidal and core radius of the cluster, respectively.

Georgiev et al. (2009) computed f_c for King (1962) models by deprojecting the density profile and then calculating the potential as a function of radius. In order to estimate a lower limit to the escape velocity of this cluster, we adopted the smallest value for f_c reported by these authors in their Table 2, i.e. 0.076. We adopt an effective radius $r_{eff} = 17.5$ pc (Maraston et al., 2004) and a cluster mass $M_{cl} = 1.13 \times 10^8 M_{\odot}$ as determined above. With these values, we get $v_{esc} = 193 \text{ km s}^{-1}$ for W3, well above the $\sim 15 \text{ km s}^{-1}$ limit proposed by G11b as the threshold for any extended star-

formation episode to happen (which would be responsible for the eMSTO observed in intermediate-age clusters).

We emphasize that this value represents a lower limit as f_c is likely higher for this cluster. According to Bastian et al. (2013a) the tidal radius is $r_t > 500$ pc for W3. From Table 1 in G14, we derive that the mean value of $\langle r_c/r_{\text{eff}} \rangle = 0.67$. Assuming that the core radius is $r_c \approx 0.67 \times r_{\text{eff}}$, this leads to $\log(r_t/r_c) = 1.63$, which would correspond to a $f_c = 0.1$, leading to a much larger $v_{\text{esc}} = 254 \text{ km s}^{-1}$ for W3.

2.2.3 Synthetic SED experiments

Having determined that the SFH of W3 is consistent with an SSP of 570 Myr, in this section we test how the SEDs built by using the SFHs of eMSTO clusters inferred by G14 compare to the observed SED of W3. With these experiments, we explore whether the inferred SFHs from eMSTO clusters are also compatible with the SED of this cluster, which satisfies all the characteristics of an eMSTO cluster of this age (~ 600 Myr), namely:

1. It has the age when a second episode of star formation is expected to have happened recently or be happening.
2. Currently it has an escape velocity well above the threshold suggested by G11b as being necessary to retain/accrete gas from which the second stellar generation will form.

This makes W3 suitable to undergo, or have recently undergone, the extended star-formation episode responsible for eMSTOs according to some authors (e.g. G14 and Correnti et al. 2015).

All the synthetic SEDs in this section and the previous one (i.e. SED fitting) were built by using Bruzual & Charlot (2003) stellar-population models of Z_{\odot} , assuming a Chabrier (2003) IMF, and computing models with ‘Padova 1994’ evolutionary tracks (Alongi et al., 1993; Bressan et al., 1993; Fagotto et al., 1994a,b; Girardi et al., 1996)

and the stellar library STELIB (Le Borgne et al., 2003). All synthetic SEDs were attenuated with the extinction value reported for W3, $A_V = 0.083$ mag, by using a Cardelli et al. (1989) extinction law and $R_V = 3.1$.

2.2.3.1 Experiments with Goudfrooij et al. (2014) SFHs

G14 analyse the eMSTOs of 18 intermediate-age clusters in the Magellanic Clouds, and report SFHs for all clusters that consist of a first, instantaneous massive burst followed by an extended period of star formation, equivalent to a small fraction of the mass of the first burst.

We would like to emphasize that the SFHs directly inferred from the eMSTO (referred by these authors as pseudo-age distributions) have little evidence of a large initial burst. From Figs. 2, 3 and 4 of G14, we see that only an extended episode of star formation is found which can be represented reasonably well by a Gaussian distribution with a FWHM of ~ 375 Myr for most clusters. However, without an initial burst this would represent a problem regarding the build up of the mass of this extended star formation episode. This is because if there is no first generation, there would not be a potential well that could accrete and retain the gas from which the next generation of stars are going to be born (i.e. it would take hundreds of Myr for the clusters to build up enough mass to exceed the suggested limit of 15 km s^{-1} escape velocity). In G14 they solve this problem invoking a first generation of stars which will be lost nearly entirely after the second episode of star formation takes place. By doing this they are able to build up such extended star formation episode and simultaneously match the inferred pseudo-age distributions from the eMSTO with no signs of an older and massive population.

For the present experiments, we have built the SEDs of synthetic clusters according to the same kind of star-formation episodes, i.e. a first, instantaneous burst of star formation at 570 Myr (i.e. the age recovered by DynBaS for W3) contributing most of the mass of the cluster, followed by an extended, Gaussian-shaped star-formation episode with a fraction of the mass of the first burst. We have made a couple of conservative assumptions and choices:

1. We do not allow the final star-formation episode to extend over the last 100 Myr of the cluster life. Young populations with current ages < 100 Myr would leave a strong signature on the integrated SED of any cluster, which is clearly incompatible with our observations of W3 (cf. §2.2.4).
2. For this experiment we have restricted our second star-formation episode to a FWHM = 100 Myr. If we were to increase the FWHM of the second star-formation episode, we would increase the difference between the SEDs of the synthetic clusters and that of W3, as we would be increasing the fraction of younger populations relative to the original instantaneous burst.

The rationale behind these choices is to favour all these extended star-formation scenarios, as we are trying to minimize the differences in the SEDs between an extended star formation episode and an instantaneous burst (our best fit SFH for W3).

In G14, the authors used the results from a simulation called SG-R1 by D’Ercole et al. (2008) to describe the dynamical evolution of intermediate-age clusters.⁷ This particular simulation was chosen due to the agreement in the reproduction of the mass fractions formed during the second, extended and first, instantaneous star-formation episodes inferred by G14 from the eMSTOs of intermediate-age clusters at their current ages (i.e. mass ratio between the second and first generation stars $M_2 : M_1 \approx 2:1$ observed today, 1–2 Gyr after their birth). For our synthetic clusters we take the values for $M_2 : M_1$ from this simulation at younger ages, i.e. between $100 \lesssim t/\text{Myr} \lesssim 1000$. These range from $M_2 : M_1 = 0.3:0.7$ (at ~ 100 Myr) to $M_2 : M_1 = 0.5:0.5$ (at ~ 1 Gyr).

Figure 2.7 shows the SFHs of synthetic multiple-generation clusters for three different mass ratios. We will refer to these synthetic clusters with extended star-formation episodes hereafter as composite stellar population (CSP) clusters. The synthesised SEDs of these CSP clusters are shown in Figs. 2.8 and 2.9 together with the observed spectrum of W3.

⁷This simulation most likely is inadequate to describe intermediate-age clusters in the SMC/LMC as we discuss in §2.2.4.1.

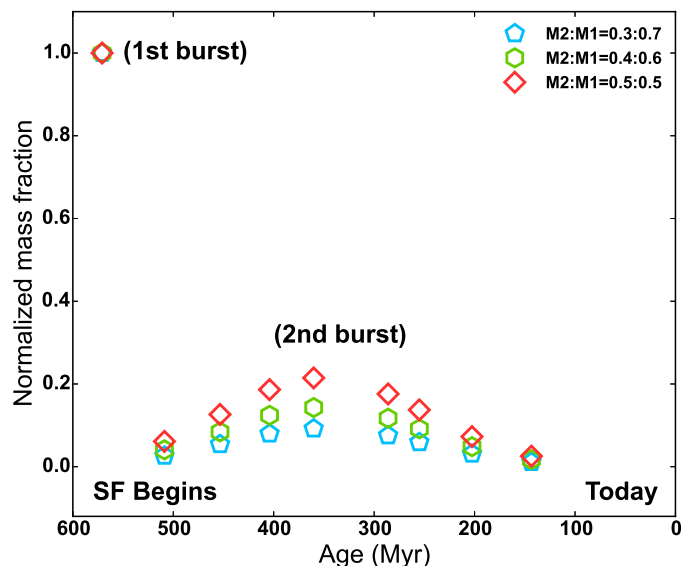


Figure 2.7: Star formation histories of three synthetic clusters. The pentagons, hexagons and diamonds represent the SFH of composite stellar population (CSP) clusters with mass ratios of $M_2 : M_1 = 0.3:0.7$, $0.4:0.6$ and $0.5:0.5$ respectively. For all CSP clusters the first star formation episode is an SSP of 570 Myr. The second episode of star formation follows a Gaussian distribution centred at 350 Myr with FWHM = 100 Myr.

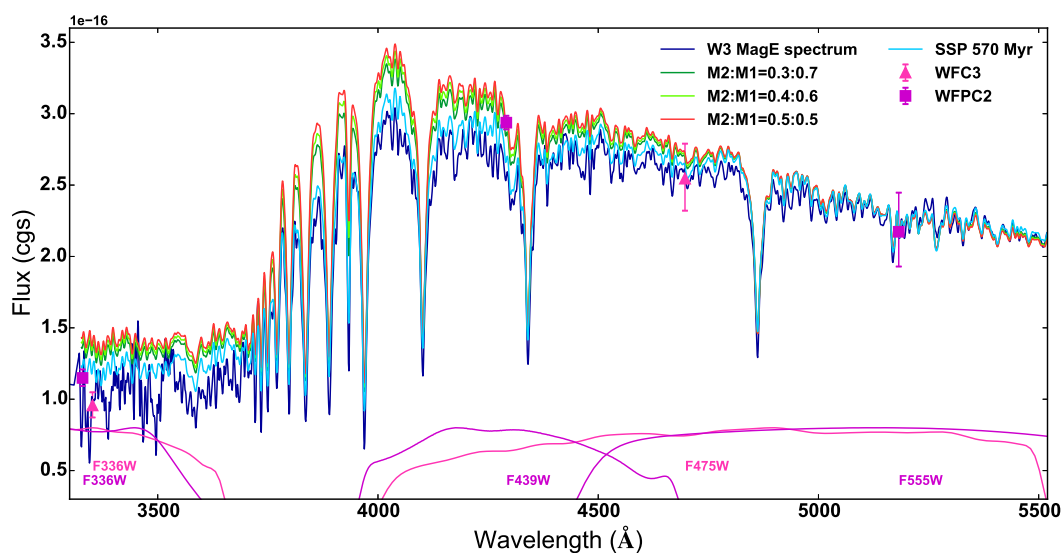


Figure 2.8: The dark blue line represents the integrated MagE spectrum of W3. *HST* WFC2 and WFC3 photometry of W3 is represented with squares and triangles, respectively. The model spectrum recovered by DynBaS for W3 is shown in cyan (SSP of age 570 Myr). Dark green, green and red lines represent the synthetic SEDs of CSP clusters with a mass ratio of $M_2 : M_1 = 0.3:0.7$, $0.4:0.6$ and $0.5:0.5$, respectively. The various SEDs are all normalized to the flux of W3 at the effective wavelength of the *F555W* filter. The transmission curves of the filters used in this work (in this wavelength range) are shown at the bottom of the figure.

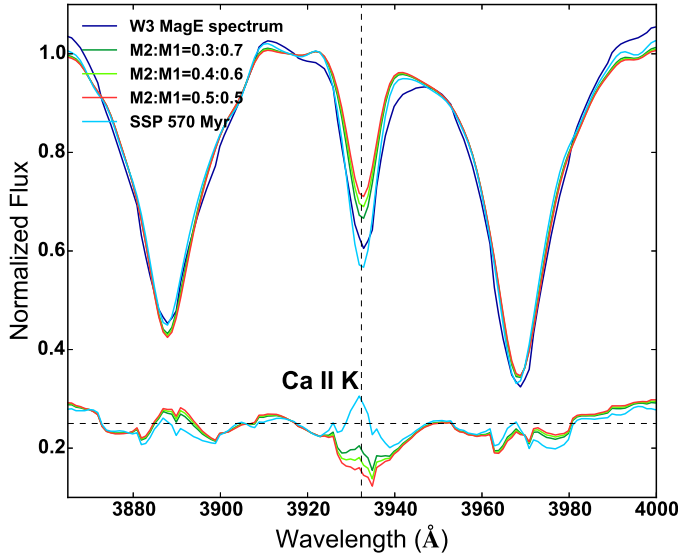


Figure 2.9: Same as Fig. 2.8, but shown as a close-up around the age-sensitive Ca II K line. For this figure the continuum of all SEDs had been normalized for a better comparison of the line profiles. All CSP synthetic clusters miss the depth and profile of this line. The DynBaS solution (570 Myr SSP) yields the best representation of this line and of the colours of W3. The bottom of the figure shows the residuals of the spectral fits.

2.2.3.2 Experiments with Goudfrooij et al. (2014) pseudo-age distributions

Although for a massive cluster of W3’s age (570 Myr) the SG-R1 simulation shows that most of the cluster mass comes from the stars of the first generation, we also explore the possibility that *this entire generation* was already lost during the early dynamical evolution of this cluster, leaving just the observed age distribution derived by G14 from the eMSTO stars.

To test this possibility, we built a second set of CSP clusters, this time following the present-day age distribution (i.e. pseudo-age distributions in G11a,b and G14). For this we assumed a simple Gaussian distribution centred at 570 Myr and with FWHM ranging from 300 to 100 Myr (cf. Fig. 2.10). The resulting SEDs are shown in Figs. 2.11 and 2.12, where they are compared directly with the observed W3 spectrum.

2.2.4 Discussion

Figure 2.8 shows a portion of the MagE spectrum of W3 together with overplotted synthetic spectra of the best SSP DynBaS solution as well as of the CSPs with SFHs shown in Fig. 2.7. For this figure, we have normalized the flux of all our synthetic cluster spectra to the observed flux of W3 at WFPC2’s $F555W$. Obviously, the MagE spectrum agrees well with the WFPC2 and WFC3 photometry (data points with error

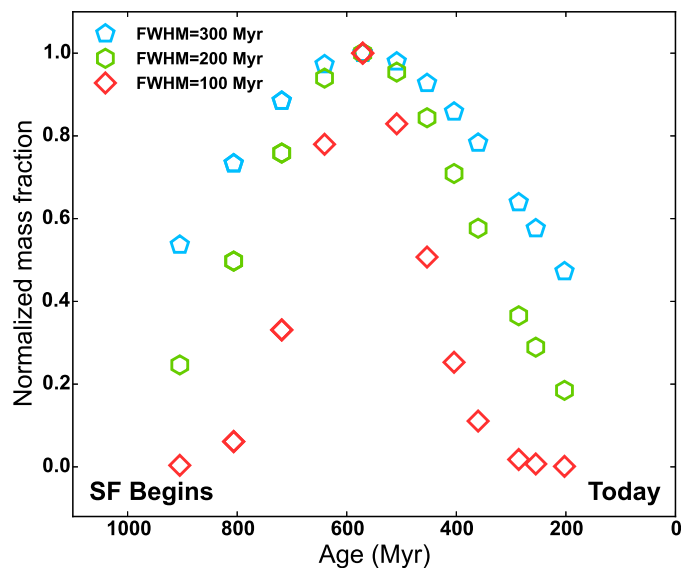


Figure 2.10: Pseudo-age distributions from G14 for three synthetic clusters. The pentagons, hexagons and diamonds represent the SFH of CSP clusters with FWHMs equal to 300, 200 and 100 Myr, respectively. All distributions are centred at an age of 570 Myr.

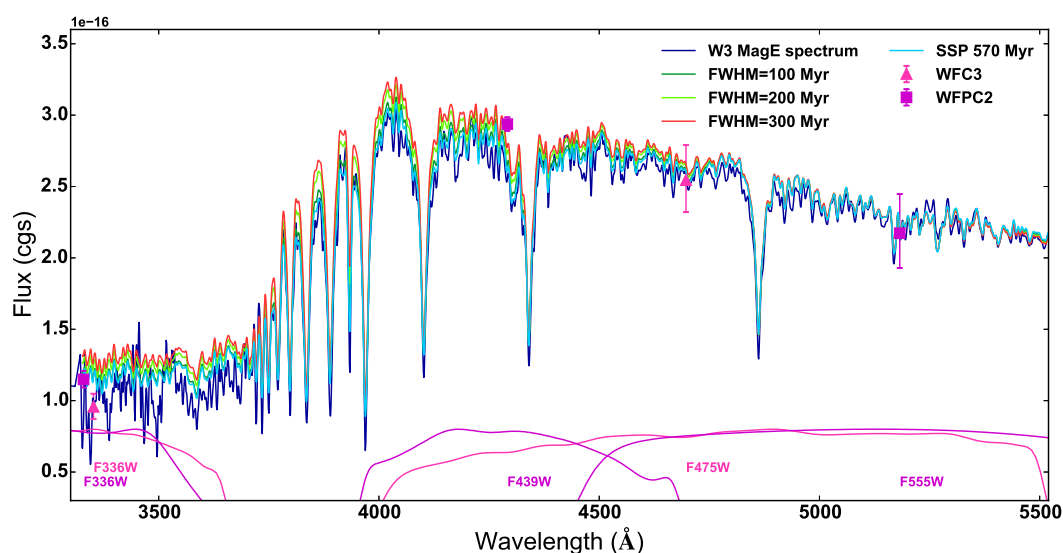


Figure 2.11: Similar to Fig. 2.8, but here we show in red, green and dark green the synthetic SEDs of CSP clusters built following the pseudo-age distributions from G14 with FWHM = 300, 200, and 100 Myr, respectively.

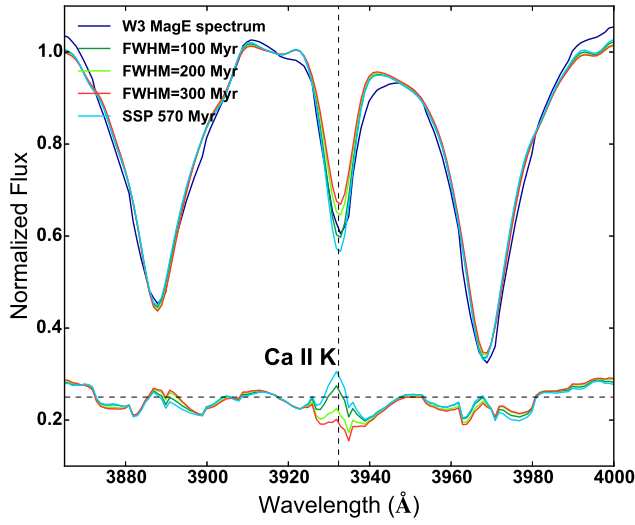


Figure 2.12: Same as Fig. 2.9, but for model CSP clusters following the pseudo-age distributions from G14. In the same way as with the predicted SFHs from G14, the DynBaS solution (570 Myr SSP) and the CSP with $\text{FWHM} \leq 100$ Myr yield the best representation of the Ca II K line of W3 when compared to the SEDs of CSP with $\text{FWHM} > 100$ Myr clusters that follow the G14 pseudo-age distributions. The bottom of the figure shows the residuals of the spectral fits.

bars). This confirms that the wiggles in flux present in the MagE spectrum are negligible compared to the overall SED. This figure shows that the DynBaS solution (570 Myr SSP) is a very good representation of the observed SED of W3, while the synthetic CSP clusters fail to reproduce the optical colours of this cluster as these CSPs are too blue ($\sim 10\%$ brighter for $3700 < \lambda/\text{\AA} < 4000$). The offsets between the DynBaS solution and the MagE spectrum presented in Fig. 2.8 are in part due to the wiggles in the continuum mentioned in §2.2.1. Once the DynBaS solution and the MagE data are both continuum-normalized, the spectra match very well as shown in Fig. 2.5.

Besides analysing the overall shape of the SED of W3 and its agreement with the SED of synthetic SSP and CSP clusters, we can also analyse the behaviour of individual spectral features that are sensitive to age. Figure 2.9 shows the same SEDs as displayed in Fig. 2.8, but now centred on a narrow region around the Ca II K line, which is very sensitive to age (for a given metallicity, this line gets deeper with age). Figure 2.9 illustrates once more how the CSP clusters fail to reproduce the observed characteristics of W3 (this time the profile of the Ca II K line), and although the SSP of 570 Myr does not reproduce perfectly the depth of this line (as it is a little bit deeper), it still does a better job than any of the CSPs. As already stated, this particular line gets deeper with age, whence even a small young component in a CSP would make this line appear significantly shallower. The differences between the W3 spectrum and the best SSP solution in the profile of this line, could be due to the finite sampling in age

of the SSP templates used for this work. If this were the case, the precise age of this cluster would be somewhere between the template of 570 Myr and the next youngest (508 Myr) one, as this spectrum will have about the same depth of the Balmer lines but the Ca II K line will be a little bit shallower than that of the 570 Myr template.

We note that the *extent* of our second episode of star formation (i.e. when the extended burst begins and ends) is limited to ~ 350 Myr (see Fig. 2.7), which is about the FWHM of the extended star-formation episode proposed to explain the eMSTOs of some intermediate-age clusters according to G11a,b and G14. If we were to consider a more extended episode of star formation (i.e. ~ 700 Myr as suggested by G14), the differences in the SEDs and the Ca II K line between W3 and the synthetic CSP clusters would become more marked due to the inclusion of even younger components to the CSP. In other words, *even with these favorable assumptions, like a short second star-formation episode (FWHM=100 Myr) and the truncation of the star formation at younger ages (no star-formation in the last 100 Myr, see Fig. 2.7), we still find considerable differences between the SEDs of a cluster with a SSP and a cluster that experienced such extended star-formation event.*

We can use the experiments with the pseudo-age distributions (§2.2.3.2 and Fig. 2.10) to place constraints on any extended SFH that may be present in W3 (i.e. the age resolution that our data offer). Extended star formation leaves a second-order imprint on a cluster's SED due to the nonlinear evolution of colour. A cluster with an extended burst of star formation centred at lookback time t will be bluer than an SSP of age t ; the effect scales as $(\Delta t/t)^2$, where Δt is the duration of star formation. Extended SFHs have been inferred from eMSTOs in the CMD, where the effect is instead first-order: the width of the MSTO increases linearly with the duration of star formation.

Figure 2.11 shows how the SEDs of synthetic clusters with the extended SFHs of Fig. 2.10 compare to the observed SED of W3. At first glance, one can see that the CSPs with the long star-formation episodes (FWHM = 200 and 300 Myr) are easily distinguished from the W3/SSP SED, since the flux in $3700 < \lambda/\text{\AA} < 4000$ is again about 10% higher than that of the W3 or SSP SEDs. But this time, the CSP cluster with the narrowest star formation episode (i.e. FWHM=100 Myr) is not very different

from the SSP or W3's SED.

If instead we focus on the Ca II K line, as shown in Fig. 2.12, we can see that the CSPs with $\text{FWHM} > 100$ Myr never reproduce the profile of this line better than the single SSP spectrum. We conclude from this that in order to produce a CSP that has an SED and shape of the Ca II K line similar to what is observed in W3, we would need to (1) decrease the contribution of the main (first) burst proposed by G14, either by reducing its mass or by reducing the period between the first and second burst to be short enough so that both bursts would be indistinguishable, and (2) reduce the extent of the second star-formation period, down to a limit where it approaches the SED of an SSP. Figure 2.12 illustrates that this would be the case for a CSP following a Gaussian distribution with a $\text{FWHM} = 100$ Myr.⁸

We note that the mean FWHM age spread claimed by G14 for a sample of 18 intermediate-age clusters is 375 Myr and the shortest FWHM is 200 Myr. These values are well above our derived limit where one could start confusing the SED of an SSP and of a brief (≤ 100 Myr) CSP event. Stellar rotation can mimic a fractional age spread of $\sim 20\%$, or ~ 100 Myr at the age of W3; Fig. 2.11 shows that W3 is perfectly consistent with such a pseudo-age spread. It is, however, strongly inconsistent with the ~ 300 – 400 Myr durations inferred from the eMSTOs in older LMC clusters.

2.2.4.1 Is the SG-R1 simulation suited to describe eMSTO clusters?

The simulation chosen by G14 to describe the dynamical evolution of intermediate-age clusters in the SMC/LMC displaying eMSTOs may not reproduce accurately their mass losses. This simulation, described in D'Ercole et al. (2008) and named SG-R1, was originally developed to study the dynamical evolution of ~ 10 Gyr old Galactic globular clusters in a strong tidal field. Due to this, there are some issues that may make it unsuitable for studies of intermediate-age SMC/LMC clusters, such as:

- The second-generation stars in this simulation have only masses between 0.1

⁸This upper limit for the extent of any prolonged star formation episode within W3 is consistent with the uncertainties/degeneracies in age estimated for this cluster cf. §2.2.2 and Appendix A.

and $0.8 M_{\odot}$. Yet, the estimated masses of stars that populate the turnoff of intermediate-age (1–2 Gyr) clusters are all $> 1 M_{\odot}$. *Hence, this simulation would not feature any stars visible today in the regions of colour–magnitude diagrams where the eMSTO is observed in intermediate-age clusters.*

- The main reason that led G14 to choose this particular simulation for describing eMSTO clusters is that the mass ratio between second- and first-generation stars yielded at the age of intermediate-age clusters is very similar to the ratio inferred from the SFH derived from the eMSTO. This ratio is $M_2 : M_1 \approx 2 : 1$ for present-day eMSTO clusters. *However, Figs. 15 and 16 of D’Ercole et al. (2008) show that one only gets this ratio for stars in the mass range $0.1 \leq M/M_{\odot} \leq 0.8$.* If one takes into account that the stars of the first generation in this simulation cover masses between 0.1 and $100 M_{\odot}$ following a standard (i.e. Kroupa) IMF, the actual mass ratio between the second- and first-generation stars decreases as there are more stars from the first generation than just the ones between $0.1 \leq M/M_{\odot} \leq 0.8$.
- The cluster in the simulation SG-R1 is tidally limited, i.e. the stars in the cluster are distributed up to the radius where a star is equally bound to the cluster and the Galaxy. This setup provides an extremely efficient way to lose stars. However, *all the intermediate-age clusters studied in G14 have tidal radii between 4.9 and 43 times larger than their core (and effective) radii according to these authors.* This fact makes mass loss in these clusters very inefficient.

To put this in context, we emphasize that the scenario of G14 requires retaining the first generation of stars (most of the cluster mass) at younger ages in order to provide enough gravitational potential to hold on to the gas expelled from evolved stars and to accrete gas from their surroundings. This gas will eventually fuel the extended (second) star-formation episode responsible for the eMSTO. Figures 2, 3 and 4 of G14 show that for these 1–2 Gyr old clusters, this second episode stopped forming stars 800–1500 Myr ago (depending on the cluster). Hence, the first-generation stars can only be lost after these ages, when they are no longer needed to hold on to the material to form the second burst. In other

words, *this implies a strong change of the tidal potential hosting each of these clusters in the last 800–1500 Myr, for which—to the best of our knowledge—there is no evidence.*

- Another critical factor is that the simulation SG-R1 assumes that the cluster is sitting in the Galactic potential tidal field, at a galactocentric distance of 4 kpc. Yet, the tidal fields of the SMC and LMC are significantly weaker than that of the Galaxy. Hence, the disruption derived from this simulation will be significantly overestimated compared to the actual one suffered by the eMSTO clusters in the SMC/LMC. We figure that this simulation could only apply to the eMSTO clusters if their densities at young ages were about two orders of magnitude lower than the densities of YMCs observed today (see Appendix B).

We conclude that the simulation SG-R1 by D’Ercole et al. (2008) is unsuitable for describing the dynamical evolution of SMC/LMC clusters with an eMSTO.

2.2.4.2 NGC 1856: a YMC with an eMSTO

The young cluster NGC 1856 represents a very interesting piece of the puzzle of the origin of the eMSTO. As mentioned before, this massive ($\sim 10^5 M_{\odot}$) young cluster with an age of ~ 300 Myr is significantly younger than any of the clusters previously reported with eMSTOs (with ages usually between 1–2 Gyr). The young age of this cluster allows us an unprecedented opportunity to understand the early evolution of a cluster with an eMSTO. In this section we combine the information derived by Milone et al. (2015); Correnti et al. (2015) from the eMSTO of NGC 1856 with previous studies of YMCs in order to place some constraints on the origin of the eMSTO.

In a previous study we analysed the YMC NGC 34: S1 (Cabrera-Ziri et al., 2014). Using DynBaS we concluded that the SFH of this cluster is consistent with an SSP of age 100 ± 30 Myr and mass $1.9 \pm 0.2 \times 10^7 M_{\odot}$. We were able to rule out any significant episode of star formation in the last 70 Myr of the cluster. G14 claim this is consistent with their scenario, as perhaps 100 Myr may not be enough for a second episode of

star formation to take place, as the Lyman-Werner photons from the first-generation stars prevent the gas from cooling down to form stars (Conroy & Spergel, 2011).

If the suggestion of G14 indeed applies, then a break in the star formation lasting ~ 100 Myr would not be consistent with the age spreads inferred from the eMSTO of the young cluster NGC 1856. For the age of this cluster (~ 300 Myr) a ~ 100 Myr delay between the first- and second-generation stars would be readily observable in its CMD. However, the distribution of stars in the eMSTO of this cluster, and the inferred age distributions, seem to be continuous with no apparent gaps (Milone et al., 2015; Correnti et al., 2015). This could mean that the beginning of the extended star-formation episode responsible for the eMSTO varies from cluster to cluster in a very peculiar way, as it has never been observed to be ongoing in *any* YMC. That is, no evidence of ongoing star formation has been found in a study of ~ 130 young ($10\text{--}1000$ Myr) massive ($10^4 - 10^8 M_{\odot}$) clusters (Bastian et al., 2013c). Nor has any evidence been found of gas reservoirs within YMCs that could fuel extended star-formation episodes with the masses suggested by these scenarios (e.g. Bastian & Strader, 2014; Cabrera-Ziri et al., 2015, more about this in §3). Hence, the alternative explanation is that it cannot be an age spread that is responsible for the eMSTO.

Niederhofer et al. (2016) found a correlation between the width of the eMSTO (or inferred age spread) and the age of the clusters in their sample, suggesting an evolutionary effect. For instance, a young cluster like NGC 1856 has an inferred MSTO age spread of 140 Myr (cf. Milone et al. 2015), while an older cluster (1 Gyr) like NGC 2108 has an inferred age spread of 230 Myr and an even older (1.45 Gyr) cluster like NGC 411 shows an MSTO spread equivalent to 516 Myr (cf. G14).

Supporting this interpretation is the recent analysis of the CMD of NGC 1856 by D’Antona et al. (2015), which suggests that the complex MSTO of this cluster is due to two populations of the same age (~ 350 Myr), one composed mainly of very rapidly rotating stars ($\omega = 0.9\omega_{\text{crit}}$), while the other is composed of slowly/non-rotating stars.

In this context, we can use W3 to test the age spread or the rotation scenarios. As seen in the previous sections, the maximum age spread present in W3 is at most 100

Myr. In the age spread scenario suggested by G14, for a cluster with such a high escape velocity, the expected age spread is typically ~ 375 Myr, inconsistent with the observations. On the other hand, in the rotational scenario, the expected MSTO spread would be the equivalent of $\sim 150 - 200$ Myr. However, the post-main sequence features, which contributed significantly to the integrated light are expected to have age spreads equivalent to < 100 Myr (Niederhofer et al., 2015). Hence, our observations are inconsistent with the age spread scenario, but consistent with those expected from the rotational scenario.

2.2.5 Summary and Conclusions from Cabrera-Ziri et al. (2016a)

We have used the SED of W3, a YMC in the merger remnant NGC 7252, and have compared it with the SED of synthetic clusters constructed with the SFHs that are proposed to explain the eMSTOs of intermediate-age clusters. We find that the SED of this cluster is consistent with that of an SSP of age 570_{-62}^{+70} Myr, mass $1.13_{-0.13}^{+0.14} \times 10^8 M_{\odot}$ and current central escape velocity above 193 km s^{-1} .

A key argument of some of the scenarios that have been proposed to explain the eMSTOs of intermediate-age clusters is based on the fact that these clusters all have masses above $10^4 M_{\odot}$. These scenarios also assume that the eMSTO clusters were a factor of 10–20 more massive at birth and had escape velocities $> 15 \text{ km s}^{-1}$, enabling them to retain the gas that fueled the extended episode of star formation responsible for the observed eMSTO (cf. Keller et al. 2011). However, our results are in strong contradiction to the prediction of these scenarios, given that the SED of W3 does not match the model SED of young clusters with an age spread similar to any of those suggested for eMSTO clusters. Yet, W3 is the most massive young cluster known to date, and its mass ($\sim 10^8 M_{\odot}$) and escape velocity ($> 193 \text{ km s}^{-1}$) exceed by orders of magnitude the masses/escape velocities (and the expected birth masses/escape velocities) of intermediate-age clusters showing eMSTOs. The near lack of significant extinction in this cluster ($A_V = 0.083$) is also in conflict with the properties of a young cluster hosting a massive reservoir of cool gas (Longmore, 2015), suggesting that cur-

rently there is no cold gas that could fuel an extended star-formation episode in the near future.

Of course, there is a possibility that this specific cluster has some intrinsic property or that there is something peculiar in its environment that has prevented any extended episodes of star formation from taking place. Yet, note that these results are in perfect agreement with previous studies of YMCs, as they all point towards a SFH of a single burst with a negligible extent (see §2.1, and references therein). Also, in the scenarios investigated here there is no explicit requirement regarding the eMSTO cluster environments that would make the results we have obtained from W3 irrelevant for constraining the origin of this phenomenon.

Additionally, the open clusters Hyades and Praesepe—composed of ~ 300 and ~ 1000 members, respectively, and each ~ 800 Myr old (Perryman et al., 1998; Kraus & Hillenbrand, 2007)—are known to have MSTOs that are inconsistent with a single isochrone, which has been attributed to spreads of a few hundred Myr in age (Eggen, 1998). Brandt & Huang (2015a) have recently proposed that age spreads are not needed to explain the broadened MSTOs in these clusters, since stellar models that include *rotation* can reproduce the same morphology with a single generation of stars. This mechanism has also been explored in the past to explain the origin of eMSTO clusters in the SMC/LMC (e.g. Bastian & de Mink 2009).

However, given the relatively small number of stars in the Hyades and Praesepe, it is hard to tell if the broadening of the turnoff observed in these open clusters is the same phenomenon as that observed in the significantly more massive ($> \sim 10^4 M_{\odot}$) intermediate-age clusters displaying an eMSTO. If this were the case, this would also challenge the suggestion that the cluster’s gravitational potential well retained the gas long enough to have these extended star formation episodes, as it is highly unlikely that these open clusters had the necessary elevated escape velocity at birth.

Piatti & Bastian (2016) have recently found evidence for eMSTO in extremely low mass clusters ($< 5000 M_{\odot}$) in the LMC, which shows that cluster mass cannot be the essential parameter. Similar hints of eMSTOs can be seen in CMD of the low-mass

Galactic open clusters NGC 752 and Tombaugh 1 (Twarog et al., 2015; Silva et al., 2016).

Finally, we would like to reiterate the important point made by G11 that, if the eMSTOs observed in intermediate-age clusters are due to the same mechanisms proposed to explain the chemical abundance patterns in GCs, then one would expect to see the same light-element abundance variations in intermediate-age clusters. However, different abundance analyses have shown no signs of these abundance patterns in the LMC intermediate-age clusters NGC 1806, 1651, 1783, 1978, and 2173 (Mucciarelli et al., 2008, 2014). Some of these clusters show an eMSTO (e.g. NGC 1783, 1651 and 1806) and have stellar masses comparable to GCs (all of these intermediate-age clusters are above $10^5 M_{\odot}$). All of these considerations suggest, again, that the eMSTO phenomenon is unrelated to the chemical anomalies found in old GCs.

2.3 Constraints from resolved LMC/SMC clusters

Recently Li et al. (2016); hereafter L16, studied the CMDs of three intermediate age (~ 1.5 Gyr) clusters in the LMC/SMC (NGC 1783, NGC 1806⁹ and NGC 411), and claimed to have found young (few hundred Myr) populations of stars in each cluster. The authors interpreted these results as a ‘smoking gun’ of a recent star formation burst within these clusters. If true, this would cause us to reconsider much of the results presented above.

These authors proposed that these three clusters were able to accrete gas while moving through the interstellar medium of their host galaxy, and eventually were able to trigger a secondary star formation event once the accreted gas density had achieved a ‘relevant threshold’. Furthermore, they also suggest that the process undergone by these clusters might be able to explain the origin of MPs in GCs.

In Cabrera-Ziri et al. (2016b) we use L16 photometric catalogs, and find that the young

⁹In the Li et al. catalogs, NGC 1806 was attributed the wrong ID, i.e. that of NGC 1696. In the catalogs the coordinates match those of NGC 1806.

Table 2.3: Number (N and N_F) and surface density (Σ_N and Σ_{N_F}) of young stars in the cluster region (before decontamination) and the reference field.

NGC	N (stars)	N_F (stars)	Σ_N ($\times 10^{-3}$ stars/arcsec ²)	Σ_{N_F} ($\times 10^{-3}$ stars/arcsec ²)	$\Sigma_N - \Sigma_{N_F}$ ($\times 10^{-3}$ stars/arcsec ²)
1783	167	311	5.32(± 0.41)	7.77(± 0.44)	-2.49(± 0.60)
1806	148	55	13.09(± 1.08)	9.17(± 1.24)	3.92(± 1.64)
411	86	34	10.95(± 1.18)	7.59(± 1.30)	3.36(± 1.76)

populations in the CMDs of these three clusters are also present in the CMDs of field regions around the clusters, challenging the associations of the young populations with these clusters. In this section I will explain how we got to that conclusion.

2.3.1 HST photometry

Here I will summarise the data described in L16 and used in their analysis. The data for clusters NGC 1783 (and its reference field) and NGC 1806 were obtained with the ACS/WFC camera aboard HST under programmes GO-10595 (PI: Goudfrooij) and GO-12257 (PI: Girardi). For the L16 study, the authors used the images taken with the filters $F435W$ and $F814W$, which correspond approximately to the Johnson–Cousins B and I bands, respectively, and which will be referred to as such in the following. For the cluster NGC 411, these authors used images obtained with the $F475W$ and $F814W$ filters of the WFC3 camera of the HST – programme GO-12257 (PI: Girardi). The filter $F475W$ is also similar to B and will be referred to as such henceforth.

To produce their stellar catalogs, L16 performed point-spread-function photometry using DAOPHOT within the IRAF environment. The reader interested in more details is referred to L16 and references therein. For the analysis in Cabrera-Ziri et al. (2016b) we used L16 photometric catalogs which were kindly provided by these authors in a private communication.

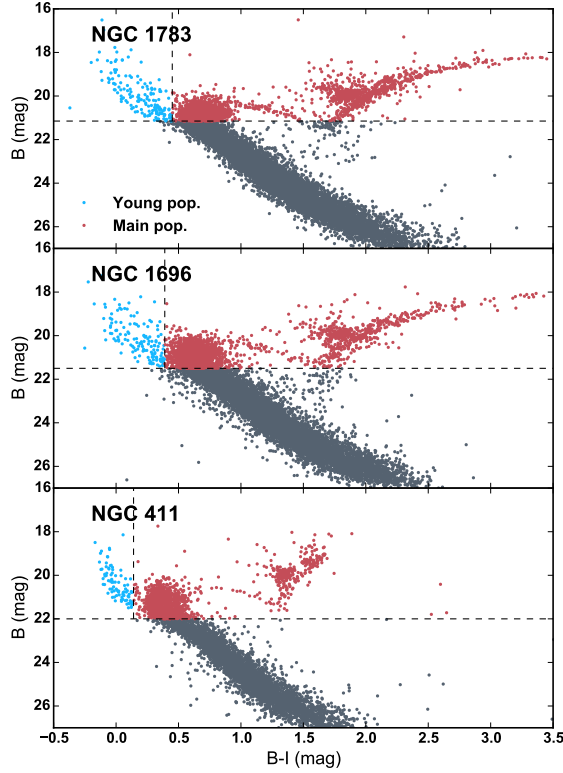


Figure 2.13: Selection of young (blue dots) and main (~ 1.5 Gyr old – red dots) populations from the CMDs (before decontamination) for the luminosity functions (cf. Fig. 2.14) and radial profiles (cf. Fig. 2.20).

2.3.2 Densities and luminosity functions of the young stars

We compared the density of young stars in the cluster (i.e. inner two core radii, as defined by L16) and in the reference field region, which was chosen to be the same as in L16. This comparison was done before applying any decontamination and the definition of the young sequences in the CMD was selected to be $B < \{21.25, 21.50, 22.00\}$ and $B - I < \{0.45, 0.39, 0.14\}$ for clusters NGC 1783, NGC 1806 and NGC 411 respectively (cf. Fig. 2.13). In Table 2.3 we report the number and (average) surface density of the young stars in the cluster and reference field region for each case. In brackets we show the standard deviation of the densities calculated \sqrt{N}/A_C and $\sqrt{N_F}/A_F$ where A_C and A_F are the solid angles (areas) of the cluster and reference field region, respectively.

The last column of the Table 2.3 shows the difference between surface densities. For NGC 1783, we find that the reference field contains significantly ($\sim 4\sigma$) more of these young stars per unit area than the cluster, while for both NGC 1806 and NGC 411, the densities of young stars in the clusters differ from 0 at the $\sim 2.3\sigma$ and \sim

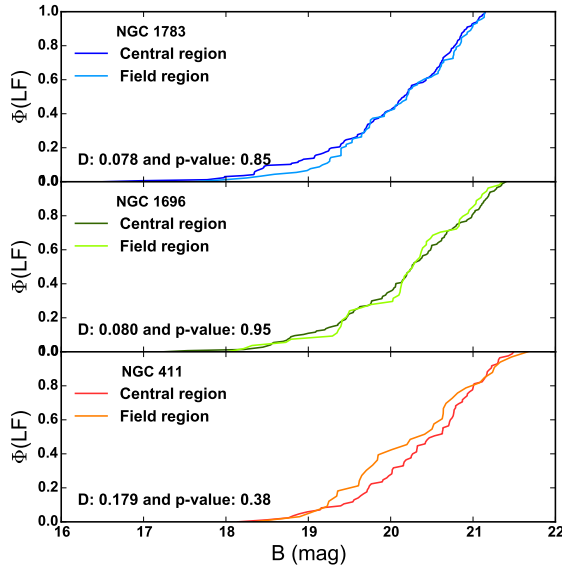


Figure 2.14: Cumulative LFs of the young populations in the clusters and field regions. In each panel we report the KS statistic, D , and p -value from our analysis of the LFs of the young populations from the field and cluster regions. We find no significant differences between them.

1.9σ respectively. From this, we find no significant overdensities of young stars in the cluster regions with respect to the reference field.

Additionally, we calculated the luminosity functions (LFs) of these young populations in the field region and compared them with the LFs of the young populations in the cluster region (also before applying any decontamination). The cumulative LFs of the young populations from clusters and field regions are shown in Fig. 2.14. They are very similar in all cases. For every cluster we applied a KS test to compare the LFs of both regions, the results are shown in Fig. 2.14 as well. From the KS test we can say that the LFs of the young populations in the field regions around the clusters, and the LFs of the stars within the clusters, do not show any significant difference.

This casts doubts on the association of these young populations with the clusters themselves as 1) there are no obvious overdensities of young stars in the cluster with respect to the reference fields, and 2) the LFs of the young populations in the cluster region do not show a significant difference to the ones in the reference field.

2.3.3 Reducing background contamination in L16

To remove the background contamination in the CMDs of the clusters, L16 used the following technique:

1. The CMD of the cluster and field region are gridded in several bins/cells.
2. The number of stars within each grid cell in the field region CMD are counted.
3. In the cluster region CMD, the same number of stars as in the corresponding grid cell of the field region CMD are randomly removed, accounting for the difference in solid angle (area) between the cluster and field regions.
4. The resulting subset of stars in the cluster CMD is considered the decontaminated CMD of the cluster.

This technique will perform well, i.e. reducing significantly the contribution of field stars, only in well populated grid cells, where Poisson uncertainties are much smaller than the number of available stars. However, if the grid cells are populated with just a few stars, the performance of this technique can be very poor. Another caveat of this method is that grid cells that contain more field stars than cluster stars end up with negative values, which are not taken into account during the analysis. This is the case of the regions of the CMDs that host the young population of the LMC/SMC field (i.e. these regions contain both positive and negative counts after using this technique).

2.3.4 Performance of L16 background decontamination

2.3.4.1 Subtracting the field from the field

To illustrate the flaw of the technique used by L16, we carry out a simple experiment. For this we have randomly assigned the stars of the L16 field region to two subsets, irrespective of their spatial location. The experiment consists of taking these two subsets of stars, and applying the L16 method to reduce the background using one subset as a primary field and the other as reference/background population. With this experiment one would expect to find very few stars at the end, as we are subtracting populations that are statistically identical. If on the contrary, we find that this test yields significant residuals, one can conclude that the technique used is not adequate.

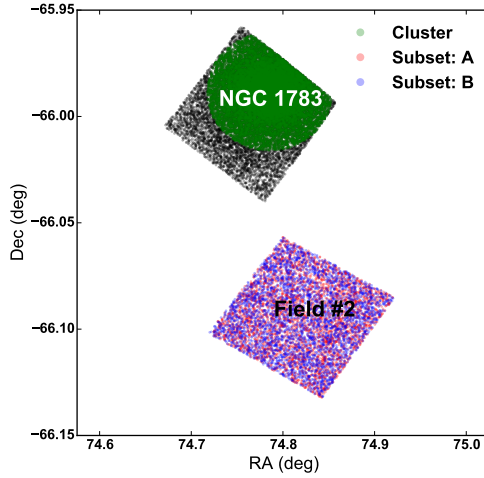


Figure 2.15: Spatial distribution of the cluster and field stars used in our experiments. Red and blue colours show the position of the stars from subset A and B respectively.

For these experiments we have used the same grid/binning as L16, i.e. grid cells of magnitude \times colour = $0.5 \times 0.25 \text{ mag}^2$ ranging from $(B - I) = -2.5$ to 3.5 mag and $B = 16$ to 27 mag .

In Fig. 2.15, we show the spatial distribution of the subsets of stars taken for our experiment. The subsets A and B, have the same number of stars and were chosen randomly. Both are distributed uniformly across the field region next to the cluster NGC 1783. The CMDs of both subsets are shown respectively in panels “A” and “B” of Fig. 2.16. The CMDs are virtually identical. As noted in §2.3.2, the young populations found in L16 are already present in the field region. We show the Marigo et al. (2008) isochrones attributed by L16 to each population for reference. The colour scale represents the log of the number of stars in each grid element.

We then proceed with our experiment, assuming that the subset A contains stars that belong to the primary field, and subset B stars form the reference/background region. After applying the technique used by L16, we were left with the CMD shown in panel “A-B” of Fig. 2.16.

In this “residual” CMD we note that this technique was efficient in removing most of the stars along the field’s MS, i.e. stars with $B > 22 \text{ mag}$. In these regions we are left with $\pm \sim 15 \text{ stars/cell}$ – the negative values correspond to grid cells where there are not enough stars to subtract, i.e. fewer stars in the grid cells of the primary than in the reference/background region, which will be discussed further in §2.3.5. When we

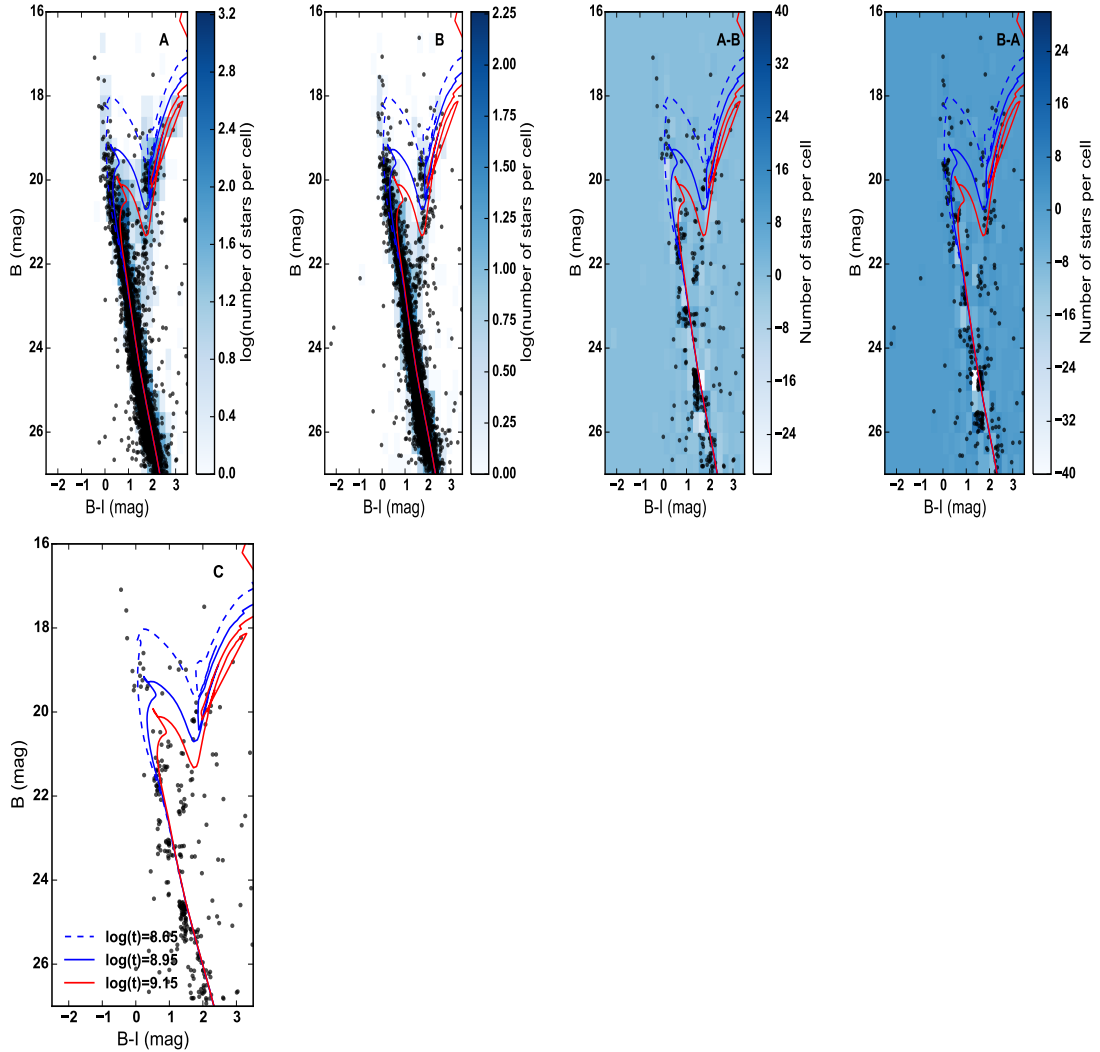


Figure 2.16: CMDs of subsets A and B are shown in panels “A” and “B” respectively. The colour scales in these two panels show the log of the number of stars in each grid element. Panel “A-B” shows the residual CMDs obtained when we applied L16’s decontamination method assuming that subset A represents the CMD of the stars in the primary field and subset B the reference/background stars. Panel “B-A” is similar to panel “A-B” but here subset that B was taken as the stars in the primary field and subset A the reference stars instead. The colour scale of panels “A-B” and “B-A” show the number of stars in each grid cell in linear scale. Panel “C” is the same as panel “A-B”, but without the colour scale. The isochrones in all panels are those attributed by L16 to the young sequences in their CMD of NGC 1783.

compare these values to the original number of stars in these grid cells ~ 200 (i.e. before applying the decontamination technique), we are left with about $\sim 8\%$ of the original number of stars in this region of the CMD.

On the other hand, there are significantly fewer stars close to the turn-off of the young populations ($B < 20$ mag) with ~ 5 stars/cell in comparison to ~ 200 stars/cell in the fainter part of the CMD. The problem with the decontamination method used by L16 is particularly evident here. After “decontaminating” this part of the CMD, the number of stars per grid cell does not change much – there are still ± 5 stars/cell. In other words, the residuals after decontamination are comparable to the original population due to low number statistics.

The same result is obtained if we take as primary-field stars the background population B and use background population A as reference-field stars, as shown in panel “B-A” of the same figure. In this technique, only grid cells with positive counts are analysed, i.e. grid cells resulting in negative counts are ignored, resulting in a bias in the analysis.

We have carried out similar tests, defining different subsets of stars A and B. Also, we have divided “Field #2” (cf. Fig. 2.15) into different spatial subsets, and carried out the same experiments in each of them. All our tests show the same results: the residuals of the young populations are present after the statistical decontamination.

We find the same results for NGC 1806 and NGC 411, the other clusters studied by L16. The presence of these residuals after our experiments also calls into question the association of the young populations with these clusters, as they show the “noise” leftover after decontaminating a CMD with this technique.

2.3.4.2 Decontaminating the cluster CMD

We have applied L16’s method to decontaminate the CMD of the clusters using the same reference field as L16 and the same CMD grids. The results obtained for NGC 1783 are shown in Fig. 2.17.

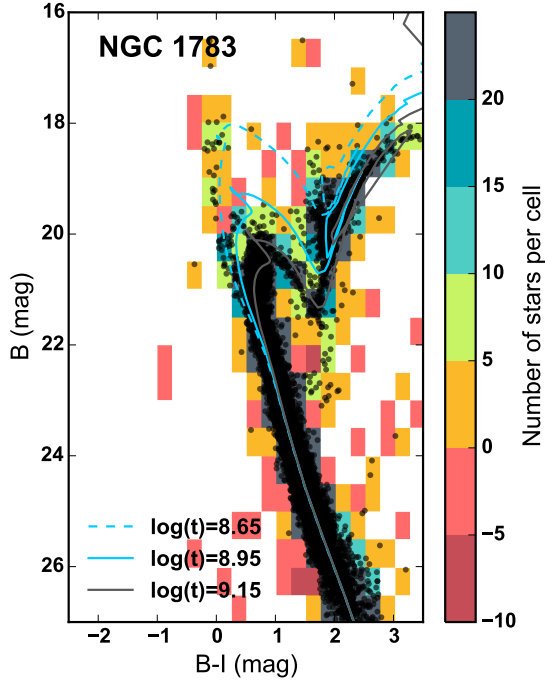


Figure 2.17: CMD of NGC 1783 produced by L16’s decontamination technique. In colour, we represent the number of stars/cell. The negative values represent the grid cells where there were more stars in the reference field than in the cluster region.

2.3.5 Significance of the L16 detections

We used the method outlined in Knoetig (2014) to calculate the probability of the stars in the on-cluster CMD to belong to the background/field and also to quantify the significance of the detections. The solution presented by Knoetig assumes that the on- and off-cluster cell counts follow a Poissonian distribution, and this method has the advantage to be applicable to cells with small and large number of counts, which is ideal in our case, as the number of counts in a cell changes significantly across the CMDs as shown in §2.3.4. We refer the reader interested in the details of this method to Knoetig (2014), as the discussion of such a rigorous analysis escapes the scope of this work.

This method depends only on three parameters: the number of stars in a cell of the on-cluster CMD, the number of stars in a cell of the off-cluster (background/reference) CMD, and the ratio of exposure times between the on- and off-cluster pointings, α . We have adopted $\alpha = 1$, as is adequate to the regions of the CMD we are interested in, i.e. those hosting the young populations; however this assumption need not necessarily be correct for the faint end of the CMD where incompleteness might play a role due to

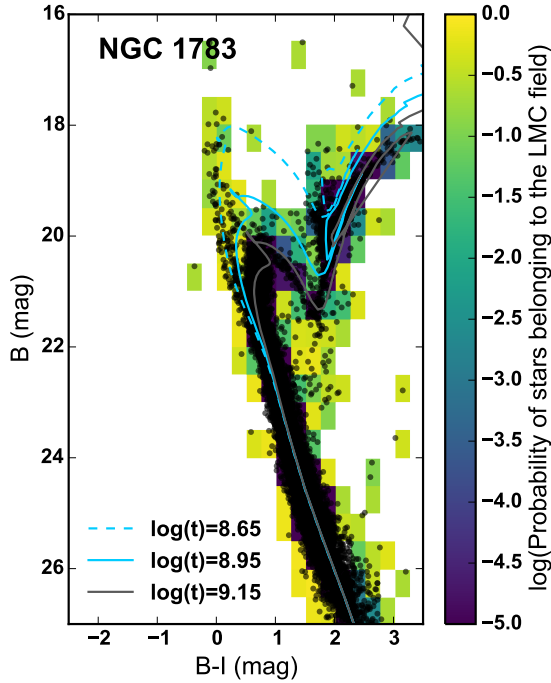


Figure 2.18: On-cluster CMD of NGC 1783, before decontamination. The colour scale represents the log of the probability of the stars in a given cell to belong to the LMC field. The main population has very low probabilities while the young population is very likely to be members of the LMC-field.

the different exposure times (minimum and maximum exposure times between the on- and off-cluster pointings are 680 s and 720 s respectively).

We use equation (23) in Knoetig (2014), to calculate the probability of the cell counts in the on-cluster CMD to be only due to background/field stars. In Fig. 2.18, we show the raw CMD of NGC 1783 (i.e. before decontamination), and in colour we represent the (log of the) probability of the stars in the on-cluster region to belong to the background/LMC-field population. Note that all cells that do not belong to the main (~ 1.5 Gyr) population, have large ($\sim 10 - 85\%$) probabilities to belong to the LMC field. On the other hand, the probability that stars along the main cluster sequence belong to the LMC field is vanishingly small, less than $10^{-4}\%$ and as small as $10^{-31}\%$ along the main sequence¹⁰.

We have also calculated the significance of the detections, S_b , defined as “if the probability were normally distributed, it would correspond to a S_b standard deviation measurement” (equation (27) in Knoetig 2014). In other words, it quantifies how much, in standard deviation (σ) units, the number of stars in a CMD cells differs from the LMC

¹⁰Note that the colour scale in Fig. 2.18 is truncated to highlight the contrast between the young and main population.

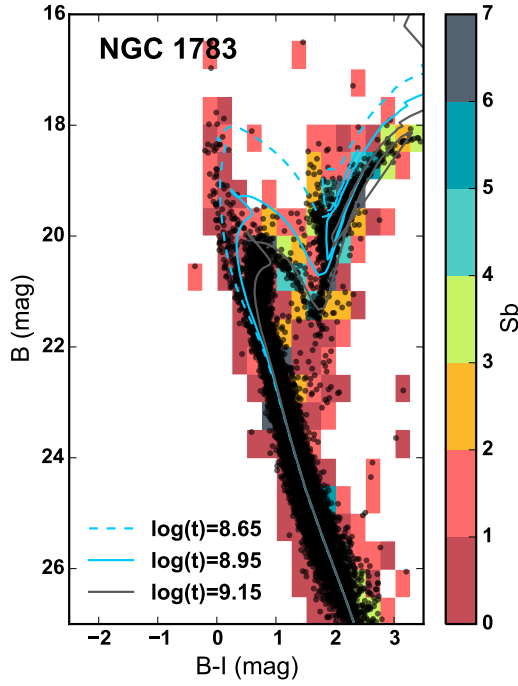


Figure 2.19: On-cluster CMD of NGC 1783, before decontamination. The colour scale represents the significance of the detection in a given cell with respect to the LMC field. The main population is detected at high (> 5) significance. On the other hand, the significance of the detection of the young population is minimal, i.e. consistent with the LMC field.

field population. Figure 2.19 shows the significance S_b of the detection of stars in a given cell with respect to the LMC field for NGC 1783. The young populations are detected with low (0 – 2) significance, while the main population is detected at high (> 5) significance.

The probability of the young populations to belong to the background/field population and significance of the detections of the young population with respect to the reference field, calculated in this section, also suggest that the young populations from the cluster CMDs belong to the surrounding field.

2.3.6 Spatial distribution of the populations

Finally, in this sub-section we analyse the spatial distributions of young populations in these clusters. In Fig. 2.20, we have the radial profiles of the main population, i.e. intermediate-age population, and the young populations found in the clusters' region before and after CMD decontamination by L16's method. The main populations were taken from $B(\text{mag}) < \{21.25, 21.50, 22.00\}$ and $B - I(\text{mag}) \geq \{0.45, 0.39, 0.14\}$ in the CMDs for clusters NGC 1783, NGC 1806 and NGC 411 respectively (cf. Fig.

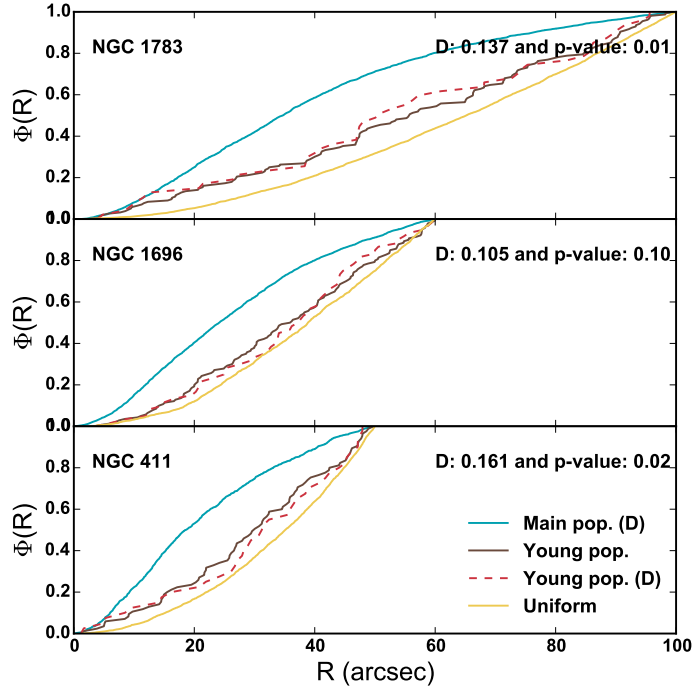


Figure 2.20: Radial profiles of the populations within the clusters. Blue lines: main intermediate-age population after CMD decontamination. Brown and pink lines: young populations, before and after applying L16’s decontamination method. Yellow line: synthetic stars distributed uniformly across the clusters. The radial profile of the young populations in these clusters is significantly less centrally concentrated than the main population.

2.13), and the young populations were selected from the same regions as for the LFs in §2.3.2.

From this figure we see that these young populations seem to be less centrally concentrated with respect to the main population of the clusters, in agreement with L16’s findings. For comparison, we have distributed randomly, *in a statistically uniform way across each cluster* (i.e. inner two core radii), 10000 artificial stars. We then perform a KS test comparing the radial profiles of the artificial stars (*uniformly distributed in space*), and the radial profiles of the young populations before any decontamination. The results of these tests are also shown in Fig. 2.20. We conclude that the radial profile of the young population in NGC 1806 is consistent with the radial profile of a uniform distribution of stars, as expected for field (i.e. background/foreground) stars. On the other hand, while the spatial distribution of young stars within NGC 1783 and 411 is not consistent with an uniform spatial distribution, these young stars are significantly less centrally concentrated than the main population of the cluster. We might not expect the young population to be perfectly described by a uniform population, even if they are (as we argue here) likely members of background, if there is a population gradient across the field.

The fact that the young populations found in L16’s results, are significantly less centrally concentrated than the main population stars, represents another reason to question the association of these young populations to these clusters. Moreover, the young population in NGC 1806 even shares the radial profile expected for uniformly distributed field stars. This is also in agreement with the results presented in §2.3.2, §2.3.4 and §2.3.5.

We note that the exact shape of the young sequences depends on the reference field adopted and the choice of bin size. On the other hand, these changes have little to no impact to the main (i.e. intermediate age) population of these clusters.

2.3.7 Summary and conclusions from Cabrera-Ziri et al. (2016b)

We have re-analysed the CMDs of three intermediate-age LMC/SMC star clusters that have been recently claimed to host new generations of stars by L16. Using the same data as L16, we have shown that these young stellar populations belong to the field population of the LMC/SMC. Our experiments have shown that an insufficient background subtraction resulted in these young populations remaining in the clusters’ CMDs. We conclude that L16 results are not evidence that these clusters host new generations of stars. This is consistent with previous studies that have looked for, but have not found evidence of multiple epochs of star-formation within young and intermediate-age clusters, including: Bastian et al. (2013c); Li et al. (2014); Cabrera-Ziri et al. (2014, 2016a); Niederhofer et al. (2015).

More sophisticated methods exist to address the issue of field contamination. In the same class as the method adopted by L16 there are applications that properly address the issues of bin edges and placements by taking into account magnitude and colour uncertainties (e.g. Kerber et al. 2002; Balbinot et al. 2010). However, more robust methods can be found that adopt an “unbinned” approach in a matched-filter framework. Implementations of the latter methods are widely spread across the Local Group dwarf galaxy and stellar stream communities (e.g. Martin et al. 2008; Bechtol et al. 2015).

Having said this, given that in all cases we would be dealing with populations in the Poisson regime, one needs to be cautious when interpreting any result obtained for such populations.

In L16, the authors proposed that these clusters were able to accrete and retain gas from their surroundings (adopting the models of Conroy & Spergel 2011), which subsequently spawned a new generation of stars. Gas accretion and the gas content of star clusters have been studied in several different contexts. So far the evidence points to clusters becoming gas free at very early ages, in most cases just after a few Myr, e.g. Hollyhead et al. (2015). Other studies have shown that clusters remain gas free, even if they are, in principle (based on escape velocity arguments), massive enough to accrete and retain gas from the surrounding, up to very old ages (e.g. Bastian & Strader, 2014; Bastian et al., 2014; Cabrera-Ziri et al., 2015, 2016a; McDonald & Zijlstra, 2015, more on this in the next chapter). All this suggests that stellar clusters are extremely inefficient at holding onto gas. Perhaps this is the reason why, to date, we have not found compelling evidence for multiple stellar generations within clusters.

We note that L16 found that the “young” stars in each of the clusters were significantly less centrally concentrated than the main stellar population, in contrast with expectations of models that invoke multiple epochs of star formation in clusters (e.g. Conroy & Spergel 2011). However, if these stars are field contaminants, as argued in the current work, the similar less centrally concentrated distribution is consistent with a field population that was not fully subtracted.

Finally, L16 adopt He enriched isochrones to explain the younger generation of stars in two of the three clusters, as standard isochrones did not fit the data (for the adopted distance and extinction of the cluster). Why material accreted from the ISM would be He enriched (and why we do not see He enriched stars forming in the field or clusters/associations today) is left unanswered.

Chapter 3

Gas content of young massive clusters

Some formation scenarios that have been put forward to explain multiple populations within Globular Clusters (GCs) require that the young massive clusters have large reservoirs of cold gas within them, which is necessary to form future generations of stars. In Cabrera-Ziri et al. (2015) we use deep observations taken with Atacama Large Millimeter/sub-millimeter Array (ALMA) to assess the amount of molecular gas within 3 young (50 – 200 Myr) massive ($\sim 10^6 M_{\odot}$) clusters in the Antennae galaxies. In this chapter I present the results of that study.

3.1 Background

The majority of the proposed formation scenarios for GCs adopt multiple generations of stars in order to explain the observed chemical anomalies. Essentially the main concept is that the chemically processed ejecta of some kinds of stars from the first generation (*polluter* stars) breed a second generation of stars with the observed “anomalies”. Several kinds of stars have been suggested to be the *polluters* namely: Asymptotic Giant Branch (AGB) stars (e.g. D’Ercole et al. 2008; Renzini 2008; Conroy & Spergel 2011 - hereafter D08, R08 and CS11 respectively), fast rotating massive stars, FRMS (e.g. Decressin et al. 2009; Krause et al. 2013), and massive stars in interacting binary systems (de Mink et al., 2009).

In all of these scenarios the ejecta from the *polluters* is expected to cool and sink into the centre of the gravitational potential well of the cluster where it will spawn future generations of stars. These models all require additional “pristine” material (i.e. the gas from which the first generation was born) to be (re)accreted by the clusters from their surroundings in order to match the chemical patterns found in GCs, or alternatively that some left over gas from the first generation stays bound in the centre of the cluster and mixes with the polluted material and subsequently forms stars (e.g. D08; CS11; Krause et al. 2013).

As mentioned previously, each type of *polluter* star is expected to have a different timescale for the second episode of star formation. For example, the AGB scenario predicts that the second star formation episode begins ~ 30 Myr after the birth of the first generation (when the super-AGB stars begin to eject their low velocity winds). This then continues until $\sim 80 - 100$ Myr, when it is truncated by prompt SNe Ia explosions. For this model this is necessary in order to match the observed abundance trends in GCs (e.g. D08 - as lower mass AGBs stars, with longer lifetimes, have different abundance yields). However, other authors have suggested that this maximum needs to be pushed to later times ($\sim 200 - 300$ Myr) in order to allow the Lyman-Werner flux density to drop sufficiently for the gas to cool and form new stars (CS11, see also R08 for an alternative long timescale AGB scenario - few 10^8 yr). On the other hand, the FRMS and the interacting binaries scenarios work on much shorter timescales (a few Myr) for the formation of the second generation.

In a series of papers, we have used observations of young massive clusters (YMCs) often seen as young GCs (e.g. Schweizer & Seitzer 1998), to probe the different models for GC formation. Some of these studies were focused on the properties of the gas within YMCs. For example Bastian et al. (2013c) analysed over 100 YMCs for evidence of ionised gas ([OIII] or $H\beta$) due to ongoing star formation, and found none. They concluded that a maximum mass of any ongoing burst within a YMC should be smaller than 2% of the mass of the population already formed. In a following work, Bastian & Strader (2014) placed limits on the amount of HI and/or dust found within 13 LMC/SMC YMCs (with ages between 15 and 300 Myr, and masses between 10^4

and $2 \times 10^5 M_{\odot}$) to be $< 1\%$ of the stellar mass, this result is at odds with the expectations of some scenarios (e.g. CS11). In addition, Longmore (2015) has shown that high levels of extinction/dust would be expected for the clusters if there were to be such large reservoirs of gas/dust within these clusters as suggested by D08 which are inconsistent with observations of YMCs. Bastian et al. (2014) also used YMCs to test a prediction from the FRMS scenario, namely that massive young clusters should remain embedded in the natal gas cloud for the first 20 – 30 Myr of the cluster’s life. However, it was found that YMCs, independent of their mass, are very efficient at expelling any gas within/near them, beginning 1 – 3 Myr after their formation. Similar results have been found in YMCs in the Antennae, where they appear to have removed the molecular gas within them over the first 10 Myr of their life clearing the gas out to a radius of ~ 200 pc (Whitmore et al., 2014).

In Cabrera-Ziri et al. (2015) we look for evidence of molecular gas necessary to form the second generation of stars within young GCs with Atacama Large Millimeter/sub-millimeter Array (ALMA) observations. Our study was centred on 3 young (< 200 Myr) massive ($\sim 10^6 M_{\odot}$) clusters in the Antennae galaxies (W32187, W32604 and W31730 – as defined in Whitmore et al. 2010). We estimate the escape velocities for these clusters to be between 50–130 km/s, well above the velocity of the stellar ejecta of the different *polluters*, allowing them in principle to be able to retain the ejecta from these stars. These clusters have very little reddening, with $E(B - V)$ ranging from 0.06 to 0.5 mag, and are amongst the 12 brightest/most massive clusters in the Antennae galaxies, which makes them ideal for this kind of study (Whitmore et al. 2010, hereafter W10).

This chapter is organised as follows: In §3.2 we present the ALMA data of these clusters and in §3.3 we show the procedure used to estimate the H_2 masses for these clusters. We discuss the Cabrera-Ziri et al. (2015) results and present its conclusions in §3.4 and §3.5, respectively.

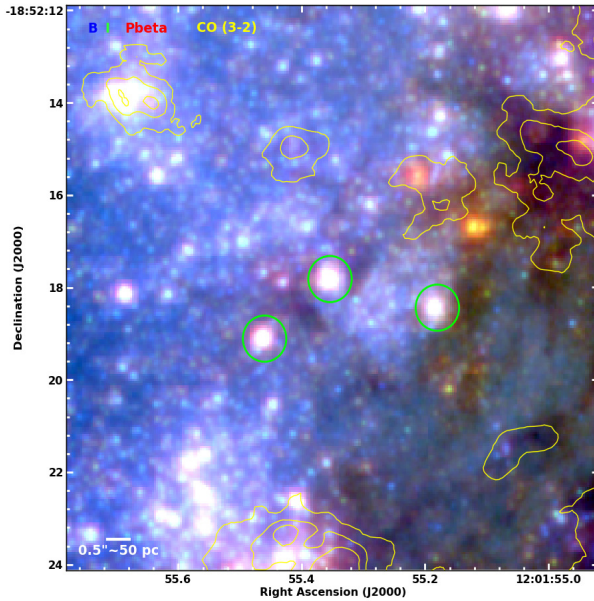


Figure 3.1: The region containing the clusters in Cabrera-Ziri et al. (2015). This composite image was made with *HST* observations where the red, green and blue colours are from Pa β , *I*-band, *B*-band images (from Whitmore et al. 2014). The contours overlaid in yellow are CO (3–2), representing flux levels of 4, 24, and 48 K km/s. The green circles highlight the clusters of interest.

3.2 ALMA data

We made use of “Band 7” (345 GHz) ALMA observations of the Antennae galaxies (NGC 4038/39) from Cycle 0 project 2011.0.00876. A detailed description of these observations and data reduction can be found in Whitmore et al. (2014), along with a formal introduction to the highest spatial resolution CO (3–2) observations of the overlap region in the Antennae.

In Fig. 3.1 we present a colour composite image of the clusters of our analysis (based on *HST* imaging); W32187, W32604 and W31730 (from east to west respectively, W10)¹. The clusters of interest are highlighted with green circles. The contours indicate the integrated CO emission, from which it can already be seen that no CO emission is associated with the clusters.

Only these clusters fulfilled the following selection criteria 1) be located in our ALMA field of view and away of any background CO emission 2) were young (< 200 Myr) and massive ($> 10^6 M_{\odot}$) 3) have near-IR spectroscopy used to determine radial velocities and velocity dispersions. There are 4 more clusters that satisfy criteria 1) and 2) but they lack near-infrared spectroscopy (i.e. with no radial velocities nor velocity

¹a.k.a. cluster S2.1, [W99]15 and S1.2 in Mengel et al. (2008).

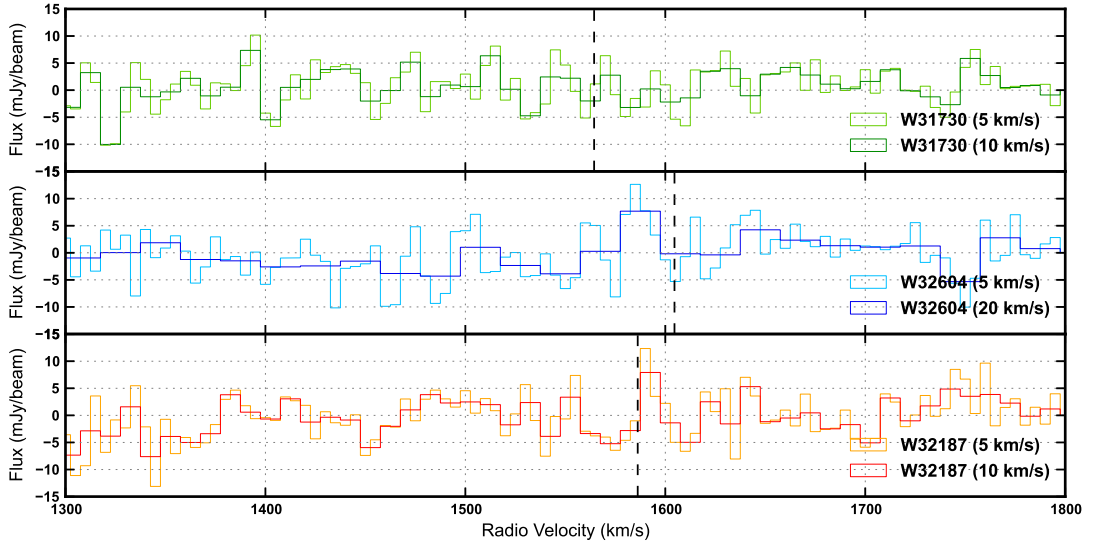


Figure 3.2: ALMA spectra of the 3 young massive clusters in the Antennae galaxies. The spectrum of each cluster is presented with the highest resolution (bins of 5 km/s) and also binned to the approximate velocity dispersion reported in M08. There is no detection of any significant CO (3–2) emission in any of the clusters studied in this work. The vertical dashed lines represents the radial velocities of each cluster from M08 corrected to LSRK. The position of the extracted spectra and rms values of the flux are reported in Table 3.1.

dispersions).

Fig. 3.2 shows the spectra of the (primary beam corrected) CO (3–2) emission towards the three clusters in units of mJy/beam. For these observations the channel spacing is 5 km/s and the synthesised beam size is $0.56'' \times 0.43''$. All spectra were extracted from single beams taken from the approximate I-band intensity peak. These positions are given in Table 3.1 together with the characteristics of each cluster (see §3.3). We noted a systematic offset of $-1.088''$ and $1.65''$ in R.A. and Dec. respectively, in the positions of the clusters reported in table 7 in W10 with respect to the ones in the HST images.

3.3 Molecular gas and stellar mass estimates

Following equation (3) in Bolatto et al. (2013):

$$M_{\text{mol}} = 1.05 \times 10^4 \left(\frac{X_{\text{CO}}}{2 \times 10^{20} \text{ cm}^{-2} (\text{K km/s})^{-1}} \right) \frac{S_{\text{CO}} \Delta v D_L^2}{(1+z)} M_{\odot} \quad (3.1)$$

we derived the H₂ gas masses for these clusters. For the H₂ mass estimates we assume a CO (1–0)-to-H₂ conversion factor of $X_{\text{CO}} = 2 \times 10^{20} \text{ cm}^{-2} (\text{K km/s})^{-1}$, a luminosity distance of $D_L = 21.8 \text{ Mpc}$ to the Antennae galaxies and a redshift of $z = 0.005688$. Finally $S_{\text{CO}}\Delta v$, is the integrated CO (1–0) line flux density, in our case given by

$$S_{\text{CO}}\Delta v = \frac{F_{\text{rms}}\Delta v}{r_{31}} \quad (3.2)$$

where F_{rms} is the rms value of the flux of our ALMA CO (3–2) spectra shown in Fig. 3.2 (we assumed this value to be the standard deviation of the flux, σ , for these spectra); Δv is the channel spacing of the spectra (5 km/s for the high resolution spectra and 10 or 20 km/s for the low resolution ones, see Fig. 3.2); and r_{31} is the CO (3–2) to CO (1–0) line ratio. We adopted $r_{31} = 0.792$; this value was obtained averaging the measurements of r_{31} reported for the Antennae on Table 2 from Zhu et al. (2003).

In Table 3.1 we present the characteristics of these clusters. The ages and photometric masses are from W10. We remeasured the sizes of these clusters and used these values to recalculate the dynamical masses of Mengel et al. (2008), hereafter M08. For the sizes, we made an empirical PSF based on ACS *V*-band drizzled images and used ISHAPE (Larsen, 1999) to measure the effective radii adopting different profiles (see Bastian et al. 2009 for more details on the technique). The derived sizes were 2.7, 1.7, and 2 times larger than reported in M08 for W32187, W32604 and W31730 respectively, which corresponds to an increase of the dynamical mass of the same proportion. We find excellent agreement between the photometric and dynamical masses.

In this table we also include F_{rms} , $S_{\text{CO}}\Delta v$ and H₂ mass. We note that the measurements presented here are 1σ upper limits for $S_{\text{CO}}\Delta v$ and H₂ mass. Already with these data we do not find clear evidence of molecular emission above the 1σ level in any of these spectra.

Table 3.1: Clusters’ ages, spectra position, photometric masses, projected half-light radii, dynamical masses, flux spectra rms, $S_{\text{CO}}\Delta v$ and H_2 mass. Values in parenthesis correspond to the binned spectra.

Cluster ID	α	δ	$\log(\text{Age})^a$	M_{ph}^a ($\times 10^6 M_{\odot}$)	r_{hp} (pc)	M_{dyn} ($\times 10^6 M_{\odot}$)	F_{rms} (mJy/beam)	$S_{\text{CO}}\Delta v$ (mJy km/s)	H_2 mass ($\times 10^5 M_{\odot}$)
W31730	12 01 55.462	-18 52 19.108	7.7	1.7	4.1	1.4	3.98 (3.21) ^b	25.11 (40.58) ^b	1.25 (2.01) ^b
W32604	12 01 55.354	-18 52 17.824	7.7	1.6	3.4	2.4	4.48 (2.84) ^c	28.29 (71.73) ^c	1.40 (3.56) ^c
W32187	12 01 55.184	-18 52 18.442	8.3	1.9	8.1	1.8	4.43 (3.47) ^b	27.98 (43.84) ^b	1.38 (2.17) ^b

^a from W10. We assumed conservative errors for these age estimates of $\pm 50\%$.

^b value for the spectrum binned to 10 km/s (similar to the velocity dispersion of 11.5 km/s reported in M08 for W31730 and W32187).

^c value for the spectrum binned to 20 km/s (similar to the velocity dispersion of 20.2 km/s reported in M08 for W32604).

3.4 Discussion

From Table 3.1 we can see that our non-detections of CO in the ALMA spectra of these clusters can be translated into upper limits on the H_2 mass estimates which are of the order of $\sim 9\%$ of the stellar mass. Having said that, we note that this estimate is subject to the choice of X_{CO} . For this study we have used the value reported for the Milky Way disk by Bolatto et al. (2013). However, several studies have shown that the X_{CO} in the Antennae is lower by a factor of 2–10 (e.g. Zhu et al. 2003; Bisbas et al. 2014) than the Milky Way value. As a consequence the H_2 mass estimate will decrease by the same factor if X_{CO} decreases, so *the values of molecular gas reported in Table 3.1 are strict upper limits.*

As mentioned in §3.1, given the age range of these clusters (50–200 Myr) we are only able to place constraints on the AGB scenario. However, this sample spans the critical timeframe where the second generation of stars is expected to be formed for this choice of *polluters* (30–300 Myr, see §3.1). There are several variations of this scenario that adopt AGB stars as the source of enrichment. In the following subsection we outline the essentials of an “AGB scenario” and some distinctions between different scenarios².

²Note that this will be focused only on the issues relevant to the results presented in this work.

3.4.1 AGB scenario: The essentials

- i A first generation (1G) is born as a simple stellar population, i.e. all the stars with the same age, and homogeneous (*pristine*) chemical composition.
- ii The remaining pristine gas that formed the 1G, is expelled from the cluster at some time during the following ~ 30 Myr by the winds of massive stars and core-collapse SNe (R08).
- iii A second generation (2G) starts to form. The first stars to be born will be from the pure (i.e. undiluted) ejecta of the most massive ($\sim 8 - 9 M_{\odot}$) AGB stars³. This material will be forming the 2G stars with the most extreme abundance patterns, that is, the most He-rich population which is also the one with the most O-poor stars observed today in old GCs. We will refer to this population as the *extreme* 2G (the extreme stars identified by Carretta et al. 2009a).
Curiously, the 2G stars are assumed to span a rather narrow mass range $0.1 - 0.8 M_{\odot}$ (D08). This preference for a truncated initial mass function (IMF) for the 2G stars in these models, would have two main consequences 1) this generation of stars will not have type II SNe that would clear the gas, interrupting the formation of the 2G; and 2) it would minimise the “mass budget problem”, i.e. the fact that one would require a 1G many times more massive than the amount of stars with primordial abundances seen today. Both consequences would be treated again in (vi) and (vii) respectively.
- iv Only after the extreme 2G is born, the cluster starts accreting pristine material from a surrounding reservoir. The second star formation episode will continue forming stars, this time with *intermediate* chemical abundances (i.e. abundances between the extreme and pristine ones) from the ejecta of the lower mass ($\lesssim 8 M_{\odot}$) AGB diluted with this accreted material.⁴

³a.k.a. super-AGB stars

⁴CS11 in their model predict a continuum accretion of pristine gas just after the 1G is formed, but the star formation is inhibited during the first 100–200 Myr given that the Lyman-Werner 1G photons have been keeping the gas warm. Due to this (ii) and (iii) never took place in this variation of the AGB scenario. D’Ercole et al. (2011) argue that this mechanism (continuous accretion) would not be able to reproduce the *extreme* populations observed in GCs, see §3.4.3.

We need to underline this point, given that the dilution is required in all the scenarios that share AGB stars as polluters. *Although several attempts have been presented, to date it still remains quite equivocal where was this pristine material stored, what triggers the accretion, what process regulates its rate, and what mechanism ends it.* However, it is possible to constrain the nature of this sequence of events with the current knowledge of the field, for example:

- Where does this pristine gas reservoir come from? This element is not clear in the scenarios so far. D08 implies that the 1G cluster is surrounded by some pristine gas, and the accretion starts after the extreme 2G is formed. On the other hand, CS11 argue that the young GC continuously accretes material, as it sweeps the surrounding interstellar medium (ISM) in a competing process against ram pressure. Later, after the number of energetic photons from the 1G drops, the gas that has been accumulated in the cluster's potential is allowed to cool down to form stars (CS11).
- In D'Ercole et al. (2011) (hereafter D11), the authors conclude that the amount of pristine gas that contributes to the 2G formation is at most equal to 10% of the 1G mass in order to reproduce the extent of the observed abundance patterns. This limit was obtained assuming high star formation efficiencies ($\sim 100\%$); if lower values were in play in the 2G formation, the mass of the gas reservoir should increase (further discussed in §3.4.2).
- The expulsion of the pristine gas mentioned in step (ii) by core-collapse SNe, should have been through a very distinct mechanism in the sense that while it is able to expel this pristine material (now polluted with Fe-peak and α -elements) away from the cluster, it does it in such way that this polluted material never reaches the pristine gas reservoir. This has been explored by R08 and Renzini (2013), concluding that if only 0.2% of the core-collapse SN ejecta would have reached the pristine gas reservoir the 2G of the cluster would exhibit [Fe/H] inhomogeneities like the ones observed in ω Cen, M22 and Terzan 5.

It has been put forward that some asymmetries in the gas distribution could

prevent the Fe-polluted material from reaching the reservoir, avoiding the contamination (cf. D08). In this case the core-collapse SNe leave an “hour glass” cavity after clearing the leftover gas from the 1G, allowing the uncontaminated material around the “hour glass” to collapse back into the cluster for step (iv).

- The accretion must be an accelerated process. The theoretical yields of the AGB stellar models predict a correlation between Na and O, in their ejecta, as a function of stellar mass/time. Given this, after the *extreme* 2G is formed, the pristine gas accretion rate should increase rapidly in time, in order to be able to dilute the material not just compensating their natural correlation trend but to a higher degree, in order to reproduce the observed Na-O anti-correlation.
- v It is assumed that the star formation of the 2G took place in bursty episodes. This premise in the models is backed by the evidence of discrete (i.e. non continuous) He and N abundances in the subpopulations of some massive GCs (e.g. NGC 6397, 2808 & 6752 - Milone et al. 2012a,b, 2013). Furthermore, this assumption also agrees with the recent discovery of a few massive GCs (e.g. NGC 6752 & 2808 cf. Carretta et al. 2012; Carretta 2014) showing clear discreteness on their light element abundance patterns, specifically, the Mg-Al anti-correlation.
- vi The formation of the 2G should end before the low-mass ($\lesssim 3 M_{\odot}$) AGB stars produce large amounts of C, which is especially the case for low metallicity AGBs (cf. R08, D’Ercole et al. 2010). The production of C would affect the sum of CNO elements which appears to be constant (within a factor of ~ 1.5) among primordial and enriched stars in GCs (e.g. Carretta et al. 2005). This requires a mechanism which should be synchronised to start operating just before these lower mass AGB go into action, otherwise (in principle) the star formation would continue. Regarding this, most authors have agreed on the role of prompt ($\sim 10^8$ yr) Ia SNe on this matter.

In CS11, the 2G star formation happens suddenly. Here an instantaneous burst of star formation gives birth to the 2G of stars after the number of Lyman-Werner

photons ($912\text{\AA} < \lambda < 1100\text{\AA}$) drops sufficiently to allow the star formation (200–300 Myr after the birth of the 1G, CS11). The star formation ends when the type II SNe from the 2G and prompt Ia SNe from the 1G start to go off, keeping the cluster gas-free for the rest of its life. In a similar manner, for R08 the formation of the 2G is likely span up to 300 Myr as well. Contrastingly, in D08 the prompt Ia SNe are expected to end the 2G formation episodes ~ 80 Myr after the 1G star formation event. In this model there will be no type II SNe from the 2G IMF since all the stars have masses well below the limit for core-collapse SNe (D08).

- vii After the 2G is formed in these models, the young cluster ends up with just a small fraction of the stars showing the chemical signature of the AGB material. In order to match the observed high fraction (close to 1:1) of enriched/non-enriched stars (i.e. ratio of “first-to-second generations of stars”) these scenarios assume that GCs underwent strong mass-loss and lost most of their first generation stars, usually 90% or more, which means that GCs were significantly more massive at birth than seen today. Furthermore, these models usually assume that the 2G stars had a truncated mass function.

In D08, the authors claim that the cluster should have been about 10 times more massive at birth, however, this value has some severe underlying assumptions. One can see from Fig. 4 of D08, that the stellar mass of the 2G is just $\sim 10^{4.5} M_{\odot}$, this corresponds to a $\sim 1/30$ th of their 1G mass ($10^6 M_{\odot}$). So only if the current (old) cluster has a particularly low fraction of enriched/non-enriched stars (1:3) and only if 1G stars were lost (all 2G stars were kept in the cluster) can one reach this value for the mass of the 1G (originally 10 times more massive). Alternatively, if the current cluster has an equal fraction (1:1) of enriched/non-enriched stars the cluster should have been 30 times more massive at birth (again, this value assumes no 2G stars escaped the cluster during its dynamical evolution).

Additionally, as mentioned in (iii), D08 assumed a truncated IMF (only forming stars with $0.1 - 0.8 M_{\odot}$) for the 2G. If the 2G would have formed following a conventional (i.e. Kroupa et al. 1993) non-truncated IMF (i.e. stars form with masses between $0.1-100 M_{\odot}$) the mass of the first generation should scale by a factor of 2

(i.e. 1G should have been 20 or 60 times more massive in the past depending on the assumed fraction of enriched/non-enriched stars of 1:3 and 1:1 respectively).

On the other hand, in CS11 the young GCs had a similar masses to those observed today (D11), while Conroy (2012) support that the GCs were at least 10–20 times more massive at birth.

Although there has not been reported any evidence of a strongly non-standard IMF in GCs or YMCs (cf. Bastian et al. 2010) this option is difficult to exclude. However, in the last few years there have been some constraints reported regarding the strong mass-loss.

Larsen et al. (2012) and Larsen et al. (2014a) studied three dwarf galaxies, and looked at the amount of GC stars which could have been lost and now form part of the field populations of their host galaxies. In both studies the authors found high GC-to-field stars ratios, concluding that these GCs could only have been at most 4–5 times more massive initially. These values are upper limits, given that it was assumed that all of the field stars that share the same metallicity as the GCs (in a broad metallicity range), formed in these clusters (i.e. no field stars formed with similar abundances) nor did they take into account that lower mass clusters would likely have been formed at the same time and have since disrupted (e.g. Kruijssen 2015), contributing to the field population. Furthermore, the recent model by Kruijssen (2015), putting GC formation into a hierarchical galaxy assembly context, also found that clusters that survive to the present epoch were likely to be only 2–3 times more massive than currently observed.

In the following subsection we will present a “toy model” designed to explore the viability and consequences of the AGB scenario, given the constraints we have just presented regarding the stellar mass and upper limits on any potential gas within the observed clusters.

3.4.2 Toy model

The “toy model” is based on the most massive young globular cluster in our sample, W32187 with a mass of $\sim 2 \times 10^6 M_{\odot}$. This cluster lies within the age range where a

second episode of star formation is expected to occur in the AGB model. We adopt the initial mass upper limits discussed above (Larsen et al., 2012, 2014a; Kruijssen, 2015), and assume that the current mass of the cluster is ~ 4 times more massive than it will be in ~ 10 Gyr⁵, i.e. assuming that the current cluster stellar mass is the initial mass. This means that as an old GC, this cluster will have a mass of $M_{\star} = 5 \times 10^5 M_{\odot}$. If we also assume a 1:1 ratio for the number of first-to-second generation stars at an age of ~ 10 Gyr, this would correspond to a mass of the second generation (2G) stars of $M_{\star}^{2G} = 2.5 \times 10^5 M_{\odot}$. This is a lower limit to the amount of gas that would need to be present, integrated over time. However, if we adopt a standard star-formation efficiency for this cluster of SFE=1/3 (e.g. Lada & Lada 2003), this means that $M_{gas}^{2G} = 7.5 \times 10^5 M_{\odot}$ of molecular gas is required to give birth to the 2G. The rest of this gas i.e. the other 2/3 that will not end up in stars, is expelled from the cluster (see §3.4.5) after the star formation takes place. Given these assumptions, *how much molecular gas would we expect at any given time within this cluster?*

To answer this question we consider the window where star formation can take place according to D08, $\Delta t = 50$ Myr (i.e. from 30–80 Myr, see §3.4.1). If the star formation is extremely rapid, in the sense that any gaseous material within the cluster is used in the star formation very quickly, e.g. $\Delta t_{SF}^{2G} = 1$ Myr⁶, we would expect to find $M_{gas}^{2G} = 1.5 \times 10^4 M_{\odot}$ (i.e., 1/50th of the total gas mass) at any given moment during this 50 Myr time window, which lies below our detection limits of $\sim 1 \times 10^5 M_{\odot}$. However, if the star formation event lasts longer, i.e. if we assume that any gas within the cluster is present for say $\Delta t_{SF}^{2G} = 10$ Myr, before being consumed in star-formation, the amount of gas at any given time would increase to $M_{gas}^{2G} = 1.5 \times 10^5 M_{\odot}$, which is above our (conservative/overestimated) detection limit for this cluster of $1.38 \times 10^5 M_{\odot}$. Moreover, if such clusters have undergone a significant mass loss (as claimed in the D08 model), then we would not be looking at the initial mass, but rather the present day values (contrary to what was assumed here). Hence, if the initial mass was significantly higher, we would expect more gas to be present in the cluster, for

⁵This value differs the original D08 scenario (as seen in §3.4.1), however, with this adjustment we take into account the Larsen et al. (2012, 2014a); Kruijssen (2015) results.

⁶We note that if we assume a slighter shorter timescale of $\Delta t_{SF}^{2G} = 0.6$ Myr our simple model is in good agreement with D08 predictions.

example if the cluster has already lost 50% of its initial mass, then these estimates would increase by a factor of 2.

CS11 suggest that Δt_{SF}^{2G} must be long ($\sim 100 - 300$ Myr) as the Lyman-Werner flux density from the first generation stars will be too high to allow the gas/dust to cool sufficiently to form stars. In this case, we would have expected to detect large amounts of gas ($> 10\%$ of the stellar mass) within all three of the clusters observed in the present work, in contrast to what is observed (an upper limit of $< 9\%$ of the stellar mass).

This simple “toy model” demonstrates the general bounds that may be expected in the AGB scenario. The actual amount of gas within the cluster depends critically on 1) the assumed SFE and 2) the time of which the ISM may exist within the cluster before being expelled or used to form 2G stars.

3.4.2.1 Summary of the toy model and comparison with previous works

Our “toy model” was developed to find the *minimum amount of gas* during the formation of a 2G needed to form the number of stars with enriched abundances (a.k.a. 2G stars in the AGB scenario) seen today in a GC. In this model we have assumed that at every Δt_{SF}^{2G} , 1/3 of all gas (regardless of its origin i.e., either ejected by AGB stars or accreted from the pristine gas reservoir) is turned into stars, while the remaining 2/3 of the gas will be lost from the cluster (this could be by means of any of the mechanisms mentioned in §3.4.5). Nevertheless, this is just an assumption. However, if this material is not cleared away from the cluster, but instead remains within the cluster, it could build up over time.

This alternative has been modelled and thoroughly developed by D08. Here, the authors assume that the gas that has not found its way into a star (i.e. 2/3 of the total gas in our case) remains in the cluster. Perhaps this material is too warm to form stars yet, but the key issue here is that it has not been expelled from the cluster (in D08 this gas will eventually cool and start forming new stars)⁷. This process results in the accumu-

⁷If the gas can cool, and remains in the cluster, it will eventually form new stars. Hence, even if the

lation of gas within the centre of the cluster. However, since the gas mass and density are increasing, D08 assume that this will also have an effect on the star formation rate (SFR), with higher densities resulting in higher SFRs. This treatment is physically motivated, but of course adds some additional assumptions and parameterisations that are beyond the scope of our simple toy model.

However, if some kind of feedback is considered (which is not the case in D08 - see §3.4.5) and would have kept the gas from cooling (so that it cannot form new stars, but it does remain in the cluster), then the gas mass will increase as a function of time inside the cluster (e.g., as in the CS11 scenario). The longer the gas accumulates within the cluster the easier it would be to detect it. Additionally, if the gas temperature increases (due to the feedback mechanism, e.g., Lyman-Werner flux) then the gas would be easier to detect, for a given amount of gas mass, with the type of observations used in the current work. Although perhaps our toy model might be considered less physically motivated than assuming some fraction of gas is retained, *we note that this approach provides a lower limit to the amount of gas expected in the cluster at any given time.*

Finally, we must remark that our unsophisticated model is in no way meant to replace the ones provided by D08/D’Ercole et al. (2010) or CS11 which are much more physically motivated, which is the reason we why we have chosen to compare against them. Nevertheless, we have shown that this simple description in our “toy model” is able to reproduce the same processes as the more elaborate model of D08, without the need to include further unconstrained parameters. Here we have shown that a good agreement is achieved between D08 model and our “toy model”, if one adopts a relatively short Δt_{SF}^{2G} of 0.6 Myr.

3.4.3 Accretion of pristine gas

CS11 have presented a model for how pristine gas may be continuously accreted at a (nearly) constant rate by the GC in order to dilute the AGB ejecta within the cluster,

SFE is low per unit time in this model (D08), it can approach unity over the full formation epoch of the 2G (assumed to be 50 Myr in this case).

and form 2G stars (such strong dilution is required on chemical grounds, e.g. D’Ercole et al. 2010). In the CS11 model, young GCs contain 10% of their initial stellar mass in gas within the cluster, and this gas acts as a net as the cluster passes through the galactic ISM, picking up further pristine material. In this case, the clusters would always be expected to have $> 10\%$ of their stellar mass in gas within them, which would be above our detection limit. Hence, this scenario is not consistent with the observations presented here.

Moreover, D’Ercole et al. (2011) have shown that any model with nearly constant accretion of pristine gas can not reproduce the observed abundance trends found in GCs. Instead, the accretion of pristine gas must be finely tuned, i.e. it cannot contribute significantly until ~ 20 Myr after the 2G begins to form. This allows for the most enriched 2G stars to form entirely from (super)AGB ejecta, while subsequent 2G stars form from a combination of AGB ejecta and pristine gas, which dilutes the abundances, and turns the predicted correlation between Na-O from AGB stars, into an anti-correlation (as mentioned in §3.4.1).

3.4.4 D’Ercole et al. (2008) prediction of the gas reservoir mass

From Fig. 3 of D08, we obtained an estimate of the amount of gas expected to be found in a young (100 Myr) massive ($10^6 M_{\odot}$) cluster, integrating the gas density profile in a radius of 25 pc (approximately the size of our beam radius). We obtained $\sim 1500 M_{\odot}$ of gas, which corresponds to a reservoir of molecular gas of $\sim 0.15\%$ of the stellar mass at an age of 100 Myr. This implies an extremely rapid Δt_{SF}^{2G} ($\Delta t_{SF}^{2G} \simeq 6 \times 10^5$ yr, see §3.4.2). As discussed in CS11, such rapid turn-over from accreted/ejected gas to stars, is likely optimistic, as it ignores the large heating effect of evolving first generation stars, i.e. stellar feedback.

In D08 the only heating source in the standard model was the thermalisation of the kinetic energy of the stellar winds. D08 ran additional models with “extra energy sources” (e.g. X-ray binaries and planetary nebulae nuclei) and found that such heating may terminate any 2G star formation (above certain threshold). However, detailed

models are required to understand the exact efficiency of stellar feedback on any material residing in the cluster. Such models have yet to be done for young GCs, however McDonald & Zijlstra (2015) have run these models for older GCs and have found that stellar feedback is very efficient at clearing out gas/dust within the cluster. Since the feedback at young ages (< 200 Myr) is significantly higher than at ~ 10 Gyr, it is likely that it can provide an effective gas/dust clearing mechanism, potentially explaining the results presented here.

Nonetheless, due to the lack of heating included in the current D08 model, the accreted/ejected gas can sink in the very centre of the cluster (< 0.1 pc), where the gas density becomes extremely high, leading to rapid and efficient star-formation. Additionally, this model assumes that the 2G of stars only make up $\sim 3\%$ of the initial mass of the first generation, which needs to be increased in order to match the relative numbers of 1G/2G stars in some clusters.

3.4.5 Why are YMCs gas free?

As mentioned in the previous section, D08 studied the possibility of models with extra energy sources (only the wind thermalisation energy was included in the standard model). They concluded that if a critical value of $Q_{cr} = 2 \times 10^{36}$ erg/s was exceeded, a $10^6 M_{\odot}$ cluster would abruptly transition from a model hosting a cooling flow, which would be collecting the AGB ejecta in the centre of the cluster, to a model hosting a wind (i.e. expelling the material from the cluster). Furthermore, they arrive at the conclusion that if a luminosity of $Q = 1.38 \times 10^{37}$ erg/s were to be reached within a massive ($10^7 M_{\odot}$) cluster, the immediate onset of a fast wind would preclude the formation of any 2G⁸. These authors proposed X-ray binaries as a possible source of this energy.

Power et al. (2009) studied the role of high mass X-ray binaries (hereafter, HMXBs) in the first few hundred Myr of GCs. In their Fig. 2, one can see the evolution of the H

⁸The equivalent value for a $10^6 M_{\odot}$ cluster was not provided in D08, but we assume it would be below this $Q = 1.38 \times 10^{37}$ erg/s limit.

ionizing photon rate over time, produced by the HMXB population of a $10^6 M_{\odot}$ cluster. In this plot one can see that even if only 50% of the high mass binaries that survive the SNe of the primary star of the binary system become HMXBs (it is assumed that only 1/3 of binaries will survive the primary SNe, i.e. $\sim 15\%$ of the initial high mass binary population), one would expect to have $Q \sim 1.5 \times 10^{40}$ erg/s and $Q \sim 2.2 \times 10^{38}$ erg/s at 30 and 80 Myr respectively. From this we see that, during the timescale where the 2G is expected to be form in D08, these Q values are several order of magnitude above the threshold ($Q_{cr} \sim 10^{36}$ erg/s) necessary to stop the star formation of the 2G in these $10^6 M_{\odot}$ clusters. However, a crucial parameter that requires further modelling is what fraction of this energy is transferred to the ISM within the cluster, and what fraction escapes the cluster directly.

This makes HMXBs a potential candidate to explain why these clusters appear to be gas free. This possibility is reinforced when considering that in these environments a single HMXB source has a typical luminosity in excess of $L_X \sim 10^{38}$ erg/s (e.g. Fabbiano et al. 2001; Wolter & Trinchieri 2004; Rangelov et al. 2012).

Another plausible mechanism able to remove the gas from the cluster could be ram pressure stripping by the ISM around the cluster, as shown in CS11. Originally, this mechanism would not be effective for the D08 scenario as it stands, due to the fact that in this model most of the gas gathered by the cooling flow would be concentrated in the innermost region ($\lesssim 0.1$ pc) of the cluster. Such an extremely concentrated volume of gas would not be sensitive to the influence of ram pressure, since this mechanism is heavily dependent on the surface area/cross section of the gas within the cluster. Hence this effect can be neglected for the current version of this model. Nevertheless, this changes if the gas were to occupy a larger volume within the cluster. For example, if this gas were to be exposed to heating (some sort of stellar feedback, currently not considered in this model e.g., Lyman-Werner photons) it would be reasonable to expect the density of this gas to decrease, and as a consequence, to cover a larger volume within the young cluster. Therefore, if this (heated) gas would now cover the central 1 pc of the cluster, the new surface of this gas would have increased by a factor of 100, and the effect of the ram pressure would increase as well in the same proportion. To

summarise, if the gas ejected by the polluter stars were not to be concentrated in a very small volume at the centre of the cluster, it is likely that the ram pressure stripping by the ISM surrounding the cluster would play a non-negligible role in the expulsion of some the gas out of the cluster.

For the moment, we can not provide a definitive answer to why YMCs are gas free, and in order to reach a definite conclusion on the possible explanation of this phenomenon, we require further studies that are beyond the scope of the current study. Nevertheless, we have shown that at least these two possibilities could play a role in its answer and should be contemplated in future studies.

3.5 Conclusions from Cabrera-Ziri et al. (2015)

We use ALMA CO(3–2) observations to search for cool gas within three young massive clusters in the Antennae merging galaxies. Some scenarios for the formation of the observed multiple populations in GCs predict that such YMCs should contain significant amounts of cool gas ($\geq 10\%$ of the initial stellar mass of the system) within them in order to form multiple generations of stars (e.g. D08, CS11). The observations of clusters W31730, W32604 and W32187 used in the current work provide upper limits of $\sim 1 \times 10^5 M_{\odot}$ of H_2 gas within the three clusters or 7.4, 8.8, and 7.3 % of their stellar mass, respectively. We note, however, that the adopted X_{CO} may be overestimated by up to an order of magnitude, which would decrease the measured upper limits by the same amount.

We have estimated the amount of gas that is expected to be present within the clusters, in various versions of the AGB scenario, and found that the exact amount depends crucially on a number of assumptions and uncertainties (e.g. the amount of first generation stars lost, star-formation efficiencies, stellar IMF variations), hence we cannot reach definitive conclusions regarding the AGB model in general.

For the D08 scenario, the results from W31730 and W32604 clusters are consistent with their prediction. However, if one were to adopt less extreme values for the main

parameters at play in the model (e.g. IMF, SFE, fraction of enriched/non-enriched stars, 1G and 2G mass loss, etc.) instead of the adopted by the authors, one would expect significant amounts of gas in these young clusters (as shown in §3.4) which would be easily detectable by our observations. On the other hand, cluster W32187 (200 Myr) in principle would lie outside the timescale for the formation of the 2G adopted in this scenario (30–80 Myr) established by the first SNe Ia explosions. Having said that, we should emphasise that the timescale of these prompt Ia SNe is highly unconstrained, and in this model there is nothing inherent in the 80–100 Myr values adopted. Current evidence suggests that these events could start as soon as just $\sim 40 - 50$ Myr or as late as 400 Myr after the 1G was formed (e.g. Ruiter et al. 2013; Maoz et al. 2010; Brandt et al. 2010). Hence, the results from this particular cluster have a constraining effect in D08 as well. Ultimately, the CS11 AGB scenario predicts gas masses well in excess of the upper limits provided here (during these ages), hence our results are in strong tension with this model.

The lack of evidence of any cold gas within these clusters suggest, that the actual levels are below our detection limits. This could be due to heating by stellar feedback and/or subsequent stripping i.e. ram pressure (CS11, Power et al. 2009; McDonald & Zijlstra 2015). However, further full radiative transfer calculations are required to assess the precise magnitude of these effects.

Although the constraints placed by our ALMA observations are not conclusive in ruling out the AGB scenario, we note that they are in agreement with a growing number of studies that have not found evidence of extended (or multiple) star-formation episodes within massive clusters. For example, no evidence of ongoing star formation has been detected (down to limits of few percent of the mass of the first generation) in young ($10^6 - 10^9$ yr) massive ($10^4 - 10^8 M_{\odot}$) clusters (cf. Bastian et al. 2013c). Also, Cabrera-Ziri et al. (2014) used an integrated optical spectrum of massive ($> 10^7 M_{\odot}$) young (~ 100 Myr) cluster, in order to estimate its star-formation history. The cluster was found to be consistent with single stellar generation, with no evidence of a secondary burst down to mass ratios of 10–20% of the current cluster mass. Additionally, Bastian & Silva-Villa (2013) and Niederhofer et al. (2015) have searched for evidence of age

spreads in resolved massive LMC/SMC clusters, and found that all are consistent with a single burst of star-formation. Altogether, the evidence from observations of YMCs places strong constraints on the AGB scenario, ruling out large areas of parameter space.

Chapter 4

Abundance variations in young massive clusters

As mentioned above, none of the models seeking to explain MPs within GCs explicitly invoke “special” conditions (for example, conditions only found in the early universe), suggesting that the same mechanisms should be operating in young massive clusters (YMCs) today. This makes YMCs ideal places to test GC formation theories (e.g. Sollima et al. 2013). Additionally, since both metal-rich (bulge) and metal-poor (halo) GCs have been observed to host MPs, and since they likely formed in very different environments and at different redshifts (e.g. Brodie & Strader 2006; Kruijssen 2014), it appears likely that the process of the formation of MPs is related to the clusters themselves, and not their host environment (cf. Renzini 2013). Consequently, the same MPs should be observable in YMCs forming in the present day.

To date, there has been no conclusive evidence of multiple episodes of star formation in YMCs (e.g. Bastian et al., 2013c; Niederhofer et al., 2015; Cabrera-Ziri et al., 2014, 2016a,b). Nor has any evidence been found of gas reservoirs within YMCs that could fuel extended star-formation episodes with the masses suggested by the formation scenarios listed above (e.g. Bastian & Strader 2014; Cabrera-Ziri et al. 2015). These studies have called into question the proposed scenarios, however, *they have not tested whether the distinctive chemical patterns characterising MPs are present within these*

clusters.

So far, no evidence of the characteristic GC abundance patterns has been found in the Milky Way open clusters in the Galactic disk (de Silva et al., 2009; Pancino et al., 2010; Magrini et al., 2014, 2015; Maclean et al., 2015); more massive ($\sim 10^4 M_{\odot}$) old open clusters were targeted by Bragaglia et al. (2012) (Berkeley 39, ~ 6 Gyr) and Bragaglia et al. (2014); Cunha et al. (2015) (NGC 6791, ~ 9 Gyr). None of these studies found signs of stars with “polluted chemistry”. Furthermore, the LMC intermediate-age (1–2 Gyr, $> 10^5 M_{\odot}$) clusters NGC 1806, 1651, 1783, 1978, and 2173 do not show signs of GC-like abundance patterns (Mucciarelli et al., 2008, 2014). *This lack of evidence of MPs in younger clusters has been suggested to be due to the fact that they have lower mass/density than the ancient GCs* (e.g. Krause et al., 2016). However, these studies have shown that a sharp mass/density limit does not apply, as there exists overlap of these properties between the samples with and without MPs.

There are clusters that are forming in the nearby universe with masses well in excess of $10^6 M_{\odot}$ (e.g. in the Antennae Galaxies; Whitmore et al. 2010). These clusters have properties similar to those expected for young GCs (cf. Schweizer & Seitzer 1998; Portegies Zwart et al. 2010), and hence we may expect that they also have formed MPs.

The traditional method to find and quantify the signatures of star-to-star abundance variation has been via high-resolution spectroscopy of individual stars in a cluster. Young clusters with masses and densities similar to early GCs are only found in external galaxies. Due to their distances (tens of Mpc), a detailed abundance analysis of their individual stars is not possible with the instrumentation currently available. While we cannot resolve these clusters into their constituent stars, Cabrera-Ziri et al. (2016c) employed a method, the *J*-band technique, devised to allow us to look for chemical anomalies, i.e. the MPs, within these clusters using their integrated near-infrared (NIR) spectrum.

4.1 RSG stars and YMCs

Davies et al. (2010) developed a technique, a.k.a *J*-band technique, whereby chemical abundances of red supergiants (RSGs) may be extracted from a narrow spectral window around $1 \mu\text{m}$ from low resolution data ($R \sim 3000$). The method is therefore extremely efficient, allowing stars at large distances to be studied, and so has tremendous potential for extragalactic abundance work. Several studies have shown that the *J*-band technique rivals the precision (± 0.1 dex) of metallicity measurements using Blue Super Giants (frequently used to determine metallicities beyond the Local Group) and is applicable over similar distances (several Mpc) with existing instruments (Gazak et al., 2015; Lardo et al., 2015).

The effective temperatures of the RSGs are constant to within ± 200 K (Davies et al., 2013) and do not depend on the stellar metallicity (Gazak et al., 2015). Within a cluster, characterised by a SSP, the RSGs all have similar luminosities and virtually identical masses, and therefore similar gravities. *In other words, for a given metallicity and stellar mass, RSGs have almost identical spectra in the J-band.*

Our method to search for MPs in YMCs exploits the fact that “RSGs all look the same”¹. So, if the mechanisms responsible of the GCs abundance variations (i.e. MPs) are in force today, and we were to compare RSGs from the field with the integrated light spectra of young clusters dominated by RSGs, we would expect to find both spectra very similar (i.e. to have similar Fe, and most of metals), and only see differences in the abundances of the elements that vary within GCs (i.e. C, N, O, Na and Al). These abundance differences will be due to the contribution of “polluted” RSGs to the integrated light of the cluster.

¹This is only true within a single stellar population. If there were a range in masses they will have different effective temperatures and luminosities.

4.2 XSHOOTER data

We will focus this pilot study on a young (~ 15 Myr) massive ($\sim 10^6 M_{\odot}$) cluster in NGC 1705, a blue compact dwarf galaxy 5.1 Mpc away, with a metallicity similar to the Small Magellanic Cloud (SMC, e.g. Annibali et al. 2009). For our analysis we use archival NIR spectroscopic data of the cluster NGC 1705: 1 obtained on Nov 23rd 2009 with the XSHOOTER spectrograph on the Very Large Telescope under ESO programme number 084.B-0468(A) (PI S. S. Larsen). The cluster was observed in a single AB nodding cycle, using the 0.9 arcsec \times 11 arcsec slit placed at parallactic angle. The total exposure time was 600 s, during which the airmass increased from 1.32 to 1.35 and the seeing from 0.98 arcsec to 1.17 arcsec. Flux standard stars were also observed and to correct for the atmospheric absorption in the NIR, telluric standard stars of spectral type late-B were observed within one hour of each science target. The data reduction consisted of subtraction of bias and dark frames, flat-fielding, order extraction and rectification, and flux and wavelength calibration. This was carried out using the standard ESO Reflex pipeline version 2.6.0. At the end of this we achieved a SNR at the J -band of > 100 per spectral bin.

4.3 Analysis

We performed a differential analysis, comparing the J -band spectrum of NGC 1705: 1 and a representative RSG median spectrum with similar metallicity. For this, we first built a suitable comparison sample by selecting SMC RSG spectra spanning a metallicity range between $-0.24 \leq [Z] \leq -0.72^2$, similar to that of NGC 1705 (Annibali et al., 2009). These spectra were taken from Davies et al. (2015), hereafter D15. Then we calculated a median and standard deviation spectra (σ) of all the RSGs in our sample. As these RSGs do not belong to dense/massive clusters we do not expect to see in them the chemical patterns characteristic of GCs stars. Hence, if the mechanisms that are responsible for the distinct abundance patterns of GCs are still acting today

² $[Z]=\log(Z/Z_{\odot})$

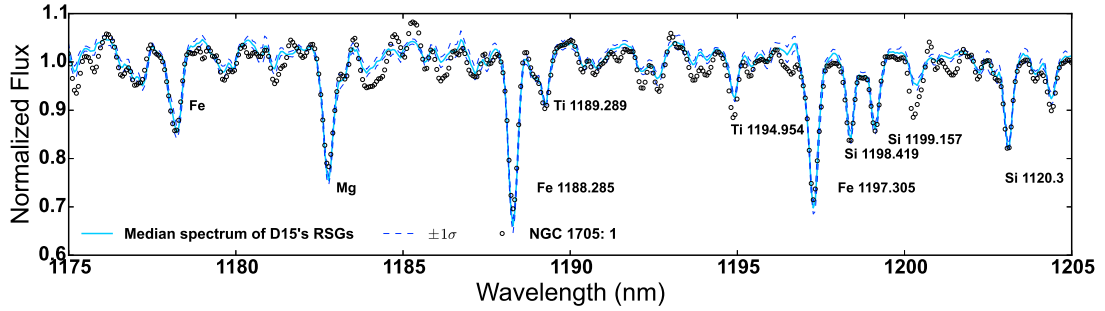


Figure 4.1: In cyan we show (part of) the median J -band spectra of the RSGs from D15. The blue dashed lines denote $\pm 1\sigma$ spectra of the D15 stars. The cluster’s spectrum is shown in black circles. All spectra have been downgraded to the same resolution ($R = 4000$). As expected, we find a good agreement between the metal lines of our cluster and the median RSG spectrum. Mg remains constant from star-to-star in most GCs, however, $[Mg/Fe]$ has been observed to be depleted in the stars of a few GCs (e.g. NGC 2808 and 7078, cf. C09). There is no evidence supporting such depletion in this cluster.

in the universe, we should observe that most metal lines (i.e. lines of species that are not seen to vary strongly in GCs – anything other than C, N, O, F, Na, Mg, Al, Si, K) should be the same in the D15 median RSG spectrum as in NGC 1705: 1, as they show no significant variation in GC stars. On the other hand, chemical species that have large variations from solar-scaled abundances in GCs (e.g. Na, O, Al and N) should be enhanced/depleted accordingly in the spectrum of NCG 1705: 1 with respect to D15 median RSG spectrum. For our analysis, all the spectra were homogenized in terms of their spectral resolution.

In Fig. 4.1, we show how the median RSGs spectrum of D15’s stars compare to the spectrum of our cluster in the region between 1175–1205 nm. As expected, we find an extremely close agreement between the metal lines of the field RSGs and our cluster, indicating that NGC 1705: 1 has a metallicity³ similar to RSG stars in the SMC. We also made use of the J -band technique (Davies et al. 2010, cf. §4.1) to make a quantitative assessment of the metallicity of this cluster and its uncertainty, yielding $[Z] = -0.4 \pm 0.1$ dex.

³Assuming that Fe, Mg, Si and Ti abundances from individual lines are representative of the metallicity Z .

4.3.1 Expectations from different GCs

Al is the only element, with strong lines in the NIR spectrum of RSGs, that shows significant abundance variations in GC stars. Na and O are other elements with evidence of strong variations from star-to-star in GCs. However, there are no Na lines in the J -band spectra of RSG. RSGs in a cluster of this age (~ 15 Myr) still contribute $\sim 50\%$ of the light in the regions where optical Na and O lines (like NaI doublets at 5682-88 Å and 6154-60 Å; and [OI] 6300 and 6363 Å lines) are found. However, carrying out a similar analysis as in the J -band is not possible, as one would need to consider how the rest of the stellar population (i.e. all other stars that are not RSGs) affect these spectral regions. Additionally, the variations in these particular lines (i.e. the difference between a star with “polluted chemistry” and a regular one) are not as large as the ones observed in the NIR Al lines. All this makes this kind of analysis significantly more complex to carry out on such features.

Extreme differences (> 1 dex) in [Al/Fe] have been observed in the stars of some GCs e.g., M 54, NGC 2808, M 80, NGC 6752 and NGC 6139 (see below). We show in Fig. 4.2, that the Al lines from NGC 1705: 1 do not show a significant enhancement when they are compared to field RSGs of similar metallicity. This is contrary to what one would expect if there were RSGs with a range of Al abundances similar to that of the GCs mentioned above. To illustrate this point, we have computed exploratory model spectra of RSGs in order to investigate how these differences in the Al lines should look. For this, we used MARCS model atmospheres (Gustafsson et al., 2008), and their spectra were computed with TURBOSPECTRUM (Plez, 2012). We assumed the following parameters for our models: $T_{\text{eff}} = 3800$ K, $\log g = 0.5$ dex, $[Z] = -0.5$ dex, $\xi = 2.0$ km s $^{-1}$, $[\alpha/\text{Fe}] = 0.0$ dex⁴ and vary the Al abundances simulating the enhancement expected of some GCs. We note that these models were not intended to measure absolute Al abundances, rather to estimate what type of variations we might expect if there were GC-like chemical anomalies in this YMC.

⁴While the assumption of a solar-scaled composition is reasonable, we expect that the errors arising from the assumption of a solar-scaled rather than an α -enhanced one has a negligible impact (within the quoted 0.1 dex errors in metallicity) on the metallicity determination (Lardo et al., 2015).

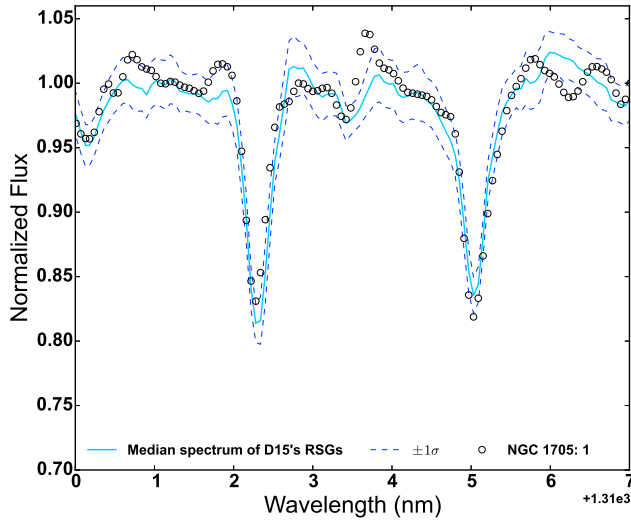


Figure 4.2: Similar to Fig. 4.1 but centred around two prominent Al lines (1312.338 and 1315.071 nm). These lines in NGC 1705: 1 and D15’s RSGs are in agreement within the observational uncertainties. This is not what would be expected if the Al of this cluster were enhanced significantly as is often observed in some GCs.

With these models we synthesised how the NIR spectra of GCs with different ranges of [Al/Fe] spread would look at young (~ 10 Myr) ages. We assumed for our calculations that 1) the ratio of enriched to non-enriched stars of young GCs is the same as the one observed today (i.e. $\sim 70:30\%$ cf. Carretta et al. 2009a; Bastian & Lardo 2015) and 2) all RSGs that dominate the NIR light of the cluster at this age had the same luminosity.

For this experiment we have compiled a homogenous sample of [Al/Fe] abundances for 25 GCs from the literature. The median number of stars per GC analysed in this sample was 12 (with a minimum of 4 stars for M79 and a maximum 100 stars for NGC 6752). We divide the [Al/Fe] spread observed in GCs in three ranges: moderate (e.g. NGC 288, M 4, M 79, or M 107); intermediate (e.g. 47 Tuc, M 12 or M 71) and extreme (e.g. NGC 2808, NGC 6752 and M 54). We define these ranges according to the difference, $\Delta[\text{Al/Fe}] = \text{mean}([\text{Al/Fe}]) - \text{min}([\text{Al/Fe}])$, between the mean [Al/Fe] abundance and the pristine [Al/Fe] abundance for the stars in these clusters. The moderate, intermediate and extreme ranges have values of $\Delta[\text{Al/Fe}] = 0.1, 0.3$ and 0.7 dex respectively. The clusters in this sample, their spreads and references are listed in Table 4.1.

In Fig. 4.3 we show the model spectra of RSG with solar Al abundance, i.e. [Al/Fe] = 0.0 dex; and Al abundances enhanced by 0.1, 0.3 and 0.7 dex, corresponding to the synthetic spectrum expected for young GCs with moderate, intermediate and extreme [Al/Fe] ranges respectively. The $\Delta[\text{Al/Fe}]$ expected for each young GC is also found in the figure.

Table 4.1: Metallicity and [Al/Fe] spreads (Δ [Al/Fe], standard deviation and maximum [Al/Fe] variation, $\Delta_{\max}([Al/Fe])$) for GCs.

Cluster	[Fe/H] (dex)	Δ [Al/Fe] (dex)	σ ([Al/Fe]) (dex)	$\Delta_{\max}([Al/Fe])$ (dex)	Reference
47 Tuc (NGC 104)	-0.77	0.27	0.16	0.67	(4)
NGC 288	-1.30	0.12	0.08	0.28	(4)
NGC 362	-1.17	0.28	0.18	0.56	(8)
NGC 1851	-1.18	0.31	0.20	0.59	(6)
M 79 (NGC 1904)	-1.57	0.09	0.07	0.20	(4)
NGC 2808	-1.15	0.71	0.46	1.32	(9)
NGC 3201	-1.53	0.57	0.29	0.81	(4)
NGC 4833	-2.01	0.57	0.32	0.81	(11)
M 3 (NGC 5272)	-1.54	0.76	0.33	1.26	(15)
M 5 (NGC 5904)	-1.34	0.48	0.28	0.82	(4)
M 80 (NGC 6093)	-1.79	0.57	0.33	1.22	(12)
M 4 (NGC 6121)	-1.17	0.10	0.05	0.20	(4)
NGC 6139	-1.59	0.69	0.25	1.17	(16)
M 107 (NGC 6171)	-1.03	0.11	0.07	0.20	(4)
M 13 (NGC 6205)	-1.57	0.77	0.36	1.16	(15)
M 12 (NGC 6218)	-1.33	0.35	0.17	0.66	(4)
M 10 (NGC 6254)	-1.57	0.41	0.22	0.60	(4)
NGC 6388	-0.44	0.51	0.23	0.75	(2)
NGC 6441	-0.39	0.15	0.13	0.37	(13,14)
M 54 (NGC 6715)	-1.51	0.95	0.57	1.37	(5)
NGC 6752	-1.51	1.06	0.43	1.65	(1,7)
M 55 (NGC 6809)	-1.93	0.27	0.17	0.52	(4)
M 71 (NGC 6838)	-0.84	0.29	0.14	0.50	(4)
M 15 (NGC 7078)	-2.36	0.57	0.30	0.93	(15)
Terzan 8	-2.27	0.23	0.17	0.50	(10)

(1) Carretta et al. (2007a); (2) Carretta et al. (2007b); (3) Carretta et al. (2009a); (4) Carretta et al. (2009b); (5) Carretta et al. (2010c); (6) Carretta et al. (2011); (7) Carretta et al. (2012); (8) Carretta et al. (2013); (9) Carretta (2014); (10) Carretta et al. (2014a); (11) Carretta et al. (2014b); (12) Carretta et al. (2015); (13) Gratton et al. (2006); (14) Gratton et al. (2007); (15) Mészáros et al. (2015); (16) Bragaglia et al. (2015)

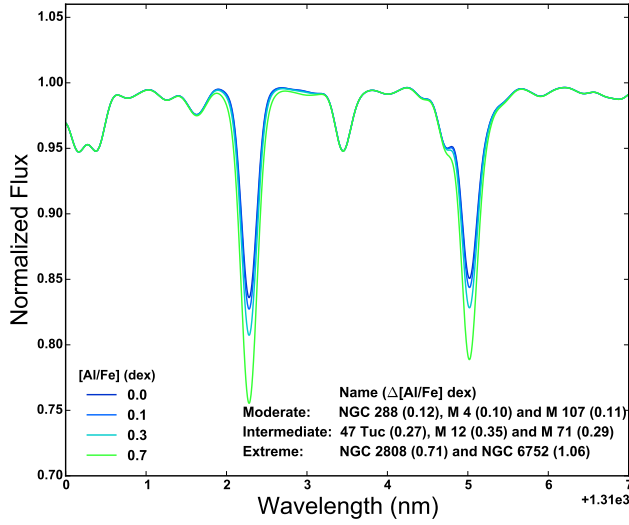


Figure 4.3: RSG models with solar-scaled (0.0 dex – as expected for the D15 RSGs) and enhanced (>0.0 dex) $[Al/Fe]$ values. We can exclude at high confidence that NGC 1705: 1 have extreme values of $[Al/Fe]$ (like NGC 2808 or NGC 6752) that depart from the solar-scaled $[Al/Fe]$ abundance of the RSGs from D15, cf. Fig. 4.2.

We conclude that if in NGC 1705: 1 there were RSGs with an extreme $[Al/Fe]$ spread, i.e. spreads similar to those expected for GCs like NGC 2808 and 6752 at young ages, we would expect to see differences between the RSGs and NGC 1705: 1 in Fig. 4.2, similar to those found between solar-scaled ($[Al/Fe] = 0.0$ dex) and extreme ($[Al/Fe] = 0.7$ dex) RSG models from Fig. 4.3. We can exclude such extreme spreads in $[Al/Fe]$ at high confidence, as the Al lines appear to be consistent with the SMC stars to within ± 0.3 dex.

4.3.2 $[Al/Fe]$ spreads: results from YMCs in the context of GCs

In this section we compare the observed $[Al/Fe]$ spreads observed in GCs with our constraints on the maximum $[Al/Fe]$ spread consistent with our observations of NGC 1705: 1.

In Fig. 4.4, we plot the observed spread of $[Al/Fe]$ in GCs as a function of the cluster $[Fe/H]$. We find a slight correlation between $\Delta[Al/Fe]$ and $[Fe/H]$ (this is also the case for the standard deviation of the $[Al/Fe]$ - bottom panel cf. Fig. 4.4 caption)⁵. We have also overplotted as a yellow upper limit our results for NGC 1705: 1. It seems that this YMCs is in agreement with what is expected for (old) GCs of similar metallicity.

⁵Pancino et al. (2017) in an homogeneous analysis of 28 GCs with an average of ~ 50 stars each (about twice our sample size), removed any remaining doubt on the fact that the extent on the Al-spread is a function of $[Fe/H]$ and cluster mass.

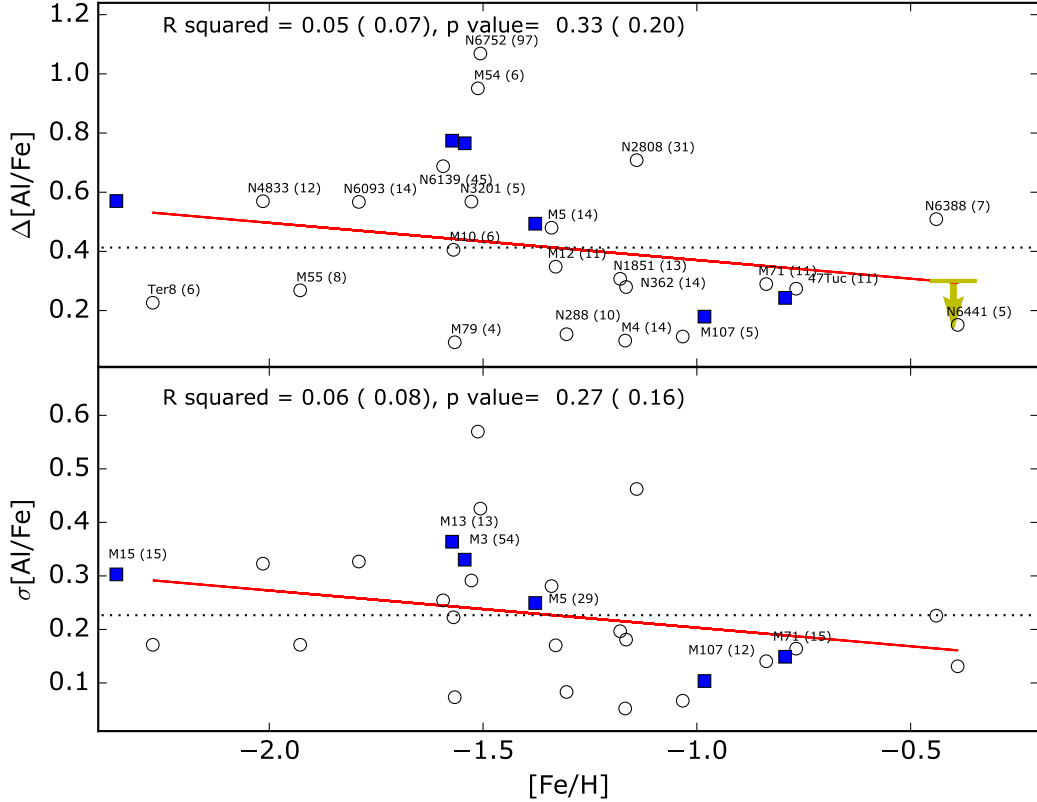


Figure 4.4: Top panel: $\Delta[\text{Al}/\text{Fe}]$ as a function of $[\text{Fe}/\text{H}]$. The upper limit for the Al spread in NGC 1705: 1 according to our analysis is shown as an upper limit. Bottom panel: Standard deviation σ of the $[\text{Al}/\text{Fe}]$ values for the stars of these clusters. The open circles represent the abundances derived by Carretta and collaborators, while the blue squares represent the Mészáros et al. (2015) APOGEE sample (blue squares). In brackets we show the number of stars with available $[\text{Al}/\text{Fe}]$. The red line is a linear fit to the Carretta data. The Pearson’s correlation coefficient is shown on the top left corners of both panels; in both cases the (anti)correlation is very weak. We also show the p-value between these distributions ($[\text{Fe}/\text{H}]$ vs. Al-spread) and one with no correlation (i.e., Pearson’s correlation coefficient = 0). We conclude that the observed Al-spread vs. metallicity distribution does not show a significant difference with respect an uncorrelated distribution, i.e. p -values > 0.25 . The values in parentheses are computed with the inclusion of the GCs M 3, M 13, and M 15 to the Carretta sample. Note that M 5, M 71 and M 107 are in common between the two datasets, thus we considered the $\Delta[\text{Al}/\text{Fe}]$ drawn from the Carretta sample to perform the fit.

4.4 Discussions and conclusions from Cabrera-Ziri et al. (2016c)

From our differential analysis of the integrated J -band spectrum of NGC 1705: 1 presented in §4.3.1, we are not able to distinguish if this YMC is more consistent with a solar $[Al/Fe]$ content or if it has a moderate or intermediate $[Al/Fe]$ enhancement range in their RSGs (i.e. $[Al/Fe] = 0.1, 0.3$ dex; respectively), like the one observed in GCs of similar metallicity cf. Fig. 4.4. In principle we can not exclude any of these possibilities (cf. Fig. 4.3). We note that from the homogeneous sample presented in Table 4.1, we find that 11 clusters ($\sim 44\%$) namely (NGC 2808, NGC 3201, NGC 4833, M 3, M 80, NGC 6139, M 13, NGC 6388, NGC 6752, M 54, NGC 7078) have extreme $[Al/Fe]$ spreads, i.e. $\Delta[Al/Fe] > 0.5$ dex, while the others have intermediate or moderate $[Al/Fe]$ spreads.

So according to this sample there is a 44:56 chance that the RSGs producing most of the NIR light in this cluster have an intermediate or moderate spread in $[Al/Fe]$. Going through a similar analysis on a larger sample of YMCs will allow us to find YMCs with extreme $[Al/Fe]$ spreads (like GCs NGC 2808 or NGC 6752), if such objects were to exist.

Alternatively if the analysis of a robust sample of YMCs were to yield the same result, i.e. all clusters having solar $[Al/Fe]$ abundances, this would lead to the following possibilities:

- All YMCs do host MPs, but only display moderate $[Al/Fe]$ spreads in their RSGs. This is highly unlikely as GCs show different levels (moderate, intermediate and extreme) of $[Al/Fe]$ spreads.
- GC stars in the RSG evolutionary stage do not show MPs. However, there is no reason in principle for this to happen, as there is evidence of MPs in GC stars at all evolutionary phases cf. P15.
- The mechanism producing extreme $[Al/Fe]$ spreads only kicks in (or makes them

evident) after ~ 15 Myr, i.e. the age of this cluster. This is the case for the D’Ercole et al. (2008) scenario to explain MPs in GCs (happening after few tens of Myr).

Or alternatively, for some reason the MPs do not become visible until after ~ 10 Gyr of evolution. As it has not been found in open or intermediate age clusters so far (cf. §4).

- The enriched population is only found in the $\sim 0.2\text{--}0.8 M_{\odot}$ stars of massive/dense clusters, i.e. only the stars alive and to which we have access in GCs. This idea has been suggested by some scenarios trying to explain the origin of MPs, (e.g. D’Ercole et al. 2008; Bastian et al. 2013b), although these particular scenarios have been ruled out on different grounds cf. §5. In spite of that, it is still a viable option and could be readily tested in the faintest MS stars of younger massive/dense clusters like intermediate-age clusters. A first approach to test this scenario is to see if it is possible to detect, beyond observational uncertainties, a splitting/broadening in the lower MS of young (massive/dense) clusters caused by an enriched population of stars. For this to be possible, the photometric observations of young massive/dense clusters must be carried out with the appropriate set of filters (cf. Sbordone et al. 2011; P15). An alternative would be direct spectroscopic observations of these faint stars, however these observations are not possible with the current instruments. Nevertheless, if an enriched population is eventually found among the $\sim 0.2\text{--}0.8 M_{\odot}$ stars of young massive/dense clusters, one would be left with an additional problem, that is, to explain why there is a threshold in the mass for this phenomenon.
- Finally, there is the possibility that none of the stars (even the low mass ones) of open clusters, YMCs and intermediate-age clusters show GC-like enrichment, and GC stars are indeed special. Then, these anomalies might be due to some special condition/mechanism (as yet unknown) only found in the early universe, $z > 2$, where/when GC formed. This condition/mechanism, if it exists, has been overlooked so far in all GC formation scenarios to date. However, we know that it should only affect stars in massive/dense systems like GCs, and not be just a

parameter of time, as only $\sim 3\%$ of the field stars in the halo (coeval with GCs) show such abundance patterns, and these stars are thought to be GC escapees cf. Carretta et al. (2010a); Martell & Grebel (2010); Martell et al. (2011); Ramírez et al. (2012); Lind et al. (2015). But at the same time, it has not been at work (or an additional mechanism should prevent it to do so) in systems somewhat more massive than GCs, like dwarf galaxies, where no evidence of such enrichment has been found (cf. Tolstoy et al. 2009; Carretta et al. 2010b).

The study of a broader sample of clusters could settle once and for all long standing questions like: are YMCs and GCs objects of the same nature? And do both share these peculiar abundance patterns? If it turns out to be that both are the same kind of objects, only observed at different ages, this would suggest a common evolution of massive/dense clusters. This would represent a huge step forward in the understanding of the formation of clusters in the early universe, as we would have a more accessible way to get data (from YMCs in nearby galaxies) to carry out studies, compared to the challenging observations of the high redshift universe. On the other hand, if YMCs prove to have none of these abundance patterns, analysing the difference between them could lead us to reveal this unknown condition/mechanism that could be responsible for the MPs.

Additionally, we note that there have been two studies on YMCs where a detailed abundance analysis of the integrated H - and K -band spectra yielded an $[Al/Fe]$ consistent with moderate/intermediate spreads ($\Delta[Al/Fe] \geq 0.5$ dex). Larsen et al. (2006) analyzed NGC 6946-1447, a young ($\sim 10 - 15$ Myr), massive ($\sim 1.7 \times 10^6 M_{\odot}$) cluster in the nearby spiral galaxy NGC 6949, and found an abundance of $[Al/Fe] = 0.25 \pm 0.18$ dex. Larsen et al. (2008) found $[Al/Fe] = 0.23 \pm 0.11$ dex for NGC 1569-B, a young ($15 - 25$ Myr) massive ($4.4 \times 10^5 M_{\odot}$) cluster in the dwarf irregular galaxy NGC 1569. Both studies are consistent with the results of our differential analysis, i.e. no evidence of extreme Al spreads in YMCs.

We note that if this unknown condition/mechanism is to be found, we should see how it would affect the constraints placed by the studies of YMCs on the scenarios proposed

for the origin of MPs in GCs.

Finally, on a cautionary note, we stress that part of our analysis is based on two assumptions: 1) that young GCs had the same [Al/Fe] distribution, as observed today in old GCs, and 2) all RSGs that dominate the NIR emission of the young GCs have the same brightness. These assumptions need not necessarily be correct. For instance if the ratio of enriched to non-enriched stars changes significantly over ~ 10 Gyr, in such way that the non-enriched stars are strongly predominant, we might not be sensitive to detect the signatures of some few Al-enriched RSGs. The same is true if for some reason, the enriched RSGs would be fainter than the non-enriched.

Chapter 5

Present day properties of GCs and expectations from formation scenarios

After decades of research, we now have a robust picture of MPs in ‘typical GCs’ based on a combination of spectroscopic and photometric studies. This information, when compared with the expectations and predictions of the GC formation scenarios, can give us important clues on their origin. In this chapter I will briefly review the most relevant constraints on these scenarios, obtained from the present day properties of GCs and their MPs.

5.1 Predicted properties

The theoretical nucleosynthetic yields of *all proposed polluters* predict a correlation between the extent (or relative variation) of the Na-O anti-correlation and the inferred difference in the He abundances between sub-populations in a given cluster. More specifically, the depletion in [O/Fe] should be accompanied by an enhancement in He. This was reviewed in Bastian et al. (2015) where it was shown that GCs with a similar extent in the Na-O anti-correlations *do not* seem to be accompanied by the same He abundance spreads, in direct contradiction with the expectations from the theoretical yields.

Furthermore, it was pointed out that all proposed polluter sources seemed to over-produce He when compared to the inferred values for the GCs in that sample. The only exception appeared to be NGC 2808, a GC with an extreme difference in He abundances of its stars.

The authors concluded that no single polluter source in that study was able to reproduce simultaneously the [Na/Fe], [O/Fe] and He-spreads of the GCs in their sample – this is regardless of the uncertainties of the theoretical yields¹. What’s more this conclusion does not depend on the way the *polluted* material is diluted by *pristine* gas.

At the time of writing this manuscript no polluter source has been identified that can account for the properties of the GCs described in Bastian et al. (2015).

5.2 Unexpected correlations

There are a number of correlations between properties of GCs and the characteristics of their MPs that are yet not accounted for by the scenarios. For example, among the most relevant we find:

- Correlation between He enhancement with GC mass: Milone et al. (2014) found that the maximum He spread of a GC –inferred from the HB morphology– is proportional to the absolute luminosity (hence mass) of a GC.
- Ratio between subpopulations: Milone et al. (2017) in a HST survey of 57 GCs, found that massive GCs host on average a larger fraction of chemically anomalous stars than GCs of lower mass. These authors found no correlation between the fraction of chemically anomalous stars and any other global property, like metallicity or Galactocentric distance. Such lack of correlation was found as well by Bastian & Lardo (2015), although for this study the authors used spectroscopic data to distinguish between subpopulations. Contrary to the Milone et al. study which focused mainly on the innermost stars in the clusters, the Bastian

¹this conclusion is also found if one were to take the abundances of extreme population stars as the “empirical composition” of the *polluted* ejecta.

& Lardo work primarily targeted more external regions of the clusters due to the intrinsic limitations of multi-object spectroscopy of crowded fields.

It is not clear if any of these relations with cluster mass implies a causality. However, if we analyse these results in the perspective of the GC formation scenarios, such trends seem unfavourable to any of them (see discussions in Bastian et al., 2015).

5.2.1 Mass budget

Although this was already discussed in detail previously (cf. §3), it is worth emphasising the severity of this evidence in the context of the mass budget problem affecting GC formation scenarios.

The number of chemically-anomalous stars in a GC can be comparable to and significantly larger than the stars with normal chemistry within the same cluster depending on the cluster mass. This makes the mass budget problem more severe, as more massive clusters would have required significantly more *polluted* material to account for such a large fraction of these stars within these clusters. This would mean, that more massive clusters were preferentially prone to lose more of their stars² during their evolution than less massive clusters.

A similar problem is found if the maximum abundance variations of some elements correlate with cluster mass, unless there is an environmental effect –affecting only the stars in the most massive clusters– which could change the yields of *polluted* material returning to the intra-cluster medium. However, such an effect is not expected in any current scenario.

As mentioned before, some scenarios have tried to change the IMF of the first and second generation of stars to alleviate the mass budget problem, however, this still does not provides a satisfactory solution to this issue.

²i.e. the first generation stars producing the *polluted* material, which would be the overwhelming majority of the stars when the cluster is young.

5.2.2 **Comments on Schiavon et al. (2013) results**

Schiavon et al. (2013) analysed the integrated light of 78 GCs in M 31, with masses ranging from 10^5 to $10^{6.5} M_{\odot}$. The authors reported a correlation between the inferred [N/Fe] enhancement and GC mass.

One could interpret this empirical evidence in two different ways. Perhaps the simpler alternative is that the [N/Fe] of the chemically anomalous population of the Schiavon et al. (2013) sample is significantly more enhanced than the chemically normal population assuming the ratio between populations in the GC of this sample is close to 1:1.

Alternatively the [N/Fe] correlation with GC mass found by Schiavon et al. (2013) may actually reflect the fact that the most massive clusters in the sample have a significantly larger contribution of chemically anomalous stars, similar to what is observed in Galactic GCs. Hence the light weighted average [N/Fe] inferred from the analysis of integrated light, might be reflecting that a larger fraction of the stars in the cluster are enhanced in [N/Fe] compared to a cluster of lower mass. Having said this, this does not exclude the possibility that the enhancement in [N/Fe] in the stars hosted in the most massive clusters in this sample is actually larger than the [N/Fe] enhancement in less massive ones, however, the current data do not allow us to distinguish whether this is the case or not.

Chapter 6

Conclusions

The main objective of this work was to place constraints on the different GC formation scenarios, placing special emphasis on the processes proposed to explain the star-to-star variations of some light elements (commonly ascribed to the presence of multiple stellar populations).

The basic hypothesis in the models put forward to explain the multiple stellar populations in GCs is that a second generation of stars is born during the early life of the GC from the chemically processed ejecta of some first generation stars in order to account for the star-to-star abundance variations observed in old GCs today.

Given that the formation scenarios proposed to explain the origin of GC do not distinguish between star/cluster formation at the present day and that of earlier epochs of the Universe, our approach consisted in comparing the properties of YMCs forming today with the expected properties of young GCs forming ~ 10 Gyr ago with similar (and sometimes greater) masses and densities.

The main constraints from the results presented in this work regard the gas content and star formation histories of young massive clusters. Namely:

- **Search for multiple star formation burst:** I have determined the star formation history of YMCs by means of fitting stellar populations models to the integrated optical spectra with a tool we have developed (DynBaS Magris et al., 2015).

These YMCs span the age range where the secondary star-formation bursts were expected to have taken place, and also possessed the mass necessary ($> 10^7 M_{\odot}$) for holding onto the polluted ejecta –based on the escape velocity arguments proposed by the scenarios. The SFHs of these clusters were consistent with a single SF burst (cf. Cabrera-Ziri et al., 2014, 2016a), at odds with the expectations of some of the scenarios for the origin of multiple stellar populations.

Similarly in Cabrera-Ziri et al. (2016c), I analysed the CMDs of LMC/SMC intermediate-age (~ 1.5 Gyr) clusters that were previously claimed to have evidence of multiple SF events (cf. Li et al., 2016). Using various statistical arguments, I showed that these young populations are present in the field regions around the clusters, and their presence in the previous CMDs was a consequence of an insufficient background subtraction. This proved that these LMC/SMC clusters do not provide evidence of young generations of stars within these clusters which is in agreement with our previous studies of YMCs.

- **Search for fuel for multiple SF-bursts:** Constraining the cool gas content of YMCs is crucial, as it tells us whether or not YMCs have the necessary material to undertake subsequent SF events attributed to the origin MPs in GCs. In Cabrera-Ziri et al. (2015), I used deep ALMA CO(3–2) observations of the overlap region of the Antennae galaxies to look for the predicted gas reservoirs within YMCs. No significant CO(3-2) emission was found in any of the YMCs, in tension with the scenarios that expected large gas reservoirs within YMCs.
- **Search for abundance variations in YMCs:** These previous studies were centred on testing the MPs formation scenarios, however they have not tested if the YMCs host MPs. In Cabrera-Ziri et al. (2016b), I used a technique to detect MPs efficiently (in a single observing night) in YMCs up to tens of Mpc away with existing instrumentation. With the next generation of instruments on the extremely large telescopes this technique could be applied in YMCs forming as far as the Coma cluster (~ 100 Mpc or $z \sim 0.02$, cf. Evans et al., 2011). The technique uses the integrated J -band spectra of YMC dominated by RSGs, and it allows us to look for evidence of the most extreme abundance variations found

in GCs (i.e. the young equivalents of clusters like NGC 2808 and NGC 6752).

From these results it is possible to conclude that the scenarios proposed to explain the origin of MPs fail to reproduce the observations of YMCs. Moreover, they all share other severe handicaps, like the “mass-budget problem”, a mismatch between the predicted abundance patterns and the observed ones, and also the inability to reproduce the observed fraction of chemically anomalous stars in GCs.

Overall, it can be concluded that currently there is no scenario proposed to explain the origin of GCs and their MPs that can fit satisfactorily all the evidence from the present day properties of GCs or the observed characteristics of YMCs.

As a by-product of our effort to understand the formation of GCs we have gathered a lot of evidence about the properties of YMCs and intermediate-age clusters. This suggests that YMCs and intermediate-age clusters formed in a very short timescale, and their giant stars seem to be chemically homogeneous. This implies perhaps that YMCs are the best example of single stellar populations in this sense, i.e. there is a negligible age spread among their stars and all seem to share a homogeneous chemical composition.

With all this evidence in hand, it is still not clear if YMCs are equivalent to young GCs or are a different kind of objects. This allows the possibility that GC formation is indeed special, and for some unknown reason it is not able to operate in the present universe.

6.1 Future work

Since none of the proposed scenarios for the formation of GCs appear to be viable, it is important to determine when/where such MPs exist, which may help determine their origin. Thus, a good way to gain some new understanding of the physics responsible of this phenomenon is to: 1) map the incidence of MPs across GC parameter space, emphasising unexplored loci, to unveil the physics of MP emergence and 2) explore

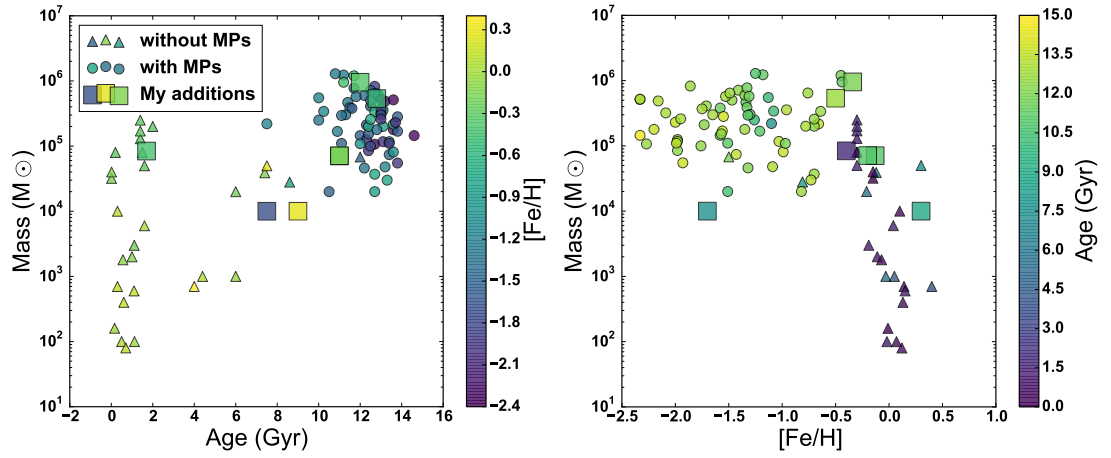


Figure 6.1: Left: Cluster mass vs. age, colour-coded is [Fe/H]. Circles and triangles represent clusters with and without MPs, respectively. The square symbols are the first clusters that could be studied in the future (data already available). Right: Cluster mass vs. [Fe/H], colour coded is the age of the cluster. Data taken from Krause et al. (2016).

the occurrence of similar mean abundance patterns in elliptical galaxies to check for a possible common origin.

Regarding the first point I propose to explore new regions (see Figure 6.1) of the parameter space:

- **High [Fe/H] GCs:** Currently the metal rich end of the Galactic GC population remains severely understudied in the context of MPs, with most studies covering only GCs in the range $-2.4 < [\text{Fe}/\text{H}] < -0.4$. There are high-dispersion spectroscopic data of metal rich ($-0.5 < [\text{Fe}/\text{H}] < -0.1$) GCs (namely NGC 6528, NGC 6553, NGC 6441, NGC 6440) from which it is possible to carry out a systematic and homogeneous study which can tell us how the abundance variations behave in these extreme metallicities. These data would be a nice complement to the recent results published by Schiavon et al. (2017b).
- **Low mass GCs:** The lack of evidence of MPs in Galactic disk open clusters (e.g. Maclean et al., 2015), may not be telling us much about the MPs in low mass clusters if there is actually an intrinsic quality missing in cluster formation today in the local Universe that makes them not suitable to compare such clusters with low mass clusters that formed together with massive old GCs. There is available UV HST photometry of very low mass ($\sim 10^4 M_{\odot}$) GCs at both extremes of the

metallicity distribution (Crater 1 $[\text{Fe}/\text{H}] = -1.7$ and NGC 6791 $[\text{Fe}/\text{H}] = +0.3$) which will increase our understanding of the MPs behaviour in those extremely low mass environments at the early epochs of GC formation.

- **Dwarf stars in intermediate-age clusters:** The absence of MPs (in evolved stars) within massive intermediate-age (1–2 Gyr, $> 10^5 M_{\odot}$) clusters (cf. Mucciarelli et al., 2008, 2014; Martocchia et al., 2017), has also suggested a cosmological effect (i.e. a special condition of the early Universe when GCs formed) for the origin of MPs. However, these studies were focused on bright RGB stars (initial masses $> 2 M_{\odot}$). Currently the highest stellar mass where there has been a successful detection of MPs, is $\sim 1.02 M_{\odot}$ for NGC 496 (cf. Niederhofer et al., 2017b). A possibility that fits the current evidence, but has yet to be explored is that the MP phenomenon is common to all (massive) clusters, however, only stars below a certain mass are affected. There is an ongoing HST survey, described in Niederhofer et al. (2017a), that is aimed at looking for the presence/absence of MPs in young and intermediate-age massive clusters. It would be interesting to probe the exact mass range ($< 1.02 M_{\odot}$) where MPs are known to be hosted in older clusters. A successful detection of MPs, i.e. a broadening/splitting of the MS of the clusters, where higher mass (evolved) stars do not show MPs (e.g. NGC 1846, Martiocchia et al. in prep), will add key constraints as it will imply that the MPs can only manifest in below a certain threshold of stellar mass. This survey includes UV photometry of NGC 1846 which could be the pilot cluster in such project. Complementary time to improve the quality of the photometry of the faintest stars has been requested already.

The second direction in which future work could be focused is the presence of the MP phenomenon in spheroids i.e. early-type galaxies (ETGs), spiral bulges and haloes. Major star formation episodes are responsible for the formation of GCs as well as massive spheroids (cf. Schweizer, 1987), so could the abundance patterns found in GCs and in these spheroids indicate a common origin?.

The recent discovery of GC-like abundance patterns (i.e. N and Al enhanced and C

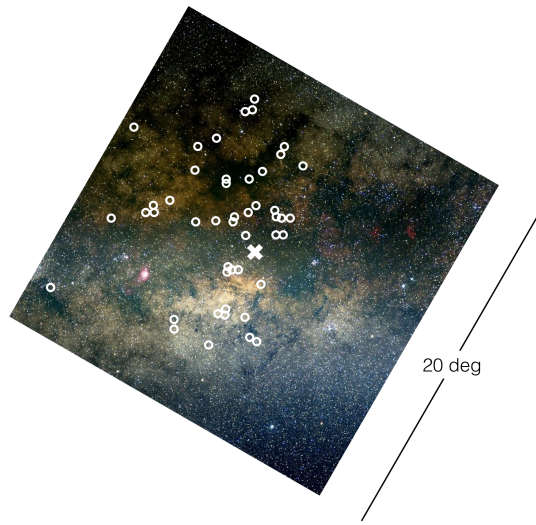


Figure 6.2: Stars with GC-like abundance patterns found by Schiavon et al. (2017a) in the inner Galaxy are shown with circles. The Galactic centre is shown with a cross. This figure was provided by R. Schiavon in a private communication.

depleted; Schiavon et al., 2017a) in the inner Galactic halo, showed that these abundance variations characteristic of MPs are not unique to GCs (cf. Figure 6.2). The numbers of these stars and their $[\text{Fe}/\text{H}]$ distribution likely excludes the possibility that they originated from disrupted/disrupting GCs. The signature abundance patterns akin to the MPs of GCs have also been found in other spheroids, for example:

- The core of M31 also shows strong CN bands, consistent with the integrated spectra of M31 and Galactic GCs (Burstein et al., 1984; Schiavon et al., 2012). Recent IFU observations of the M31 bulge have also found signs of MPs characteristic of GCs in the form of a population with significant Na enhancement (cf. Zieleniewski et al., 2015).
- Ultra compact dwarfs are systems with properties that are in-between those of GC and dwarf galaxies in terms of their mass, size, etc. Strader et al. (2013), found very high abundances of N and Na in a ultra compact dwarf galaxy satellite of M60 in the Virgo cluster.
- Integrated light analysis of ETGs have determined the presence of Na and N enhancement (e.g. Schiavon, 2007; Conroy et al., 2014).

Our lack of understanding of the origin of these abundance patterns prevents us from taking advantage of this phenomenon in the cosmological context of galaxy formation, or in the context of nucleosynthesis and stellar evolution.

One could use existing models based on empirical spectral libraries (e.g. FSPS – Conroy & van Dokkum, 2012) and combine them with synthetic stellar atmospheres (e.g. ATLAS12 – Kurucz, 2005) in order to account for relative changes in the spectra of the stars due to the changes of the abundances of the relevant elements that are found to vary in GC stars. By comparing these models to the integrated light of ETGs we would learn if the spectra of ETGs can be matched with a combination of normal and anomalous stars (i.e. stars with GC abundance variations). If so, does the stellar contribution of the “enriched population” agree with that estimated by Schiavon et al. (2017a) for the inner Galaxy? This could indicate that MPs are a manifestation of a more general phenomenon that is characteristic of the physical processes responsible for star formation in all spheroidal systems.

All the possible results from these studies, whether or not they turn out to be a positive or negative detection of MPs in each of the cases, would add fresh constraints on the origin of MPs. Any future scenarios proposed to explain their origin will have to address these results.

Appendix A

Degeneracies of the continuum normalized fit of NGC 7252: W3

As mentioned in §2.2.2, we use the SSP solution from the DynBaS fit to the continuum normalized spectrum, as the best estimate of the age of NGC 7252: W3. This fit yielded an age for this cluster of 570 Myr. In this appendix we look for possible degeneracies in our age estimate (i.e. if some other combinations of multiple populations reproduce the W3 spectrum equally well as our best solution), conducting fits to our data using grids of synthetic multiple-population clusters.

This experiment is the same as that we carried out to study the degeneracies on the SFH of NGC 34: S1 in Cabrera-Ziri et al. (2014). Here we built a grid of synthetic cluster spectra, in which each element represents a cluster with two star formation events. These spectra were built using the same continuum-normalized Bruzual & Charlot (2003) models we used for our DynBaS fits (cf. §2.2.2). In this grid each synthetic cluster consists of a massive population with always the same age, 570 Myr (Pop. I from here on), followed or preceded by a less massive second population of a different age (Pop. II). The ages for Pop. II in this grid range from 1 Myr to 1 Gyr and are distributed almost uniformly in log space. The masses of Pop. II could take values ranging from 10 to 90 per cent of the mass of Pop. I.

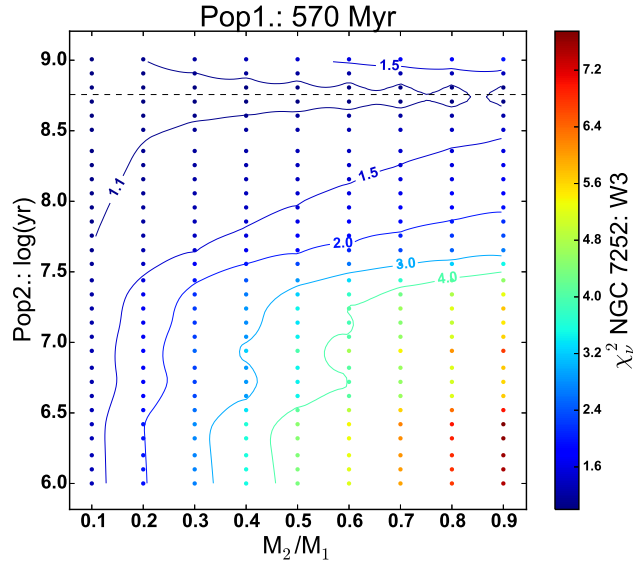


Figure A.1: Results of fitting the normalized spectrum of W3 with each element of a grid of synthetic cluster spectra. The Pop. I age for each element is always the same, i.e. 570 Myr (our best DynBaS SSP solution), which is represented with the dashed horizontal line in this plane. The vertical axis represents the age of the secondary (less massive) population, Pop. II, while the horizontal axis denotes the mass ratio between the first and second population. In colour we represent the χ^2_ν for each of these fits. For $\chi^2_\nu > 1.1$, we can spot the differences by eye between the synthetic clusters and the data (specially in the CaII K line), so those solutions are immediately excluded.

In Fig. A.1 we show the results of the fits of the continuum normalized MagE spectrum of W3 to each of the elements in this grid. In this figure we colour coded the solutions as a function of their χ^2_ν . The contours denote constant values of χ^2_ν . For practical reasons, we have normalized all these values dividing each of them by the χ^2_ν of our DynBaS1D solution (i.e. SSP 570 Myr). We found that for fits with $\chi^2_\nu > 1.1$, it is possible to distinguish by eye that the spectral fits are poor (i.e. fail to reproduce the depths/profiles of some Balmer lines and the CaII K line), and such solutions are excluded. For reference, the differences between solutions with $\chi^2_\nu < 1.1$ and $\chi^2_\nu > 1.1$, are similar (or greater) to the differences between the FWHM = 100 and 200 Myr spectra and the spectrum of W3 in Fig. 2.12, respectively.

Overall, this parameter space has a similar behaviour to the one found for NGC 34: S1 in Cabrera-Ziri et al. (2014), in the sense that we do not see any other region with a local χ^2_ν minimum which could host/hide another solution that represents a fit as good

(or better) than the DynBaS SSP solution. This figure also shows that the region with $\chi^2_\nu < 1.1$ (i.e. the region where it is not possible to distinguish a multiple population solution from a SSP solution) basically comprises all the synthetic clusters with a secondary burst (Pop. II) of age 508 and 640 Myr (which are the row of dots below and above the dashed line respectively) regardless of their mass. This region lies exactly within the uncertainties reported in §2.2.2 DynBaS fit solution, 570^{+70}_{-62} Myr. This is also in agreement with the upper limit of 100 Myr for the width of an extended star formation event centred at 570 Myr, where this multiple population solution represents a fit as good as the SSP solution (cf. Fig. 2.12 and the discussion in the text about this figure).

From this experiment, we conclude that the possible degeneracies in the SFH of this cluster, i.e. any multiple population solution as good as our SSP solution, lie within the uncertainties in the age of W3 reported in §2.2.2. We note that these uncertainties/degeneracies are significantly smaller than the age spread expected for this cluster according to the scenarios that attribute the eMSTO in intermediate-age clusters to extended star formation events.

Appendix B

Cluster disruption in the SMC/LMC

Here we discuss the feasibility of applying the strong Galactic tidal field of the D’Ercole et al. (2008) models to the intermediate-mass clusters in the SMC/LMC studied by G14.

Most of the dynamical mass loss in the D’Ercole et al. (2008) model of multiple-generation clusters is induced by stellar evolution, i.e. by the change of the gravitational potential due to massive stars ending their lives. This mass loss depends sensitively on how extended a cluster is — D’Ercole et al. (2008) achieve the high second-to-first generation ratio required by G14 only by assuming that the cluster fills its Roche lobe (their SG-R1 simulation), allowing it to lose stars efficiently as the gravitational potential changes. Hence, this model can only be applied to the SMC/LMC clusters if the ratio between the cluster radius and the tidal radius r_h/r_t is the same as in the D’Ercole et al. (2008) model. This ratio is $r_h/r_t = \{0.187, 0.115\}$ in Roche lobe-filling clusters with King parameters $W_0 = \{5, 7\}$ (e.g. Lamers et al., 2010). Independently of the cluster’s mass, this translates directly to a ratio between the half-mass density $\rho_h = 3M/8\pi r_h^3$ and the tidal density $\rho_t = 3\Omega^2/2\pi G$ (where $\Omega = V/R$ is the orbital angular velocity within the cluster’s host galaxy, assumed to have a flat rotation curve) of $\eta \equiv \rho_h/\rho_t = \{153, 658\}$ for $W_0 = \{5, 7\}$. In other words, the simulation SG-R1 *requires* that

$$\rho_h = \frac{3\eta\Omega^2}{2\pi G}. \quad (\text{B.1})$$

Table B.1: Cluster galactocentric distances, orbital angular velocities and half-mass densities required for the SG-R1 simulation in D’Ercole et al. (2008).

Galaxy	R	Ω	$\rho_h(W_0 = 5)$	$\rho_h(W_0 = 7)$
MW	4	5.6	51	221
SMC	3.5	1.8	5.0	21
LMC	2	3.1	15	66
LMC	3	2.2	8.0	34
LMC	4	1.8	5.2	22

Radii are in kpc, angular velocities in $(100 \text{ Myr})^{-1}$, and densities in $M_\odot \text{ pc}^{-3}$.

This density can be evaluated using the known rotation curves for the SMC and LMC (Alves & Nelson, 2000; Stanimirović et al., 2004). Table B.1 lists Ω and ρ_h for a number of galactic environments, such as the Milky Way at a radius of $R = 4 \text{ kpc}$ (as in D’Ercole et al. 2008, assuming a circular velocity of $V = 220 \text{ km s}^{-1}$), the SMC at $R = 3.5 \text{ kpc}$, and the LMC at $R = \{2, 3, 4\} \text{ kpc}$. The table shows that the SMC and LMC require densities $5 < \rho/M_\odot \text{ pc}^{-3} < 70$, with median values of $\rho_h = \{8.3, 36\} M_\odot \text{ pc}^{-3}$ for $W_0 = \{5, 7\}$, which is up to an order of magnitude lower than in the D’Ercole et al. (2008) model used by G14.

To determine whether the above low densities are still reasonable for young stellar clusters, we compare them to the densities of local-Universe YMCs listed in Portegies Zwart et al. (2010). The median density of the YMCs (ages $< 10 \text{ Myr}$) in their comprehensive sample is $\rho_h = 10^3 M_\odot \text{ pc}^{-3}$, i.e. between 1 and 2 orders of magnitude higher than the low densities required by G14 to apply the D’Ercole et al. (2008) model to SMC/LMC clusters. Out of the 30 YMCs, only 3 (χ Per, NGC 4038: W99-16, and NGC 4449: N-2) have densities lower than $50 M_\odot \text{ pc}^{-3}$. For reference, the only YMC younger than 10 Myr in the LMC (R136) has $\rho_h > 600 M_\odot \text{ pc}^{-3}$.

Therefore, the observed densities of recently-formed YMCs are too high for the D’Ercole et al. (2008) model to apply. The only way in which this application could be appropriate is if the intermediate-age clusters of G14 represent the low-density end of some larger, initial cluster population, of which the high-density YMCs were subsequently destroyed. However, there is no known mechanism that destroys high-density clusters

more easily than low-density ones. The main disruption agents in gas-rich galaxies are tidal evaporation and tidal shocks by giant molecular clouds, both of which *favour* the survival of high-mass, high-density clusters (e.g. Kruijssen, 2015).

We conclude that applying the simulation SG-R1 by D'Ercole et al. (2008) to YMCs in the SMC and LMC requires either extremely rare or carefully-tuned conditions, making it highly unlikely that this model applies to the clusters considered by G14.

Bibliography

- Alongi M., Bertelli G., Bressan A., Chiosi C., Fagotto F., Greggio L., Nasi E., 1993, *A&AS*, 97, 851
- Alves D. R., Nelson C. A., 2000, *ApJ*, 542, 789
- Anders P., Grijs R. D., v. Alvensleben U. F., Bissantz N., 2004, *MNRAS*, 347, 17
- Annibali F., Tosi M., Monelli M., Sirianni M., Montegriffo P., Aloisi A., Greggio L., 2009, *AJ*, 138, 169
- Balbinot E., Santiago B. X., Kerber L. O., Barbuy B., Dias B. M. S., 2010, *MNRAS*, 404, 1625
- Bastian N., Lardo C., 2015, *MNRAS*, 453, 357
- Bastian N., Niederhofer F., 2015, *MNRAS*, 448, 1863
- Bastian N., Silva-Villa E., 2013, *MNRAS*, 431, L122
- Bastian N., Strader J., 2014, *MNRAS*, 443, 3594
- Bastian N., de Mink S. E., 2009, *MNRAS*, 398, L11
- Bastian N., Emsellem E., Kissler-Patig M., Maraston C., 2006a, *A&A*, 445, 471
- Bastian N., Saglia R. P., Goudfrooij P., Kissler-Patig M., Maraston C., Schweizer F., Zoccali M., 2006b, *A&A*, 448, 881
- Bastian N., Gieles M., Goodwin S. P., Tranco G., Smith L. J., Konstantopoulos I., Efremov Y., 2008, *MNRAS*, 389, 223

- Bastian N., Tranco G., Konstantopoulos I. S., Miller B. W., 2009, *ApJ*, 701, 607
- Bastian N., Covey K. R., Meyer M. R., 2010, *ARA&A*, 48, 339
- Bastian N., Konstantopoulos I. S., Tranco G., Weisz D. R., Larsen S. S., Fouesneau M., Kaschinski C. B., Gieles M., 2012, *A&A*, 541, A25
- Bastian N., Schweizer F., Goudfrooij P., Larsen S. S., Kissler-Patig M., 2013a, *MNRAS*, 431, 1252
- Bastian N., Lamers H. J. G. L. M., Mink S. E. D., Longmore S. N., Goodwin S. P., Gieles M., 2013b, *MNRAS*, 436, 2398
- Bastian N., Cabrera-Ziri I., Davies B., Larsen S. S., 2013c, *MNRAS*, 436, 2852
- Bastian N., Hollyhead K., Cabrera-Ziri I., 2014, *MNRAS*, 445, 378
- Bastian N., Cabrera-Ziri I., Salaris M., 2015, *MNRAS*, 449, 3333
- Bastian N., et al., 2016, *MNRAS*, 460, L20
- Bastian N., et al., 2017, *MNRAS*, 465, 4795
- Bechtol K., et al., 2015, *ApJ*, 807, 50
- Bisbas T. G., Bell T. A., Viti S., Barlow M. J., Yates J., Vasta M., 2014, *MNRAS*, 443, 111
- Bolatto A. D., Wolfire M., Leroy A. K., 2013, *ARA&A*, 51, 207
- Bragaglia A., Gratton R. G., Carretta E., D'Orazi V., Sneden C., Lucatello S., 2012, *A&A*, 548, A122
- Bragaglia A., Sneden C., Carretta E., Gratton R. G., Lucatello S., Bernath P. F., Brooke J. S. A., Ram R. S., 2014, *ApJ*, 796, 68
- Bragaglia A., Carretta E., Sollima A., Donati P., D'Orazi V., Gratton R. G., Lucatello S., Sneden C., 2015, *A&A*, 583, A69
- Brandt T. D., Huang C. X., 2015a, *ApJ*, 807, 24

- Brandt T. D., Huang C. X., 2015b, *ApJ*, 807, 25
- Brandt T. D., Tojeiro R., Aubourg É., Heavens A., Jimenez R., Strauss M. A., 2010, *AJ*, 140, 804
- Bressan A., Fagotto F., Bertelli G., Chiosi C., 1993, *A&AS*, 100, 647
- Bressert E., et al., 2010, *MNRAS*, 409, L54
- Brodie J. P., Strader J., 2006, *ARA&A*, 44, 193
- Brodie J. P., Schroder L. L., Huchra J. P., Phillips A. C., Kissler-Patig M., Forbes D. A., 1998, *AJ*, 116, 691
- Bruzual G., 2010, *Phil. Trans. R. Soc. A*, 368, 783
- Bruzual G., Charlot S., 2003, *MNRAS*, 344, 1000
- Burstein D., Faber S. M., Gaskell C. M., Krumm N., 1984, *ApJ*, 287, 586
- Cabrera-Ziri I., Bastian N., Davies B., C. G. M., A. G. B., Schweizer F., 2014, *MNRAS*, 441, 2754
- Cabrera-Ziri I., et al., 2015, *MNRAS*, 448, 2224
- Cabrera-Ziri I., et al., 2016a, *MNRAS*, 457, 809
- Cabrera-Ziri I., et al., 2016b, *MNRAS*, 459, 4218
- Cabrera-Ziri I., Lardo C., Davies B., Bastian N., Beccari G., Larsen S. S., Hernandez S., 2016c, *MNRAS*, 460, 1869
- Caldwell N., Harding P., Morrison H., Rose J. A., Schiavon R., Kriessler J., 2009, *AJ*, 137, 94
- Cardelli J. A., Clayton G. C., Mathis J. S., 1989, *ApJ*, 345, 245
- Carretta E., 2014, *ApJL*, 795, L28
- Carretta E., Gratton R. G., Lucatello S., Bragaglia A., Bonifacio P., 2005, *A&A*, 433, 597

- Carretta E., Bragaglia A., Gratton R. G., Lucatello S., Momany Y., 2007a, *A&A*, 464, 927
- Carretta E., et al., 2007b, *A&A*, 464, 967
- Carretta E., et al., 2009a, *A&A*, 505, 117
- Carretta E., Bragaglia A., Gratton R., Lucatello S., 2009b, *A&A*, 505, 139
- Carretta E., Bragaglia A., Gratton R. G., Recio-Blanco A., Lucatello S., D’Orazi V., Cassisi S., 2010a, *A&A*, 516, A55
- Carretta E., et al., 2010b, *A&A*, 520, A95
- Carretta E., et al., 2010c, *ApJ*, 714, L7
- Carretta E., Lucatello S., Gratton R. G., Bragaglia A., D’Orazi V., 2011, *A&A*, 533, A69
- Carretta E., Bragaglia A., Gratton R. G., Lucatello S., D’Orazi V., 2012, *ApJL*, 750, L14
- Carretta E., et al., 2013, *A&A*, 557, 138
- Carretta E., Bragaglia A., Gratton R. G., D’Orazi V., Lucatello S., Sollima A., 2014a, *A&A*, 561, A87
- Carretta E., et al., 2014b, *A&A*, 564, A60
- Carretta E., et al., 2015, *A&A*, 578, A116
- Chabrier G., 2003, *PASP*, 115, 763
- Charbonnel C., 2016, *EAS*, 80, 177
- Chien L.-H., Barnes J. E., 2010, *MNRAS*, 407, 43
- Chien L.-H., Barnes J. E., Kewley L. J., Chambers K. C., 2007, *ApJ*, 660, L105
- Cid Fernandes R., González-Delgado R. M., 2010, *MNRAS*, 403, 780

- Cid Fernandes R., Mateus A., Sodré L., Stasińska G., Gomes J. M., 2005, *MNRAS*, 358, 363
- Clark J. S., Negueruela I., 2002, *AA*, 396, L25
- Conroy C., 2012, *ApJ*, 758, 21
- Conroy C., Spergel D. N., 2011, *ApJ*, 726, 36
- Conroy C., van Dokkum P., 2012, *ApJ*, 747, 69
- Conroy C., Graves G. J., van Dokkum P. G., 2014, *ApJ*, 780, 33
- Cordero M. J., Hénault-Brunet V., Pilachowski C. A., Balbinot E., Johnson C. I., Varri A. L., 2017, *MNRAS*, 465, 3515
- Correnti M., Goudfrooij P., Puzia T. H., de Mink S. E., 2015, *MNRAS*, 450, 3054
- Crowther P. A., Schnurr O., Hirschi R., Yusof N., Parker R. J., Goodwin S. P., Kassim H. A., 2010, *MNRAS*, 408, 731
- Cunha K., et al., 2015, *ApJ*, 798, L41
- D'Antona F., Criscienzo M. D., Decressin T., Milone A. P., Vesperini E., Ventura P., 2015, *MNRAS*, 453, 2637
- D'Ercole A., Vesperini E., D'Antona F., McMillan S. L. W., Recchi S., 2008, *MNRAS*, 391, 825
- D'Ercole A., D'Antona F., Ventura P., Vesperini E., Mcmillan S. L. W., 2010, *MNRAS*, 407, 854
- D'Ercole A., D'Antona F., Vesperini E., 2011, *MNRAS*, 415, 1304
- D'Ercole A., D'Antona F., Vesperini E., 2016, *MNRAS*, 461, 4088
- Dalessandro E., Lapenna E., Mucciarelli A., Origlia L., Ferraro F. R., Lanzoni B., 2016, *ApJ*, 829, 77

- Davies B., Figer D. F., Kudritzki R.-P., MacKenty J., Najarro F., Herrero A., 2007, *ApJ*, 671, 781
- Davies B., Kudritzki R.-P., Figer D. F., 2010, *MNRAS*, 407, 1203
- Davies B., Hoare M. G., Lumsden S. L., Hosokawa T., Oudmaijer R. D., Urquhart J. S., Mottram J. C., Stead J., 2011, *MNRAS*, 416, 972
- Davies B., et al., 2013, *ApJ*, 767, 3
- Davies B., Kudritzki R.-P., Gazak Z., Plez B., Bergemann M., Evans C., Patrick L., 2015, *ApJ*, 806, 21
- Decressin T., Meynet G., Charbonnel C., Prantzos N., Ekström S., 2007a, *A&A*, 464, 1029
- Decressin T., Charbonnel C., Meynet G., 2007b, *A&A*, 475, 859
- Decressin T., Charbonnel C., Siess L., Palacios A., Meynet G., Georgy C., 2009, *A&A*, 505, 727
- Dias B., Coelho P., Barbuy B., Kerber L., Idiart T., 2010, *A&A*, 520, 85
- Dupree A. K., Strader J., Smith G. H., 2011, *ApJ*, 728, 155
- Eggen O. J., 1998, *AJ*, 116, 284
- Evans C. J., et al., 2011, *A&A*, 527, A50
- Fabbiano G., Zezas A., Murray S. S., 2001, *ApJ*, 554, 1035
- Fagotto F., Bressan A., Bertelli G., Chiosi C., 1994a, *A&AS*, 104, 365
- Fagotto F., Bressan A., Bertelli G., Chiosi C., 1994b, *A&AS*, 105, 29
- Figer D. F., MacKenty J. W., Robberto M., Smith K., Najarro F., Kudritzki R. P., Herrero A., 2006, *ApJ*, 643, 1166
- Fouesneau M., Lançon A., 2010, *A&A*, 521, A22

- Gallagher J. S., Smith L. J., 1999, MNRAS, 304, 540
- Gazak J. Z., Bastian N., Kudritzki R.-P., Adamo A., Davies B., Plez B., Urbaneja M. A., 2013, MNRAS, 430, L35
- Gazak J. Z., Davies B., Kudritzki R.-P., Bergemann M., Plez B., 2014, ApJ, 788, 58
- Gazak J. Z., et al., 2015, ApJ, 805, 182
- Georgiev I. Y., Hilker M., Puzia T. H., Goudfrooij P., Baumgardt H., 2009, MNRAS, 396, 1075
- Georgy C., Ekström S., Granada A., Meynet G., Mowlavi N., Eggenberger P., Maeder A., 2013, A&A, 553, A24
- Girardi L., Bressan A., Chiosi C., Bertelli G., Nasi E., 1996, A&AS, 117, 113
- Girardi L., Rubele S., Kerber L., 2009, MNRAS, 394, L74
- González J. J., 1993, PhD thesis, Univ. California, p. 172
- Goudfrooij P., Puzia T. H., Kozhurina-Platais V., Chandar R., 2009, AJ, 137, 4988
- Goudfrooij P., Puzia T. H., Kozhurina-Platais V., Chandar R., 2011a, AJ, 737, 3
- Goudfrooij P., Puzia T. H., Chandar R., Kozhurina-Platais V., 2011b, AJ, 737, 4
- Goudfrooij P., et al., 2014, ApJ, 797, 35
- Goudfrooij P., Girardi L., Rosenfield P., Bressan A., Marigo P., Correnti M., Puzia T. H., 2015, MNRAS, 450, 1693
- Gratton R. G., Lucatello S., Bragaglia A., Carretta E., Momany Y., Pancino E., Valenti E., 2006, A&A, 455, 271
- Gratton R. G., et al., 2007, A&A, 464, 953
- Gratton R. G., Carretta E., Bragaglia A., 2012, A&AR, 20, 50
- Grijs R. D., et al., 2004, MNRAS, 352, 263

- Gustafsson B., Edvardsson B., Eriksson K., Jørgensen U. G., Nordlund Å., Plez B., 2008, *A&A*, 486, 951
- Harris W. E., 1996, *AJ*, 112, 1487
- Harris J., Zaritsky D., 2009, *AJ*, 138, 1243
- Heavens A. F., Jimenez R., Lahav O., 2000, *MNRAS*, 317, 965
- Hesser J. E., Bell R. A., 1980, *ApJ*, 238, L149
- Hibbard J. E., Mihos J. C., 1995, *AJ*, 110, 140
- Hollyhead K., Bastian N., Adamo A., Silva-Villa E., Dale J., Ryon J. E., Gazak Z., 2015, *MNRAS*, 449, 1106
- Jordán A., et al., 2004, *ApJS*, 154, 509
- Keller S. C., Mackey A. D., Costa G. S. D., 2011, *ApJ*, 731, 22
- Kerber L. O., Santiago B. X., Castro R., Valls-Gabaud D., 2002, *A&A*, 390, 121
- King I., 1962, *AJ*, 67, 471
- Knoetig M. L., 2014, *ApJ*, 790, 106
- Koleva M., Prugniel P., Bouchard A., Wu Y., 2009, *A&A*, 501, 1269
- Konstantopoulos I. S., Bastian N., Smith L. J., Westmoquette M. S., Trancho G., Gallagher J. S., 2009, *ApJ*, 701, 1015
- Kraft R. P., 1979, *ARA&A*, 17, 309
- Kraft R. P., 1994, *PASP*, 106, 553
- Kraus A. L., Hillenbrand L. A., 2007, *AJ*, 134, 2340
- Krause M., Charbonnel C., Decressin T., Meynet G., Prantzos N., Diehl R., 2012, *A&A*, 546, L5

- Krause M., Charbonnel C., Decressin T., Meynet G., Prantzos N., 2013, *A&A*, 552, 121
- Krause M. G. H., Charbonnel C., Bastian N., Diehl R., 2016, *A&A*, 587, A53
- Kroupa P., Tout C. A., Gilmore G., 1993, *MNRAS*, 262, 545
- Kruijssen J. M. D., 2014, *Class. Quantum Gravity*, 31, 244006
- Kruijssen J. M. D., 2015, *MNRAS*, 454, 1658
- Kudryavtseva N., et al., 2012, *ApJ*, 750, L44
- Kurucz R. L., 2005, *Mem. Soc. Astron. Ital. Suppl.*, 8, 14
- Lada C. J., Lada E. A., 2003, *ARA&A*, 41, 57
- Lamers H. J. G. L. M., Baumgardt H., Gieles M., 2010, *MNRAS*, 409, 305
- Lardo C., Davies B., Kudritzki R.-P., Gazak J. Z., Evans C. J., Patrick L. R., Bergemann M., Plez B., 2015, *ApJ*, 812, 160
- Larsen S. S., 1999, *A&AS*, 139, 393
- Larsen S. S., 2002, *AJ*, 124, 1393
- Larsen S. S., 2004, *A&A*, 416, 537
- Larsen S. S., 2009, *A&A*, 494, 539
- Larsen S. S., Brodie J. P., 2002, *AJ*, 123, 1488
- Larsen S. S., Richtler T., 1999, *A&A*, 345, 59
- Larsen S. S., Richtler T., 2004, *Astronomy and Astrophysics*, 427, 495
- Larsen S. S., Richtler T., 2006, *A&A*, 459, 103
- Larsen S. S., Brodie J. P., Hunter D. A., 2004, *AJ*, 128, 2295
- Larsen S. S., Origlia L., Brodie J. P., Gallagher J. S., 2006, *MNRAS*, 368, L10

- Larsen S. S., Origlia L., Brodie J. P., Gallagher J. S., 2008, *MNRAS*, 383, 263
- Larsen S. S., et al., 2011, *A&A*, 532, A147
- Larsen S. S., Strader J., Brodie J. P., 2012, *A&A*, 544, L14
- Larsen S. S., Brodie J. P., Forbes D. A., Strader J., 2014a, *A&A*, 565, 98
- Larsen S. S., Brodie J. P., Grundahl F., Strader J., 2014b, *ApJ*, 797, 15
- Le Borgne J.-F., et al., 2003, *A&A*, 402, 433
- Leitherer C., et al., 1999, *ApJS*, 123, 3
- Li C., de Grijs R., Deng L., 2014, *Nat*, 516, 367
- Li C., de Grijs R., Deng L., Geller A. M., Xin Y., Hu Y., Faucher-Giguère C.-A., 2016, *Nat*, 529, 502
- Lind K., et al., 2015, *A&A*, 575, L12
- Longmore S. N., 2015, *MNRAS*, 448, L62
- Longmore S. N., et al., 2014, *Protostars and Planets VI*, p. 291
- Mackey A. D., Broby Nielsen P., 2007, *MNRAS*, 379, 151
- Mackey A. D., Nielsen P. B., Ferguson A. M. N., Richardson J. C., 2008, *ApJ*, 681, L17
- Maclean B. T., Silva G. M. D., Lattanzio J., 2015, *MNRAS*, 446, 3556
- Magrini L., et al., 2014, *A&A*, 563, A44
- Magrini L., et al., 2015, *A&A*, 580, A85
- Magris G., P. J. M., Mateu C., A. G. B., Cabrera-Ziri I., Mejía-Narváez A., 2015, *PASP*, 127, 16
- Maoz D., Sharon K., Gal-Yam A., 2010, *ApJ*, 722, 1879

- Maraston C., Kissler-Patig M., Brodie J. P., Barmby P., Huchra J. P., 2001, *A&A*, 370, 176
- Maraston C., Bastian N., Saglia R. P., Kissler-Patig M., Schweizer F., Goudfrooij P., 2004, *A&A*, 416, 467
- Marigo P., Girardi L., Bressan A., Groenewegen M. A. T., Silva L., Granato G. L., 2008, *A&A*, 482, 883
- Marino A. F., et al., 2014, *MNRAS*, 437, 1609
- Marshall J. L., et al., 2008, *Proc. SPIE*, 7014, 701454
- Martell S. L., Grebel E. K., 2010, *A&A*, 519, A14
- Martell S. L., Smolinski J. P., Beers T. C., Grebel E. K., 2011, *A&A*, 534, 136
- Martin N. F., de Jong J. T. A., Rix H.-W., 2008, *ApJ*, 684, 1075
- Martocchia S., et al., 2017, *MNRAS* submitted
- McCraday N., Graham J. R., 2007, *ApJ*, 663, 844
- McCraday N., Gilbert A. M., Graham J. R., 2003, *ApJ*, 596, 240
- McDonald I., Zijlstra A. A., 2015, *MNRAS*, 446, 2226
- McLaughlin D. E., van der Marel R. P., 2005, *ApJS*, 161, 304
- Mengel S., Lehnert M. D., Thatte N. A., Vacca W. D., Whitmore B., Chandar R., 2008, *A&A*, 489, 1091
- Mészáros S., et al., 2015, *AJ*, 149, 153
- Miller B. W., Whitmore B. C., Schweizer F., Fall S. M., 1997, *AJ*, 114, 2381
- Milone A. P., Bedin L. R., Piotto G., Anderson J., 2009, *A&A*, 497, 755
- Milone A. P., Piotto G., Bedin L. R., Cassisi S., Anderson J., Marino A. F., Pietrinferni A., Aparicio A., 2012a, *A&A*, 537, A77

- Milone A. P., Marino A. F., Piotto G., Bedin L. R., Anderson J., Aparicio A., Cassisi S., Rich R. M., 2012b, *ApJ*, 745, 27
- Milone A. P., et al., 2013, *ApJ*, 767, 120
- Milone A. P., et al., 2014, *ApJ*, 785, 21
- Milone A. P., et al., 2015, *ApJ*, 808, 51
- Milone A. P., Marino A. F., D'Antona F., Bedin L. R., Costa G. S. D., Jerjen H., Mackey A. D., 2016, *MNRAS*, 458, 4368
- Milone A. P., et al., 2017, *MNRAS*, 464, 3636
- Moll S. L., Mengel S., Grijs R. D., Smith L. J., Crowther P. A., 2007, *MNRAS*, 382, 1877
- Morax E., 2016, *EAS*, 80, 73
- Mucciarelli A., Carretta E., Origlia L., Ferraro F. R., 2008, *AJ*, 136, 375
- Mucciarelli A., Origlia L., Ferraro F. R., Pancino E., 2009, *ApJ*, 695, L134
- Mucciarelli A., Dalessandro E., Ferraro F. R., Origlia L., Lanzoni B., 2014, *ApJL*, 793, L6
- Niederhofer F., Georgy C., Bastian N., Ekström S., 2015, *MNRAS*, 453, 2070
- Niederhofer F., Bastian N., Kozhurina-Platais V., Hilker M., Mink S. E. D., Cabrera-Ziri I., Li C., Ercolano B., 2016, *A&A*, 586, A148
- Niederhofer F., et al., 2017a, *MNRAS*, 464, 94
- Niederhofer F., et al., 2017b, *MNRAS*, 465, 4159
- Ocvirk P., Pichon C., Lançon A., Thiébaud E., 2006, *MNRAS*, 365, 46
- Pancino E., Carrera R., Rossetti E., Gallart C., 2010, *A&A*, 511, A56
- Pancino et al. 2017, *A&A* (accepted), p. arXiv:1702.06083

- Pasquini L., Mauas P., Käufel H. U., Cacciari C., 2011, *A&A*, 531, A35
- Peacock M. B., Zepf S. E., Finzell T., 2013, *ApJ*, 769, 126
- Perryman M. A. C., et al., 1998, *A&A*, 331, 81
- Piatti A. E., Bastian N., 2016, *A&A*, 590, A50
- Piotto G., et al., 2015, *AJ*, 149, 91
- Plez B., 2012, *Astrophysics Source Code Library*, p. 1205.004
- Portegies Zwart S. F., McMillan S. L. W., Gieles M., 2010, *ARA&A*, 48, 431
- Power C., Wynn G. A., Combet C., Wilkinson M. I., 2009, *MNRAS*, 395, 1146
- Prantzos N., Charbonnel C., 2006, *A&A*, 458, 135
- Ramírez I., Meléndez J., Chanamé J., 2012, *ApJ*, 757, 164
- Rangelov B., Chandar R., Prestwich A., Whitmore B. C., 2012, *ApJ*, 758, 99
- Renzini A., 2008, *MNRAS*, 391, 354
- Renzini A., 2013, *Mem. Soc. Astron. Ital.*, 84, 162
- Roediger J. C., Courteau S., Graves G., Schiavon R. P., 2014, *ApJS*, 210, 10
- Rossa J., van der Marel R. P., Böker T., Gerssen J., Ho L. C., Rix H.-W., Shields J. C., Walcher C.-J., 2006, *AJ*, 132, 1074
- Rubele S., Girardi L., Kozhurina-Platais V., Kerber L., Goudfrooij P., Bressan A., Marigo P., 2013, *MNRAS*, 430, 2774
- Ruiter A. J., et al., 2013, *MNRAS*, 429, 1425
- Salaris M., Cassisi S., Pietrinferni A., 2016, *A&A*, 590, A64
- Sandage A., 1986, *ARA&A*, 24, 421
- Sbordone L., Salaris M., Weiss A., Cassisi S., 2011, *A&A*, 534, A9

- Scheepmaker R. A., Haas M. R., Gieles M., Bastian N., Larsen S. S., Lamers H. J. G. L. M., 2007, *A&A*, 469, 925
- Schiavon R. P., 2007, *ApJ*, 171, 146
- Schiavon R. P., Caldwell N., Morrison H., Harding P., Courteau S., Macarthur L. A., Graves G. J., 2012, *AJ*, 143, 14
- Schiavon R. P., Caldwell N., Conroy C., Graves G. J., Strader J., Macarthur L. A., Courteau S., Harding P., 2013, *ApJ*, 776, L7
- Schiavon R. P., et al., 2017a, *MNRAS*, 465, 501
- Schiavon R. P., et al., 2017b, *MNRAS*, 466, 1010
- Schweizer F., 1987, in Faber S. M., ed., *Nearly Normal Galaxies: From the Planck Time to the Present*. Springer-Verlag, New York, p. 18
- Schweizer F., Seitzer P., 1998, *AJ*, 116, 2206
- Schweizer F., Seitzer P., 2007, *AJ*, 133, 2132
- Schweizer F., Seitzer P., Brodie J. P., 2004, *AJ*, 128, 202
- Seth A. C., Blum R. D., Bastian N., Caldwell N., Debattista V. P., 2008, *ApJ*, 687, 997
- Sidoli F., Smith L. J., Crowther P. A., 2006, *MNRAS*, 370, 799
- Silva-Villa E., Larsen S. S., 2010, *A&A*, 516, A10
- Silva J. V. S., Carraro G., Anthony-Twarog B. J., Bidin C. M., Costa E., Twarog B. A., 2016, *AJ*, 151, 6
- Sirianni M., Nota A., Marchi G. D., Leitherer C., Clampin M., 2002, *ApJ*, 579, 275
- Smith L. J., Gallagher J. S., 2001, *MNRAS*, 326, 1027
- Sollima A., Gratton R. G., Carretta E., Bragaglia A., Lucatello S., 2013, *MNRAS*, 433, 1276

- Stanimirović S., Staveley-Smith L., Jones P. A., 2004, *ApJ*, 604, 176
- Stolte A., Grebel E. K., Brandner W., Figer D. F., 2002, *A&A*, 394, 459
- Storey P. J., Hummer D. G., 1995, *MNRAS*, 272, 41
- Strader J., et al., 2013, *ApJ*, 775, L6
- Tojeiro R., Heavens A. F., Jimenez R., Panter B., 2007, *MNRAS*, 381, 1252
- Tolstoy E., Hill V., Tosi M., 2009, *ARA&A*, 47, 371
- Trancho G., Bastian N., Schweizer F., Miller B. W., 2007a, *ApJ*, 658, 993
- Trancho G., Bastian N., Miller B. W., Schweizer F., 2007b, *ApJ*, 664, 284
- Trancho G., Konstantopoulos I. S., Bastian N., Fedotov K., Gallagher S., Mullan B., Charlton J. C., 2012, *ApJ*, 748, 102
- Twarog B. A., Anthony-Twarog B. J., Deliyannis C. P., Thomas D. T., 2015, *AJ*, 150, 134
- Van Loon J. T., 2010, *Phil. Trans. R. Soc. A*, 368, 801
- VandenBerg D. A., Brogaard K., Leaman R., Casagrande L., 2013, *ApJ*, 775, 134
- Vázquez G. A., Leitherer C., Heckman T. M., Lennon D. J., de Mello D. F., Meurer G. R., Martin C. L., 2004, *ApJ*, 600, 162
- Weisz D. R., Dolphin A. E., Skillman E. D., Holtzman J., Dalcanton J. J., Cole A. A., Neary K., 2013, *MNRAS*, 431, 364
- Wheeler J. C., Sneden C., Truran J. W., 1989, *ARA&A*, 27, 279
- Whitmore B. C., 2003, In: *A decade of Hubble Space Telescope science. Proceedings of the Space Telescope Science Institute Symposium*, p. 153
- Whitmore B. C., Schweizer F., Leitherer C., Borne K., Robert C., 1993, *AJ*, 106, 1354
- Whitmore B. C., et al., 2010, *AJ*, 140, 75

Whitmore B. C., et al., 2014, *ApJ*, 795, 156

Wolter A., Trinchieri G., 2004, *A&A*, 426, 787

Yang W., Meng X., Bi S., Tian Z., Li T., Liu K., 2011, *ApJ*, 731, L37

Yang W., Bi S., Meng X., Liu Z., 2013, *ApJ*, 776, 112

Zeidler P., et al., 2015, *AJ*, 150, 78

Zhu M., Seaquist E. R., Kuno N., 2003, *ApJ*, 588, 243

Zieleniewski S., Houghton R. C. W., Thatte N., Davies R. L., 2015, *MNRAS*, 452, 597

de Mink S. E., Pols O. R., Langer N., Izzard R. G., 2009, *A&A*, 507, L1

de Silva G. M., Gibson B. K., Lattanzio J., Asplund M., 2009, *A&A*, 500, L25

de Wit W. J., Testi L., Palla F., Zinnecker H., 2005, *A&A*, 437, 247

van Dokkum P. G., 2001, *PASP*, 113, 1420